



CZECHOSLOVAK ASSOCIATION FOR CRYSTAL GROWTH

 **Fyzikální ústav**
Akademie věd ČR, v. v. i.

**Development of Materials Science
in Research and Education**

Proceedings of the 18th Joint Seminar

K. Nitsch

M. Rodová

Editors

Hnanice, Hotel Happy Star

Czech Republic

2 - 5 September 2008

Published by the Czechoslovak Association for Crystal Growth (CSACG)
CZ-162 00 Praha 6, Cukrovarnická 10, Czech Republic

Editors: K. Nitsch, M. Rodová
© 2008 CSACG, Praha, Czech Republic. All rights reserved.

ISBN 978-80-254-0864-3

The seminar is organized by

**the Czechoslovak Association for Crystal Growth and
the Slovak Expert Group of Solid State Chemistry and Physics**

under sharing of

**the Institute of Physics Academy of Science of the Czech Republic and
the Slovak Society for Industrial Chemistry**

Conference Chairman

Dr. K. Nitsch

Chairman of the Czechoslovak Association for Crystal Growth
Institute of Physics Academy of Sciences of the Czech Republic
Cukrovarnická 10, 162 00 Praha 6

Phone +420 220 318 557

Fax +420 233 343 184

E-mail: nitsch@fzu.cz

Conference Co-Chairman

Prof. M. Koman

Chairman of the Slovak Expert Group of Solid State Chemistry and Physics
Faculty of Chemical and Food Technology, Slovak Technical University
Radlinského 9, 812 37 Bratislava

Phone +421 259 325 623

Fax +421 252 493 198

E-mail: marian.koman@stuba.sk

Conference Secretary

Miroslava Rodová

Institute of Physics Academy of Sciences of the Czech Republic
Cukrovarnická 10, 162 00 Praha 6

Phone +420 220 318 429

Fax +420 233 343 184

E-mail: rodova@fzu.cz

FOREWORD

This year's seminar "Development of Materials Science in Research and Education" is already the eighteenth in the succession of seminars held by the Czechoslovak Association for Crystal Growth and the Slovak Expert Group of Solid State Chemistry and Physics regularly every year alternating in the Czech Republic and Slovak Republic since 1991. It is organised by the Czechoslovak Association for Crystal Growth and the Slovak Expert Group of Solid State Chemistry and Physics under the auspices of the Institute of Physics Academy of Science of the Czech Republic and the Slovak Society for Industrial Chemistry at a resort of Hnanice - Znojmo situated about 50 km south of Brno. The objectives of this meeting are to offer the opportunity for the Czech and Slovak teachers and scientists and guests from other countries working in the field of crystal growth and materials science to present their recent results and to exchange ideas and information.

The scientific sessions will cover the following topics of materials science:

- 1/ Trends in development of materials research.
- 2/ Education of materials science at the universities.
- 3/ Information on the research programmes of individual institutions.
- 4/ Information on equipment for preparation and characterisation of materials.
- 5/ Results of material science research.

The sessions will include talks and orally presented short contributions. The time allocated for talks is 30 minutes, for short contributions 20 minutes including the time for discussion. Although the official languages of the seminar are Czech, Slovak and English, the presentation of the abstracts is only in English.

This booklet contains the abstracts of all contributions, which reached us before July 31, 2008. The required camera-ready format of the abstracts makes it impossible for the editors to take any responsibility for the technical and language quality of the contributions. This responsibility rests entirely with the authors.

Editors

CONTENTS

EDUCATION OF MATERIAL SCIENCES AT MTF STU ACCORDING TO NEW STUDY PROGRAMMES SUBMITTED FOR ACCREDITATION	6
<i>Mária Behúlová and Peter Grgáč</i>	
HAFNIUM CARBIDE CERMETS	8
<i>Vlastimil Brožek, Pavel Ctibor, Dong-Ik Cheong, and Eun-Pyo Kim</i>	
DSC CALORIMETRY FOR AN IRON(II) COMPLEX SHOWING THE SPIN CROSSOVER ABOVE ROOM TEMPERATURE	10
<i>Ľubor Dlháň, Ivan Šalitroš, Olaf Fuhr, and Roman Boča</i>	
CRYSTALLITE SIZE AND SINTERABILITY OF TUNGSTEN	12
<i>Vlastimil Brožek, Jaroslav Maixner, Jiří Domlátil, Jan Janča, and Marek Eliáš</i>	
STUDY OF DIFFUSIVITY IN TERNARY SYSTEMS - DIFFUSION JOINTS OF Ni/Ni ₃ Al-Fe AND Ni/Ni ₃ Al-Ti	14
<i>Jaromír Drápala, Petr Kubíček, and Jana Sudrová</i>	
LPE GROWTH OF III-V SEMICONDUCTORS FROM RARE-EARTH TREATED MELTS	16
<i>Jan Grym, Olga Procházková, Jiří Zavadil, and Karel Žďánský</i>	
TiAl-Nb BASED ALLOY PREPARED BY MECHANICAL ALLOYING	18
<i>Jan Juřica and Monika Losertová</i>	
COMPOSITION, SYMMETRY AND STRUCTURE OF TETRANUCLEAR Cu ₄ Ox ₆ L ₄ COMPLEXES	20
<i>Marian Koman, Gregor Ondrejovič, and Adela Kotočová</i>	
STUDY OF ZnO-B ₂ O ₃ -P ₂ O ₅ -WO ₃ GLASSES	22
<i>Ladislav Koudelka, Jiří Šubčík, Petr Mošner, and Ivan Gregora</i>	

INFLUENCE OF INITIAL SUPERSATURATION ON NUCLEATION AND GROWTH IN CLOSED SYSTEMS	24
<i>Zdeněk Kožíšek, Pavel Demo, Alexei Sveshnikov, and Petra Tichá</i>	
THE DETERMINATION OF THE BAR SHAPE CERAMIC MATERIAL YOUNG'S ELAS- TICITY MODULUS BY MEANS OF THE BEND DEFORMATION.....	26
<i>Jozef Krajčovič and Igor Jančuška</i>	
STUDY OF GROWTH OF LEAD HALIDE SINGLE CRYSTALS FROM THE MELT ..	27
<i>Robert Král and Antonín Cihlár</i>	
HEAT CAPACITY, ENTHALPY AND ENTROPY OF CA(SR)-NB-O MIXED OXIDES 29	
<i>Jindřich Leitner, Květoslav Růžička, David Sedmidubský, and Pavel Svoboda</i>	
FIELD STIMULATED CARBON BLACK AGLOMERATION IN POLYSTYRENE MA- TRIX	31
<i>Jan Lipták and Ladislava Turczynová</i>	
BOND AND GRIND-BACK SILICON-ON-INSULATOR.....	33
<i>Michal Lorenc, Jan Šik, and Miloš Pospíšil</i>	
PREPARATION OF TiNB BASED ALLOY BY ELECTRON BEAM MELTING.....	35
<i>Monika Losertová, Jan Juřica, Jaroslav Veselý, and Jaromír Drápala</i>	
PREPARATION OF A NANOPARTICULAR SUSPENSION IN THE NEW WATER JET MILL (WJM) DEVICE USING CAVITATION DISINTEGRATION.....	37
<i>Jiří Luňáček, Richard Dvorský, and Aleš Slíva</i>	
SPECTRAL REFLECTOMETRY OF SiO ₂ THIN FILMS ON THE SILICON WAFER .	39
<i>Jiří Luňáček, Zdeněk Potůček, Milena Luňáčková, Petr Hlubina, and Dalibor Ciprian</i>	
SCINTILLATION PROPERTIES OF IMPURITIES IN YAG AND LUAG LPE FILMS	41
<i>Jiří A. Mareš, Martin Nikl, Petr Průša, and Alena Beitlerová</i>	

STRUCTURE AND PROPERTIES OF BOROPHOSPHATE GLASSES WITH TeO_2 AD- DITIONS.....	43
<i>Petr Mošner, Kateřina Vosejpková, Ladislav Koudelka, and Miroslav Vlček</i>	
PROFESSOR JAN KAŠPAR (TO 100TH BIRTHDAY ANNIVERSARY)	45
<i>Karel Nitsch</i>	
ELECTROCHEMICAL AND VAPOR DEPOSITION OF ZnO ON MICROPOROUS GAP AND GaAs SUBSTRATES.....	47
<i>Dušan Nohavica, Petr Gladkov, and Zdeněk Jarchovský</i>	
LUMINESCENCE OF CHALCOHALIDE GLASSES DOPED WITH PR AND YB.....	49
<i>Jiří Oswald, Karla Kuldová, Božena Frumarová, and Miroslav Frumar</i>	
MAGNETIC PROPERTIES OF MONONUCLEAR Co(II) AND Ni(II) COMPLEXES	50
<i>Blažena Papánková, Roman Boča, Ľubor Dlháň, Ingrid Svoboda, Hartmut Fuess, and Ján Titiš</i>	
NANOTECHNOLOGY IN EDUCATION.....	52
<i>Ivana Pilarčíková, Josef Sedláček, Jan Lipták, and Andrej Mlích</i>	
PHOTOLUMINESCENCE OF ERBIUM DOPED KTAO_3 CRYSTALS.....	54
<i>Zdeněk Potůček, Zdeněk Brykner, and Vladimír Trepakov</i>	
SCINTILLATION RESPONSE OF THE LIQUID PHASE EPITAXY GROWN YAG:Ce THIN FILMS.....	56
<i>Petr Průša, Jiří A. Mareš, Martin Nikl, Miroslav Kučera, Karel Nitsch, Alena Beitlerová, Natalia Solovieva, and Tomáš Čechák</i>	
TMA STUDY ON STRUCTURAL RELAXATION OF Ce -DOPED Na-Gd PHOSPHATE GLASSES	58
<i>Miroslava Rodová, Mária Chromčková, Marek Liška, and Karel Nitsch</i>	
RECRYSTALLIZATION ANNEALING OF WIRES ON THE BASE W-Re UNDER VAR- IOUS CONDITIONS	60
<i>Kateřina Skotnicová and Jaromír Drápala</i>	

GROWTH AND CHARACTERIZATION OF GAN:MN LAYERS	62
<i>Zdeněk Sofer, David Sedmidubský, Josef Stejskal, Jiří Hejtmánek, Miroslav Marýško, Karel Jurek, Vladimír Havránek, Anna Macková, and Michal Václavů</i>	
NUCLEATION OF VOIDS IN SOLID MATERIALS: TIME LAG	64
<i>Alexej Sveshnikov, Pavel Demo, Petra Tichá, and Zdeněk Kožíšek</i>	
DEVELOPMENT OF 150 MM SILICON WAFER FOR X-RAY SPACE OPTICS	66
<i>Jan Šik, Petr Kostelník, Miloš Pospíšil, and René Hudec</i>	
DETERMINATION OF DISTRIBUTION COEFFICIENTS OF ADMIXTURES IN TUNGSTEN AND MOLYBDENUM SINGLE CRYSTALS	68
<i>Jan Štěpánek and Kateřina Skotnicová</i>	
ASSESSMENT OF CALCIUM IONS CONCENTRATION IN SETTING CEMENT PASTES WITH VARIOUS WATER/CEMENT RATIOS	70
<i>Petra Tichá, Pavel Demo, Šárka Hošková, Alexej Sveshnikov, and Zdeněk Kožíšek</i>	
MAGNETIC CZOCHRALSKI GROWTH OF SILICON	72
<i>Lukáš Válek, Jan Šik, and Michal Lorenc</i>	
GROWTH OF INP CRYSTALS FOR RADIATION DETECTORS AND OTHER APPLICATIONS	74
<i>Ladislav Pekárek and Roman Yatskiv</i>	

ABSTRACTS

EDUCATION OF MATERIAL SCIENCES AT MTF STU ACCORDING TO NEW STUDY PROGRAMMES SUBMITTED FOR ACCREDITATION

M. Behúlová, P. Grgač

Slovak University of Technology in Bratislava, Faculty of Materials Science and Technology in Trnava, Paulínska 16, 917 24 Trnava, Slovak Republic,
maria.behulova@stuba.sk

1. Introduction. The complex accreditation of institutions providing high school education in the Slovak Republic involves not only accreditation of study programmes but as well as evaluation of the quality of the fulfillment of their mission in the area of education, research and/or art according the laws in force [1]. The process of accreditation is performed by Accreditation Commission in agreement with approved plan and given criteria, requirements and standards [2,3]. Findings of accreditation will serve for the diversification of high schools to the three types: universities, high schools and professional high schools in compliance with the main purpose of complex accreditation to provide to government, university and scientific community and to public the real image about the quality of single universities and high schools.

Table 1 Study programmes submitted for accreditation

BACHELOR PROGRAMMES (Bc.)	MASTER PROGRAMMES (MSc. Eng.)
1. Applied Informatics and Automation in Industry	1. Applied Informatics and Automation in Industry
2. Materials Engineering	2. Materials Engineering
3. Production Devices and Systems	3. Non-metallic Materials Processing and Application
4. Mechatronics of Production Devices and Systems	4. Surface engineering of advanced materials
5. Computer-Aided Production Technologies	5. Production Devices and Systems
6. Production Technologies	6. Machining and Assembly
7. Industrial Management	7. Computer-Aided Design and Production
8. Personnel Policy in Industrial Plant	8. Forming
9. Production Quality	9. Welding
10. Environmental Engineering	10. Industrial and Art Casting
11. Work Safety and Health Protection	11. Industrial Management
12. Teaching Practical Subjects within Engineering Majors	12. Personnel Management in Industrial Plant
	13. Production Quality Engineering
	14. Integrated Safety
	15. Teaching of Engineering Professional Subjects
POSTGRADUAL PROGRAMMES (Ph.D.)	
1. Automation and ICT Implementation in Processes	6. Materials Engineering
2. Industrial Management	7. Non-metallic Materials Processing and Application
3. Production Quality Engineering	8. Surface engineering of advanced materials
4. Integrated Safety	9. Didactics of Engineering Professional Subjects
5. Production Devices and Systems	10. Machine Technologies and Materials

2. Accreditation of study programmes at the MTF STU. In the framework of accreditation of the Slovak University of Technology in Bratislava, the Faculty of Materials Science and Technology in Trnava was preparing the Accreditation File from the October 2007 to the February 2008. The process of document preparation was influenced by changes in legislative in 2007 and by ambiguous interpretation of some evaluation criteria applied for the first time. Despite of this, the MTF STU submitted to the Accreditation Commission the proposal of Bachelor (Bc.), Master (MSc., Eng.) and postgraduate (PhD.) study programmes (Table 1) with new curricula exceeding a simple re-accreditation [4]. In the field of education, the accreditation was focused on the high quality, proficiency and rationalization of teaching process with the aim to reduce the number of subjects taught at the faculty and to unify the term, number

of contact hours, content and the form of examination of single subjects. In the first step of new curricula development, the subjects compulsory for all majors were defined covering e. g. at bachelor study in particular Fundamentals of Natural Science, Production Technologies, Materials, Informatics, Management, Environmental Science and Languages. For each term, two optional subjects from the area of Social Sciences were offered. In the next step, the menu of subjects providing by institutes of the faculty for the study programmes guaranteed at given institute was prepared. From this menu, guarantees of study programmes had to choose and include to their curricula given number of subjects. Finally, the curricula of proposed study programmes were completed by compulsory, optional and and/or eligible subjects of specialization in order to accomplish the core of knowledge for corresponding study branch.

3. Education of Materials Science. In the field of Materials Science, one Bc. study programme and three MSc. and PhD. study programmes are proposed for accreditation. The study programme Surface engineering of advanced materials will be provided only in English. In comparison with currently accredited study programmes, the reduction of the number of Bc. study programmes occurred but the offer for PhD. programmes was extended. According to the decrease in number of week contact hours, the education of some fundamental subjects was restricted. For example, the overall number of subjects taught at Bc. programme Materials Engineering dropped from 77 to 60. On the other hand, these restrictions referred to the material subjects in curricula of another study programmes. The following subjects related to materials science are included to curricula of suggested „non-material” study programmes [5]:

SUBJECT	BACHELOR PROGRAMMES*	MASTER PROGRAMMES*
Materials Science I	compulsory for all programmes	
Materials Science II	3, 4, 6, 12	
Mechanical Testing and Defectoscopy	3, 4, 10, 11	8, 10
Heat Treatment	6	
Technologies of Material Production	6	
Utility Properties and Material Selection	6	
Methods of Structure and Material Properties Examination	12	
Progressive Materials and Technologies		5, 6, 7, 8, 9, 10, 15
Degradation Processes and Life Prediction		5, 6, 10
Theory of Phase Transformations		10

* according to Table 1

4. Conclusion. The main intention of the chosen philosophy of submitted curriculum proposals was to increase the quality and efficiency of education process and research work at the MTF STU. Application of new study programmes and new curricula should reduce current high pedagogical duties of university teachers and provide them better conditions and opportunities for intensive basic and applied research work and successful fulfillment of the mission of the school as a technical university.

- [1] Zákon č. 131/2002 Z. z. o vysokých školách v znení neskorších predpisov.
- [2] <http://www.akredkom.sk/> (9.06.2008)
- [3] <http://www.minedu.sk/data/USERDATA/VysokeSkolstvo/KPpVZVS/> (9.06.2008)
- [4] Annual Report 2007. Faculty of Materials Science and Technology. Trnava, 2007.
- [5] Akreditačný spis MTF STU v Trnave. MTF STU, 2008.

HAFNIUM CARBIDE CERMETS

Vlastimil Brožek¹, Pavel Ctibor², Cheong Dong-Ik³, Kim Eun-Pyo³

¹Institute of Chemical Technology, Technická 5, 166 28 Praha 6

²Institute of Plasma Physics v.v.i., Za Slovankou 3, 182 00 Praha 8

³IAC - Chungnam National University, Daejeon, South Korea

Among most important metal matrix composites (MMC) we can find cemented carbides, predominantly tungsten carbide with cobalt binder. For high temperature applications the Co binder must be replaced with metals with higher melting point, namely with tungsten (m.p.3420°C), eventually tantalum or molybdenum (m.p.2996°C and 2630°C, respectively). The use of rhenium (m.p.3180°C) is economically non-realistic. Tungsten carbides WC or W₂C with decomposition temperature 2785°C should be also replaced by ZrC (m.p.3530°C) or HfC (the absolutely highest m.p.3820°C), or also their nitrides (ZrN and HfN, m.p.2980 and 3305°C, resp.). Bulk parts from these systems can be produced by powder metallurgy techniques. Such a parts are used namely for its high resistance to molten alkali metal, up to 1100°C and 860 kN/m², as pump parts for transferring molten Na in fast reactors. Pure sintered ZrC, ZrN and HfC parts serve as crucibles and boats for melting by el. current transfer. Their high melting point, high el. conductivity and low evaporation rate are favorable in production of electrodes for underwater oxy-electric cutting of steel and thermionic cathodes for equipment working under low vacuum.

It is well known that sintering above 2000°C is complicated and in the case of W with its high m.p. is it nearly unsatisfactory. Sintering under pressure - either HP or HIP is limited by an upper boundary of both the pressure and temperature. The most efficient commercial HIP from ASEA company has limit at 1850°C and 0.15 GPa. These parameters we have overcome by use of the device of BELT-type. Samples of W+HfC were sintered at 2000°C and 5.5 GPa. However the character of it was “grains of HfC incorporated by a pressure in the (quite well) sintered W matrix“ (see Fig.1). Joining or chemical interaction of the components was not attained; a bonding was only mechanical due to the shape of HfC particles. Therefore as the next step we have tested plasma spraying.

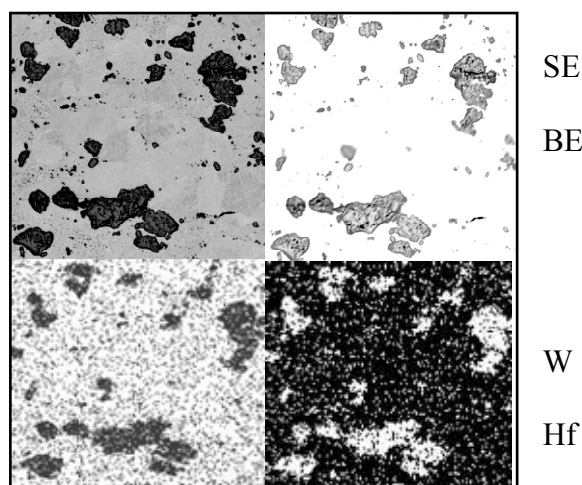


Fig.1 Cross-section of sintered W-HfC cermet

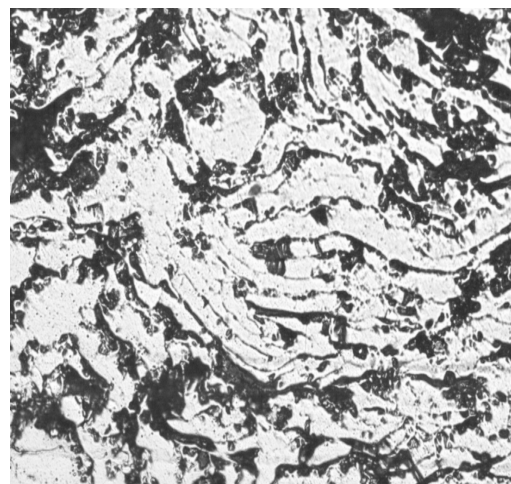


Fig.2 Plasma sprayed W-HfC cermet

A mixture of the W powder (Osram Sylvania, Bruntál), particle size 32-60 μm was mixed with 10 vol% of HfC (Sigma-Aldrich) and fed into the plasma of the WSP[®] generator by means of Ar carrying. Coatings 0.1 mm thick were sprayed on graphite substrates [1]. Metallographic study has shown different and more equal HfC particles, compare to BELT, and namely the change of their shape, which improves the cohesion with the W matrix (Fig.2). Some of the here presented results are only for bulk samples due to their better dimensional fit to the appropriate testing equipment.

Microhardness on polished cross sections was measured on polished cross sections by Hanemann head with Vickers indenter at 1 N load, see Table I.

Table I

Sample W+10HfC	As-sintered	Annealed at 1550°C in Ar	Plasma sprayed
HV [GPa] in metal	7.8 ± 2.9	9.1 ± 4.1	n.a.
HV [GPa] in carbide	9.7 ± 2.9	13.2 ± 1.7	13.0 ± 5.0

Coefficient of thermal expansion (CTE) was measured in Apparatus Setsys16/18 (SETARAM, France), Ar, in range 500-1550°C, see Fig.3

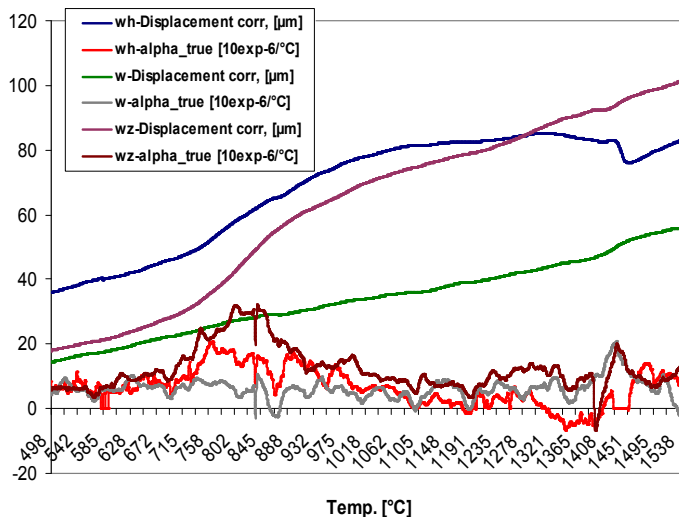


Fig. 3 – Dilatometric curves

w – tungsten
(CTE 6.18 $\mu\text{m}/\text{m}$ on heating and 2.58 $\mu\text{m}/\text{m}$ on cooling)
wz – W + 10ZrC
(CTE 12.20 $\mu\text{m}/\text{m}$ on heating and 3.54 $\mu\text{m}/\text{m}$ on cooling)
wh – W + 10HfC
(CTE 6.77 $\mu\text{m}/\text{m}$ on heating and 5.36 $\mu\text{m}/\text{m}$ on cooling)

The large standard deviation of the microhardness value at plasma sprayed sample is due to the dimensions of the lamellas versus the indent. The results could be partly diminished by the surrounding tungsten and the hardness of the HfC itself even higher. Shearing tests were carried out on samples having shape which does not allow the standardized measurement arrangement. Therefore modifications of the apparatus must have been done. The shear strength was 3.4 ± 0.3 GPa at room temperature.

The research will continue by studying of mechanical and physical properties of plasma sprayed materials and also at higher working temperatures. The materials are sensitive to surface oxidation in air from 700°C.

The Chungnam National University, Daejeon, South Korea should be acknowledged for financial support of the research, Agreement IUCF No. 2007-0336-2.

[1] V. Brožek, P. Ctibor, Cheong Dong-Ik, Kim Eun-Pyo, Proc. METAL, 13-15.5.2008, ed. TANGER Ltd., ISBN 978-80-254-1987-8.

DSC CALORIMETRY FOR AN IRON(II) COMPLEX SHOWING THE SPIN CROSSOVER ABOVE ROOM TEMPERATURE

Ľ. Dlháň¹, I. Šalitroš^{1,2}, O. Fuhr² and R. Boča¹

¹ Institute of Inorganic Chemistry, Technology and Materials, Slovak University of Technology, SK-812 37 Bratislava, Slovakia,

² Institute for Nanotechnology, Research Centre, Karlsruhe, PB-3640, D-76021, Germany

lubor.dlhan@stuba.sk

The iron(II) spin crossover complexes are excellent candidates for potential information technology applications. For this purpose, however, it is necessary to find a system working at ambient temperature and possessing a large thermal hysteresis loop. Several iron(II) complexes with bis-pyrazol-pyridine moiety almost reach these requirements [1,2]. Here we present magnetic properties and DSC investigations of iron(II) mononuclear complex **1** with general formula $[\text{Fe}^{\text{II}}(\text{L}^3)](\text{BF}_4)_2$, where L^3 is a tridentate ligand 4-ethynyl-2,6-bis(pyrazol)pyridine [3]. This system was subjected to X-ray structural (Fig. 1), magnetometric, and calorimetric studies.

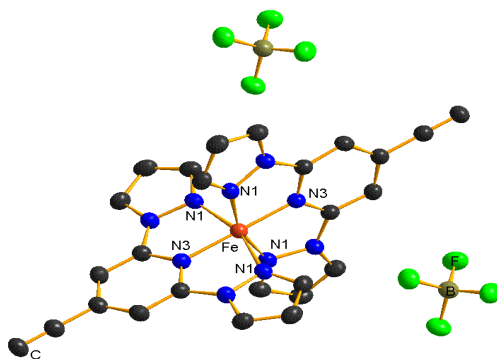
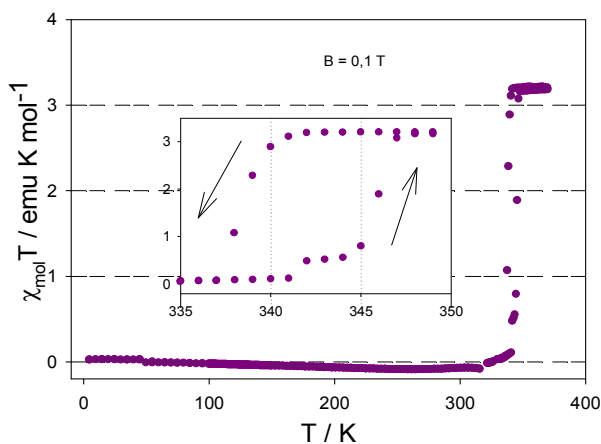


Fig. 1. View of the molecular structure of **1**.

The magnetic data for **1** (Fig. 2) show a gradual increase of the product function χT between $T = 5$ and 300 K; above this limit the rapid increase is observed. At $T_{\text{on}}^{\uparrow} = 344$ K an on-set of the sharp jump into the high-spin state ($S = 2$) is registered. At $T_{\text{off}}^{\uparrow} = 347$ K the spin transition is almost complete and a further heating alters the product function only slightly. In the cooling direction a thermal hysteresis occurs. The on-set return to the low-spin state ($S = 0$) is at $T_{\text{on}}^{\downarrow} = 340$ K and it is complete at $T_{\text{off}}^{\downarrow} = 336$ K.



The heat flow for **1** has been recorded with DSC apparatus (Diamond, Perkin Elmer) in the heating a cooling regime as shown in Fig. 3. The responses of the free aluminum container (baseline) and the calibrant material (copper) have been recorded with the same scan rate (10 K min^{-1}) allowing calculating the molar heat capacity C_p , and the C_p/T function. Their integration gave the molar enthalpy and entropy of the spin transition, respectively.

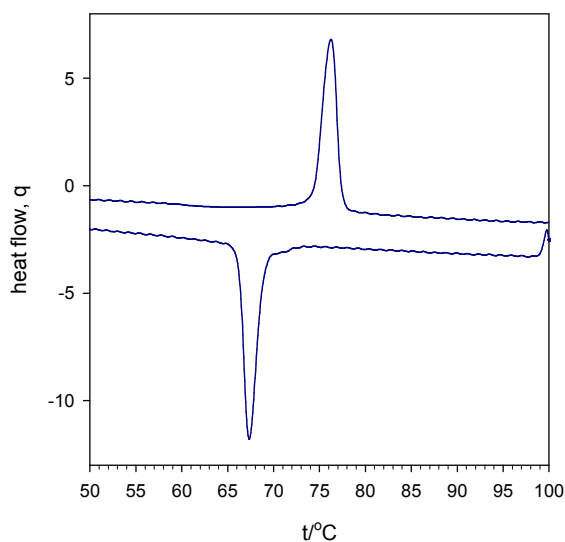


Fig. 3. Heat flow for **1** on heating (peak up) and cooling (peak down) regime.

Acknowledgments – Grant agencies and project sponsors (Slovakia: VEGA 1/0213/08, APVV 0006-07, COST-0006-06, VVCE 0004-07; Germany: DFG; ESF: COST D-35) are acknowledged for financial support.

- [1] C. Rajadurai, F. Schramm, S. Brink, O. Fuhr, M. Ghafari, R. Kruk, M. Ruben, *Inorg. Chem.* 45 (2006) 10019.
- [2] C. Rajadurai, F. Schramm, O. Fuhr, M. Ruben, *Eur. J. Inorg. Chem.* (2008) in press.
- [3] N.T.Madhu, I. Salitos, F. Schramm, S. Klyatskaya, O. Fuhr, M. Ruben, *Comptes Rendues Chemie* (submitted).

CRYSTALLITE SIZE AND SINTERABILITY OF TUNGSTEN

V. Brožek¹, J. Maixner², J. Domlátil², J. Janča³, M. Eliáš³

¹ Institute of Plasma Physics v.v.i., Academy of Sciences of the Czech Republic,
Za Slovankou 3, 182 00 Prague 8, Czech Republic

² Institute of Chemical Technology, Technická 5, 166 28 Prague 6, Czech Republic

³ Department of Physical Electronics, Masaryk University Brno, Kotlářská 2,
61137 Brno, Czech Republic.

jiri.domlatil@vscht.cz

Introduction

Sintering activity is defined by various approaches. For high melting point metals the experimental sintering activity determination according Agte is traditionally preferred [1]. Its definition is based on the measurement of and comparison of the density of a product sintered at defined conditions, i.e. with the admixture of 3 % of Ni at the pressure 0.5 MPa and temperature 1350°C, with the theoretical density. These measurements were completed by our own modification based on the knowledge that the sintering activity could be influenced also by the activity of Ni binder. There exist various forms of Ni having different reactivity also at similar powder size and specific surface area (e.g. Raney nickel or carbonyl nickel). That is why we have done analogous experiments also with silver, which is known to be absolutely nonwettable versus tungsten ($\Theta = 180^\circ$). Silver serves only as temporary binder of the compressed W powder before the sintering.

Highly reactive tungsten can be prepared by specific reduction of tungsten oxide or by the reduction of specific precursors – in our case tungstates. During their reduction so called tungsten bronzes are produced [2]. These bronzes are further reduced to produce a matrix of elemental W with cation component in the form of an oxide (e.g. PbO, CaO) or elemental metal (e.g. Fe, Ni).

Tungsten powder preparation

- a) Tungsten powder prepared by hydrogen reduction of APT at 1100°C. product Osrám Sylvania Bruntál
- b) Powdered tungsten prepared by plasmachemical reduction of WO_3 or Na_2WO_4 in capacitive coupled RF hydrogen plasma at 600°C. [3]

Tungsten powder sintering

The mixture of tungsten and nickel/or silver in the mass ratio 99:1 was pressed on the hydraulic press PITE 30. The value of the compressing pressure was 100 MPa and the loading time was 4-5 s. The sintering took place in a vacuum furnace PVG-80. The heating of the furnace is graphite. Hydrogen was employed as the process gas. argon as carrier and cooling gas. The operation of the furnace was controlled by computer according to the selected sintering program.

Crystallite size calculation

Calculations using Scherrer equation consider whole XRD peak broadening to be a result of crystallite size influence. This assumption is valid if there is neither internal stress nor high concentration of dislocations in the sample. This fact is however difficult to confirm or suspend. At the calculation utilizing K_β the difference between reflections (110) and (200) is higher than the value suffered by the sole influence of the crystallite size.

Table 1 - Comparison of different tungsten products density (selected examples)

	Theory (g/cm ³)	Measured (g/cm ³)	Density (rel %)	Crystallite size Starting powder		Crystallite size After sintering	
				2 theta 40.26	2 theta 58.24	2 theta 40.26	2 theta 58.24
W-heating rod	19.25-30	19.181	99.63	unknown		56.7	32.7
Product Plansee Reutte	19.25-30	18.919	97.98	unknown		68.2	70.6
Sheet URSS (Russia)	19.25-30	18.085	93.68	unknown		173	147
W - Magnetron sputtering				Evapored from W-sheet-target		22.0	9.9
Product Sylvania Tungsten Bruntál Ltd, sintered +3 % Ni	18.650	15.081	80.86	291	245	65.1	49.2
Product Sylvania Tungsten Bruntál Ltd, sintered +1 % Ag	19.15	15.866	82.85	217	171	829	461
APT reduced in H-plasma Sintered + 1% Ni	19.1070	17.68	92.53	22.0	20.1	64.2	48.6
Na ₂ WO ₄ red. in H-plasma Sintered + 1 % Ag	19.15	17.831	93.11	48.6	--	52.1	31.9
W-spheroidized according [4]	19.25	18.778	97.54	291	245	165.9	149.0
BELT-sintered W/WC 90/10	18.95	18.053	95.26	22.0	20.1	81.4	54.6
BELT-sintered W/HfC 95/05	18.505	17.632	95.28	22.0	20.1	36.1	41.5

Conclusion

The relation between sintering activity of tungsten and size of its crystals, measured by XRD, was confirmed qualitatively. The experimental technique for the sinterability examination was not exactly the same for all samples. However in frames of very similar experimental conditions the proportion between high final density and small initial crystal size was proven at all variants. After sintering the recrystallization and grain coarsening of individual polycrystals took place. This tendency was observed at the sintering of W reduced at temperatures from 600°C to 1100°C.

Acknowledgment to VZ MSM 002162241 CZ and MSM 6046137302

References

- [1] C. Agte and J. Vacek, Tungsten and molybdenum, SNTL Praha 1954.
- [2] G. Hägg (1935) in H. Remy, Inorganic Chemistry II, SNTL Praha 1962, p.198
- [3] M. Eliáš, Z. Frgala, J. Janča, V. Brožek, J. Adv. Oxid. Tech., Vol. 7. 1. (2004) 91-97.
- [4] V. Brožek, V. Dufek, K. Neufuss, L. Šarman, Materials Week & Exhibition MATERIALICA, October 1-4. 2001 Munich, CD-G5-918

STUDY OF DIFFUSIVITY IN TERNARY SYSTEMS – DIFFUSION JOINTS OF Ni/Ni₃Al-Fe AND Ni/Ni₃Al-Ti

Jaromír Drápala¹, Petr Kubíček², Jana Sudrová¹

¹ Vysoká škola báňská – Technical University of Ostrava, Department of Non-ferrous metals, Refining and Recycling, 15, Av. 17. listopadu, 708 33 Ostrava – Poruba,

² Na čtvrti 14, 700 30 Ostrava-Hrabůvka, Czech Republic

Jaromir.Drapala@vsb.cz

Diffusion phenomena in multi-component metallic systems have been studied at diffusion joints Ni/Ni₃Al-Fe and Ni/Ni₃Al-Ti. Chemical composition of the found intermetallic compound corresponded to the phase γ' of the ternary system Ni-Al-Me. At first, specimens in the form of cylinders (diameter 10 mm) were joined by two technologies: electron beam welding and resistance butt welding. The specimens were placed in evacuated quartz ampoules and annealed at the temperature 1050 °C for the time 100 hours and then quenched into water. They were examined metallographically in the states before and after the annealing, their micro-hardness in the diffusion joint area was measured and the global (ICP-AES, SPECTRO MAX) chemical analysis was carried out and concentration profiles of individual components were explored by the X-ray (WDX, EDX) micro-analysis. The obtained concentration profiles were evaluated applying the modified Matano-Boltzmann method utilizing the concentration curves for which optimum types of regressions were found (polynomials of second to fourth grade). In addition, a transfer matrix method by L.R. Ram-Mohan and M.A.A. Dayananda [1] was applied, which enabled to determine interdiffusion flows and the correspondent interdiffusion coefficients of particular diffusion joints.

At first, the Matano plane position was determined from the found concentration profiles by means of the material balance and then dependencies of diffusion coefficients of all the components as functions of the distance from the interface $D(x)$ and of the concentration of elements $D(c)$. We found anomalous behaviour of diffusion joints in the system Ni/Ni₃Al-Fe, which was characterized by the „plateau“ creation in the area of the solid solution γ Ni adjacent to the phase boundary – Fig. 1. Furthermore, a slight decline of the iron level was found on the side of the intermetallic phase compared to the area γ Ni. This phenomenon is the subject of further study. The situation was entirely different in case of the Ti behaviour and both Ti and Al showed a positive concentration jump, whereas it was surprisingly established that the level of Ti and Al was nearly constant in the area of the intermetallic phase γ' – Fig. 2. Nevertheless, the interdiffusion coefficients of the specimens containing titanium were on the average by an order lower than the interdiffusion coefficients of the specimens containing iron.

Polynomial functions of individual concentration profiles were utilized for determinations of interdiffusion flows and interdiffusion coefficients applying the method [1]. We present the results in figs 3 and 4 as examples.

This work was supported by Ministry of Education, Youth and Sports of the Czech Republic in projects of the Grant Agency No. 106/06/1190 „Study of crystallization processes in multi-component alloys with the aim to determine regularities of

interaction of elements and structure formation“ and MSM No. 6198910013 „Processes of preparation and properties of highly pure and structural defined materials“.

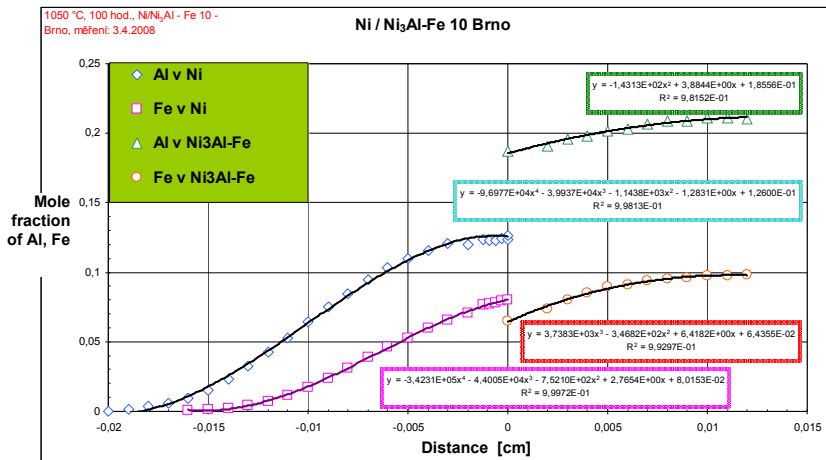


Fig. 1 Concentration profiles of Al, Fe in Ni₃AlFe/Ni diffusion joint after annealing 1050 °C/100 h.

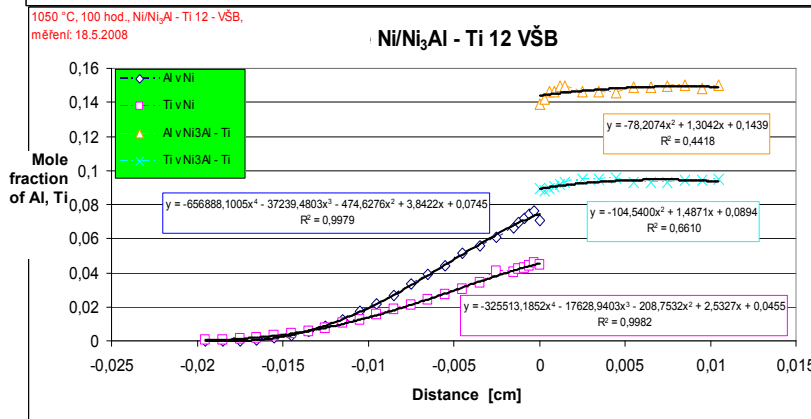


Fig. 2 Concentration profiles of Al, Ti in Ni₃AlTi/Ni diffusion joint after annealing 1050 °C/100 h.

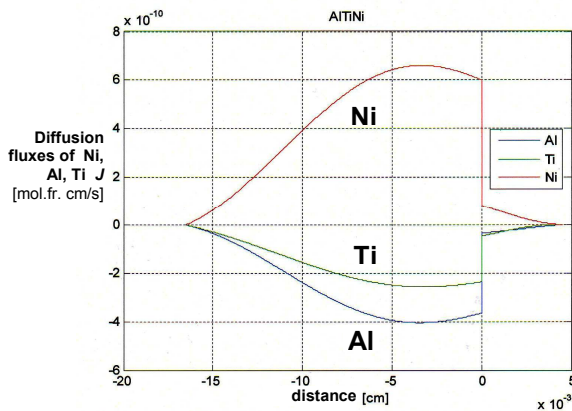


Fig. 3 Diffusion fluxes in Ni₃AlTi/Ni diffusion joint

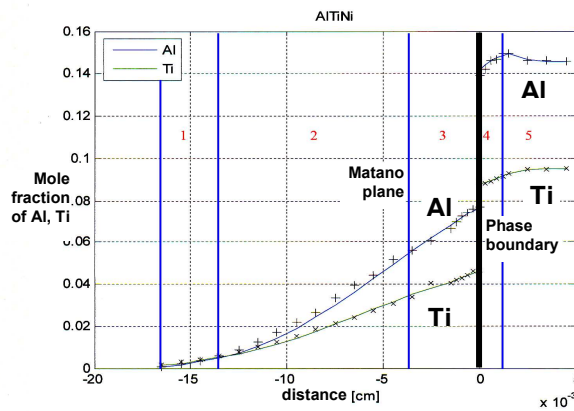


Fig. 4 Calculated concentration profiles of Ni₃AlTi/Ni by method [1].

References:

- [1] L.R. Ram-Mohan, M.A.A. Dayananda, Acta Materialia, Vol. 54 (2006) 2325.
- [2] J. Sudrová, Study of the segregation and diffusion effects in multicomponent systems Ni/Ni₃Al – Me, Thesis, VŠB – TU of Ostrava, Ostrava, (2008) 121 p.

LPE GROWTH OF III-V SEMICONDUCTORS FROM RARE-EARTH TREATED MELTS

Jan Grym, Olga Procházková, Jiří Zavadil, Karel Žďánský
 Institute of Photonics and Electronics AV CR, Chaberska 57, 182 51 Praha 8
 grym@ufe.cz

Substantial research activity has been carried out on rare-earth (RE) doped semiconductor materials for optoelectronics [1]. Achieving doping effects of REs during growth from the liquid phase has proven difficult in most III-V compounds; the high chemical reactivity and the low solid solubility restrain introduction of RE atoms into the crystal lattices [2]. On the contrary, the enhanced chemical affinity of REs towards most species of shallow impurities leads to the formation of insoluble aggregates in the melt. At suitable growth conditions, these aggregates are rejected by the growth front and are not incorporated into the grown layer: gettering of impurities is observed. Removal of deleterious impurities is essential in applications such as PIN photodiodes or nuclear particle detectors, where high electron and hole drift velocities are appreciated [3].

We demonstrate the gettering phenomenon on InP and InGaAsP epitaxial layers prepared from praseodymium treated melts (Fig. 1). Increasing the RE content in the melt,

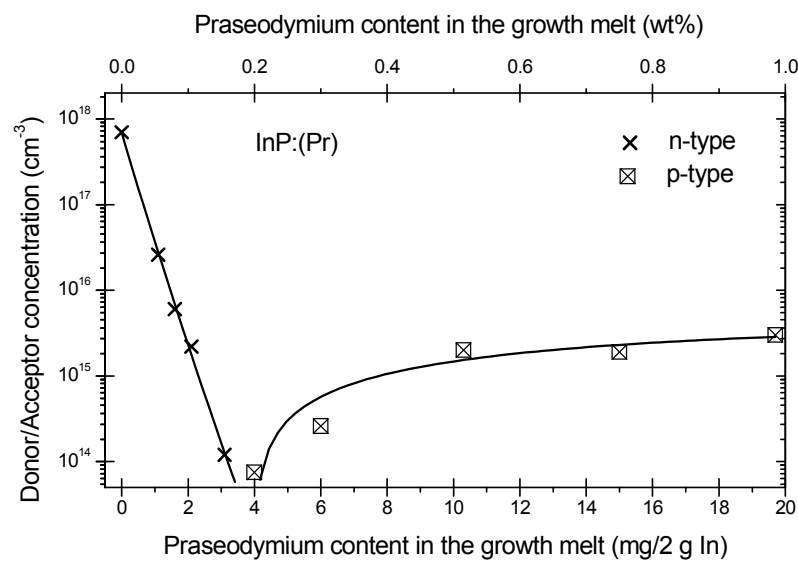


Fig. 1: Dependence of the donor/acceptor concentration on Pr content in the growth solution.

simultaneous gettering of shallow impurities occurs. Donor impurities are preferentially gettered due to their high affinity towards Si and group VI elements. Preferential gettering leads to the conductivity conversion from n- to p-type. Further increase of Pr admixture results in moderately elevated acceptor concentrations. This elevation is caused by either the incorporation of new impurities to the melt

with REs or increased p-type activity of amphoteric impurities. Admixtures of Pr (i) provoke conductivity conversion at relatively low concentration in the melt, (ii) do not influence the growth rate, and (iii) under appropriate growth conditions lead to lowered dislocation densities and good surface morphology.

Typical PL spectrum comparing layers grown with and without RE admixture is shown in Fig. 2. The observed radiative transitions in studied InP samples could be grouped into three categories: band-edge (BE) transitions at about 1.418 eV (875 nm), shallow impurity related transitions at 1.38 eV (900 nm), and deep-level transitions at

1.14 eV (1090 nm). The peak LO is the phonon replica of the shallow impurities related peak. The high energy band (BE) results from the decay of excitons. Fine structure of

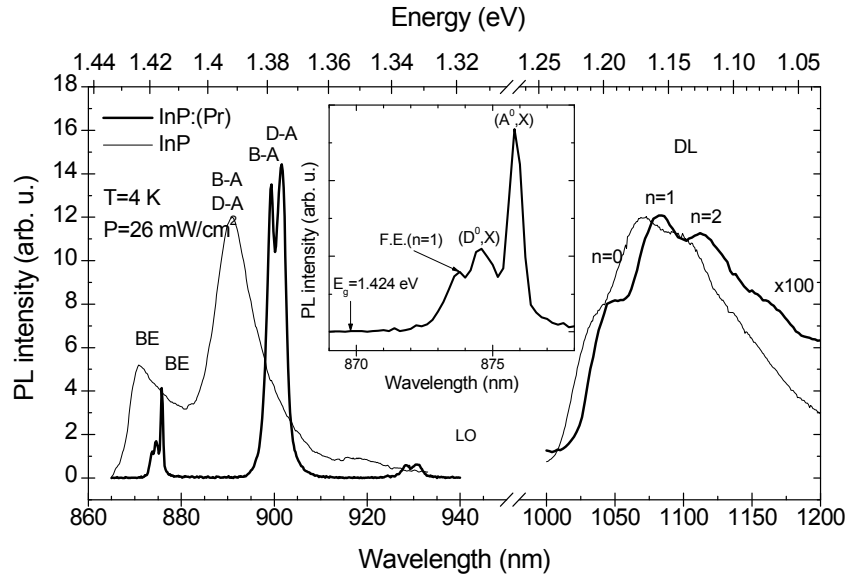


Fig. 2: PL spectra of conventionally grown InP layer and that prepared with optimized Pr addition

excitonic transitions is usually well resolved in the case of high purity samples. The shallow impurities related peak is an unresolved convolution of band-acceptor (B-A) and donor-acceptor pair (D-A) transitions in the case of zero admixtures, while separate peaks are well resolved at low excitation power on samples prepared with REs. The long-wavelength part is

usually dominated by Mn related band consisting of three partly resolved peaks at 1.184 eV ($n=0$), 1.145 eV ($n=1$) and 1.107 eV ($n=2$), which are interpreted as a zero phonon line, and one, and two phonon replicas, respectively (Fig. 2). This characteristic band, observed in majority of samples, whether rare-earth treated or not, is attributed to recombination of free or loosely bound electrons with holes bound to the Mn acceptor occupying an In site.

We prepared high purity InP layers of both n- and p-type conductivity with carrier densities diminished to the order of 10^{14} cm^{-3} . Fabrication of simple detector structures based on p-type InP layers with a Schottky barrier and p-n junction are currently under way. Schottky contacts with a large barrier height can be prepared solely on p-type InP [4]. InP epitaxial layers grown from suitable RE-treated melts show p-type conductivity without the need of intentional doping with shallow acceptors. The preliminary detection performance will be evaluated by means of a multi-channel analyzer on the basis of magnitude of pulses generated in detecting α -particles. The influence of the InGaAsP active region purification by Pr treatment on the performance of double-heterostructure LEDs in the near-infrared region (1200 nm) will be discussed.

The support of the Czech Science Foundation projects 102/08/P617 and 102/06/0153 is gratefully acknowledged.

- [1] A.J. Kenyon, Progress in Quantum Electronics 26 (2002) 225.
- [2] A. Kozanecki, R. Groetzschel, Journal of Applied Physics 68 (1990) 517.
- [3] E. Hokelek, G.Y. Robinson, Journal of Applied Physics 54/9 (1983) 5199.
- [4] O. Procházková, J. Grym, J. Zavadil, K. Žďánský, Journal of Crystal Growth 275/1-2 (2005) e959.

TiAl-Nb BASED ALLOY PREPARED BY MECHANICAL ALLOYING

J. Juřica, M. Losertová

VŠB-Technical University of Ostrava, faculty of Metallurgy and Material Engineering,
av. 17. listopad, 708 33 Ostrava, Czech Republic
jan.jurica.fmmi@vsb.cz

Intermetallic compounds based on the Ti-Al system offer combination of good oxidation resistance and suitable mechanical characteristics, especially high specific strength at higher temperatures than commercial Ti alloys [1].

Experimental alloy was prepared from Ti and Al powder and a Nb wire with diameter of 0.24 mm. Backfill containing 15.042 g Ti, 8.473 g Al and 6.4 g Nb was mechanically alloyed in ball planetary mill with steel container and five steel balls (BPR=18.3). The Ti-Al-Nb powder mixture was milled during 72 hours with rate of 150 rpm.

The particle size of powder alloy prepared was determined using the laser particle sizer ANALYSETTE 22 COMPACT, FRITSCH. The results of statistic distribution of particle sizes are summarized in the graph on the fig. 1.

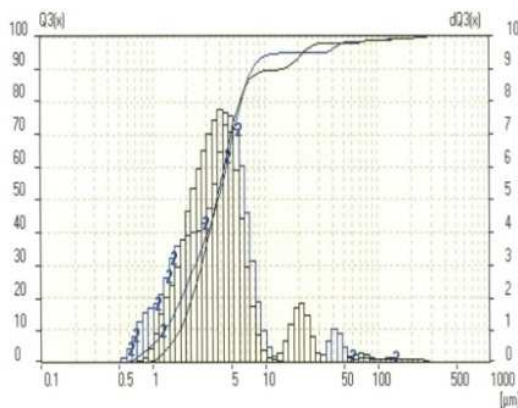


Fig. 1. Statistic distribution of particle size of TiAl-Nb based alloy for 2 measurements after 72 hours milling

The powder mixture was cold compacted under press of 4 MPa using glycerol binder. The compacted specimens were sintered in furnace at the temperature 1050 °C during 4 hours in flowing Ar (4N6) gas.

Microhardness measurement was carried out by Leco LM-100 instrument with load of 0.025 N. Microhardness impacts were performed across specimen diameter with the step of 1 mm. The values obtained from the measurement are shown in fig. 2.

Metallographic study was carried out on compacted and sintered specimens using stereomicroscope Olympus SZX 7 and metallographic microscope Olympus GX51 (fig. 3).

The aim of this work was to prepare TiAl-Nb based intermetallic alloy using mechanical alloying. The compacted and sintered alloy had the mean content of 42 weight % Ti, 18 weight % Al, 19 weight % Nb. In the microstructure, the (Nb, Ti)₂Al phase with 82 weight % Nb, 14 weight % Al and 4 weight % Ti was found (table 1). The great amount of oxygen was determined that was in relation with the large-scale oxidation of the feed powder material.

The Table 1 summarizes the results of phase and microstructure analysis performed by scanning electron microscope JEOL JSM-6490LV with EDS INCA X-ACT probe (fig. 4).

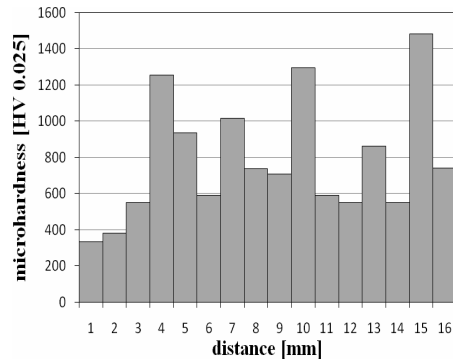


Fig. 2. Results of microhardness measurement of sintered TiAl-Nb specimen.

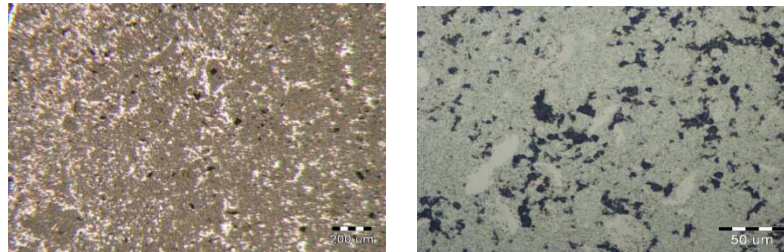


Fig. 3. Sintered TiAl-Nb specimen a) stereograph (80x), b) optical micrograph (500x).

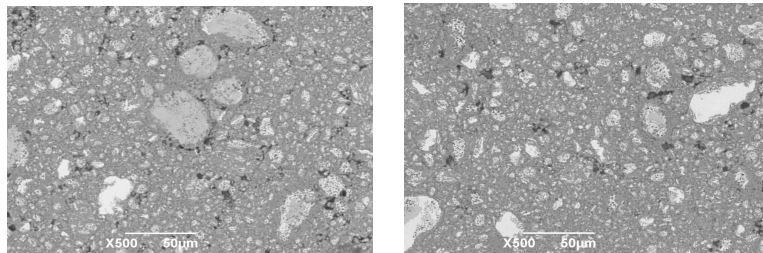


Fig. 4. Microstructure of compacted and sintered TiAl-Nb specimen (500x).

Table 1. Results of microanalysis measurement of TiAl-Nb specimen

Element Phase	Ti [weight %]	Al [weight %]	Nb [weight %]	O [weight %]
$(\text{Nb, Ti})_2\text{Al}$	3.694	14.010	82.296	-
Phase 1	42.583	18.624	18.891	19.901
Phase 2	42.351	18.994	20.778	17.626
Phase 3	43.296	20.238	19.588	16.789

The present work has been supported by the Ministry of Education of the Czech Republic under the project No. 6198910013.

[1] Loria, E.A., Intermetallics 9 (2001) 997–1001.

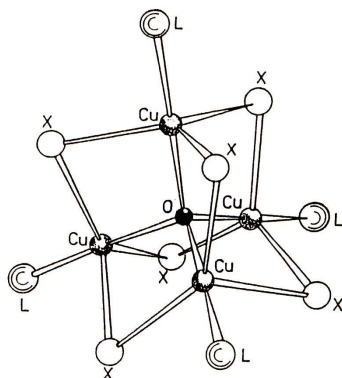
COMPOSITION, SYMMETRY AND STRUCTURE OF TETRANUCLEAR $\text{Cu}_4\text{OX}_6\text{L}_4$ COMPLEXES

M. Koman, G. Ondrejovič and A. Kotočová

Department of Inorganic Chemistry, Slovak Technical University, Radlinského 9, SK-812 37, Bratislava, Slovakia,

marian.koman@stuba.sk

A large number of tetranuclear copper(II) complexes $\text{Cu}_4\text{OX}_6\text{L}_4$ (where X = Br, Cl and L = monodentate O-, S-, N-, P- and Sb- donor atom ligands) have been prepared and structurally studied¹⁻⁴. In these complexes a central oxygen atom is tetrahedrally coordinated to four copper(II) atoms, the copper atoms are bridged in pairs by six halide atoms, and the ligands L complete trigonal bipyramidal coordination of the copper atoms (Fig. 1). In the ideal case, the structure can be described as an oxygen atom at the centre of both a tetrahedron of copper atoms, OCu_4 , and an octahedron of halide atoms, OX_6 .



The tetranuclear $\text{Cu}_4\text{OBr}_x\text{Cl}_{(6-x)}(\text{OPPh}_3)_4$ complexes (where $x = 0, 0.2, 0.5, 1.0, 1.0, 1.5, 2.0, 2.2, 2.5, 2.8, 3.2, 3.5, 4.0, 4.5, 5.0, 5.7, 5.8, 6$) were prepared and studied by IR spectra and powder diffraction measurements⁵. The dependence of the tetrahedral OCu_4 core vibration and the cubic lattice parameter on x for $\text{Cu}_4\text{OBr}_x\text{Cl}_{(6-x)}(\text{OPPh}_3)_4$ complexes indicates the $\text{Cu}_4\text{OBr}_x\text{Cl}_{(6-x)}$ core size with increasing number of large bromides, without observable change of symmetry.

Fig. 1. Structure of $\text{Cu}_4\text{OX}_6\text{L}_4$ complexes.

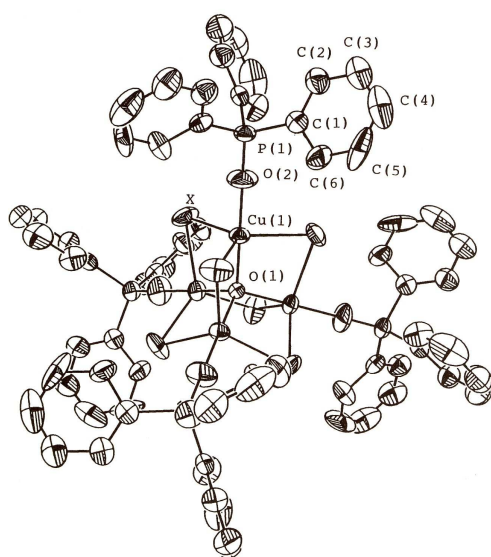


Fig. 2. Structure of $\text{Cu}_4\text{OBr}_3\text{Cl}_3(\text{OPPh}_3)_4$ complex.

Single-crystal structure determination for $\text{Cu}_4\text{OBr}_3\text{Cl}_3(\text{OPPh}_3)_4$ complex showed space group $Fd\bar{3}$ [$a_0 = 25.470(2)\text{\AA}$, $R = 0.0495$] and confirmed the structural type with a central oxygen atom being tetrahedrally coordinated to four copper(II) atoms and the copper atoms bridged in pairs by six halide atoms⁵. The bridging positions are occupied by atoms X = Br, Cl statistically in ratio 0.5 : 0.5 with interatomic Cu – X distances of $2.461(2)\text{\AA}$ (Fig. 2). The position and orientation of the $\text{Cu}_4\text{OBr}_3\text{Cl}_3(\text{OPPh}_3)_4$ molecule requires a linear arrangement of atoms O1, Cu1, O2, P1, because all of them are in special positions.

Identical crystal structure with same space group *Fd3* has the $\text{Cu}_4\text{OBr}_4\text{Cl}_2(\text{OPPh}_3)_4$ compound [$a_0 = 24.776(3)\text{\AA}$, $R = 0.067$]⁶.

Recently, new groups of tetranuclear complexes with monodentate nitrogen donor ligands of pyridine type have been prepared. The $\text{Cu}_4\text{OCl}_6(4\text{-Mepy})_4$ (4-Mepy – 4-methylpyridine) complex crystallizes in the triclinic crystallographic system [space group P-1, $R = 0.068$]. Independent part of the unit cell contains four symmetrically independent molecules of the same composition. The decrease of the symmetry is the cause of various manners of orientation of pyridine rings. This orientation is modified by the intramolecular coupling of the trigonal bipyramidal coordinations through bridging chlorides, by the distortion of trigonal bipyramidal coordination to tetragonal pyramidal geometry and through the in-plane and out-of plane pyridine ring tilting including the puckering of the pyridine rings and the tilting of corresponding methyl groups. Correlations involving bond lengths and bond angles in the molecular structure of the $\text{Cu}_4\text{OCl}_6(4\text{-Mepy})_4$ complex present in the unit cell showed that the donor-acceptor behaviour involving the π -back donation into the pyridine rings of the 4-Mepy ligands is most effectively stimulated by orientation of the pyridine rings closely to one of the three Cu—Cl bonds⁷.

The $\text{Cu}_4\text{OBr}_2\text{Cl}_4(4\text{-Mepy})_4$ complex crystallizes in the triclinic crystallographic system too [space group P-1, $R = 0.133$]. The unit cell contains eight symmetrically independent molecules with following compositions: four molecules of $\text{Cu}_4\text{OBr}_1\text{Cl}_5(4\text{-Mepy})_4$, two molecules of $\text{Cu}_4\text{OBr}_2\text{Cl}_4(4\text{-Mepy})_4$ and two molecules $\text{Cu}_4\text{OBr}_3\text{Cl}_3(4\text{-Mepy})_4$.

The change of the neutral ligands leads to decrease of symmetry in crystal structures of tetranuclear complexes with minimally disturbed molecular structures.

Financial support of the Slovak Ministry of Education (VEGA project 1/4454/07) is gratefully acknowledged.

- [1] H. T. Dieck and H. P. Brehm, *Chem. Ber.* 102 (1969) 3577.
- [2] D. Makáňová and G. Ondrejovič, *Polyhedron* 8 (1989) 2469.
- [3] D. Makáňová, I. Kováčik and G. Ondrejovič, *J. Prakt. Chem.* 333 (1991) 389.
- [4] D. S. Brown, T. G. Hopkins and A. H. Norbury, *Inorg. Nucl. Chem. Lett.* 9 (1973) 971.
- [5] V. Jorík, M. Koman, D. Makáňová, D. Mikloš, A. Broškovičová and G. Ondrejovič, *Polyhedron* 15 (1996) 3129.
- [6] M. Koman, unpublished results.
- [7] G. Ondrejovič, M. Koman and A. Kotočová, *Chem. Pap.*, submitted for publication.

STRUCTURE AND PROPERTIES OF WO₃-CONTAINING ZINC BOROPHOSPHATE GLASSES

L. Koudelka¹, J. Šubčík¹, P. Mošner¹, I. Gregora²

¹Department of General and Inorganic Chemistry, Faculty of Chemical Technology, University of Pardubice, 532 10 Pardubice,

²Institute of Physics, Academy of Sciences of the Czech Republic, Na Slovance 2, 18221 Praha

ladislav.koudelka@upce.cz

Tungsten-oxide based materials are known for their electrochromic and photochromic properties [1] resulting in a wide range of applications like smart windows, display devices or sensors. WO₃-based glasses reveal mostly dark blue colour, which is ascribed to the presence of part of tungsten atoms in a lower valence as W(V) [2]. Alkali phosphate glasses are able to incorporate large amounts of tungsten oxide [2]. The addition of WO₃ improves chemical durability of alkali phosphate based glasses against atmospheric moisture [3]. This contribution is devoted to the study of formulating of zinc borophosphate glasses with tungsten oxide WO₃ and the effect of WO₃ on its structure and properties.

Glasses of the compositional series (1-x)[0.5ZnO-0.1B₂O₃-0.4P₂O₅]-xWO₃ were prepared by the reaction of ZnO, WO₃, H₃BO₃ and H₃PO₄ by heating of the mixture up to 1200-1260°C with a subsequent cooling in air to the room temperature. Glasses were prepared within the concentration range of x = 0-0.5 WO₃. Homogeneous glasses were obtained within the concentration range x = 0-0.4 WO₃ and microcrystalline inclusions were observed in the glasses with 45 and 50 mol% WO₃. The obtained glasses were blue coloured which was caused by the presence of W⁵⁺ ions in the glasses which were identified by the electron spin resonance measurements.

It was observed that the density of the glass samples, increase with increasing WO₃ content within the range of 3.13-5.02 g/cm³, while the molar volume stays nearly unchanged. The dissolution rate of the studied glasses in distilled water, measured at the room temperature, changes within the range of 3.3x10⁻⁷ – 20.7x10⁻⁷ g.cm⁻².min⁻¹ with increasing WO₃ content

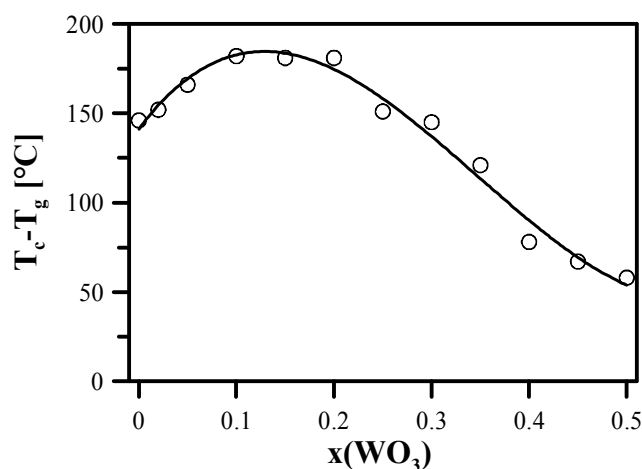


Fig 1. Thermal stability of the (1-x)[0.5ZnO-0.1B₂O₃-0.4P₂O₅]-xWO₃ glasses.

Thermal analysis showed that the glass transition temperature increases with increasing WO_3 content. All prepared glasses crystallize on heating and some of the glass samples crystallize in several steps. The crystallization temperature as well as thermal stability of the glasses, evaluated from the difference between temperature of the first crystallization (T_c) and the glass transition temperature (T_g), reveal a maximum at $x = 0.15-0.20$ (see Fig. 1). X-ray diffraction analysis of crystalline products, obtained by annealing the glassy samples above their crystallization temperature, revealed that crystalline products consist mostly of $\text{Zn}_2\text{P}_2\text{O}_7$ and BPO_4 in glasses with a low WO_3 content and with increasing WO_3 content various tungstate phases as $\text{W}_{18}\text{O}_{49}$, $\text{W}_{12}\text{PO}_{38.5}$, PW_8O_{26} were identified in crystallization products.

Raman spectra of the glasses reveal the incorporation of tungsten oxide into the structural network of the glasses and the depolymerization of phosphate chains in the glasses. Raman spectra reflect the presence of WO_x units in the structural network of the studied glasses by the presence of very strong vibrational bands in the spectral region of $800-1000\text{ cm}^{-1}$. In the Raman spectra with a low WO_3 content the band of 931 cm^{-1} , ascribed to the vibrations of terminal $\text{W}=\text{O}$ or $\text{W}-\text{O}^-$ bonds, whereas at the glasses with a high WO_3 content the band $810-830\text{ cm}^{-1}$, ascribed to $\text{W}-\text{O}-\text{W}$ vibrations dominates Raman spectra. Infrared spectra reflect these structural changes in a similar way.

^{31}P MAS NMR spectra reveal the depolymerization of phosphate network, whereas ^{11}B MAS NMR spectra show the prevailing presence of boron in BO_4 coordination and a small increase in the number of BO_3 units with increasing WO_3 content. Boron NMR spectra also reveal the transformation of $\text{B}(\text{OP})_4$ units into $\text{B}(\text{OP})_{4-x}(\text{OW})_x$ units with increasing WO_3 content in the studied glasses.

- [1] C G. Granqvist, Sol. Energy Mater. Sol. Cells, 60 (2000) 201.
- [2] F. Studer, H. Rih, B. Raveau., J. Non-Cryst. Solids 107 (1988) 101.
- [3] C. de Araujo W. Strojek, L. Zhang, H. Eckert, G. Poirier, S. J. L. Riberio, Y. Messaddeg, J. Mater. Chem. 16 (2006) 3277.

The authors are grateful for the financial support from the research project No. 0021627501 of the Ministry of Education of Czech Republic and to the Grant Agency of the Czech Republic (Grant No. 104/07/0315).

INFLUENCE OF INITIAL SUPERSATURATION ON NUCLEATION AND GROWTH IN CLOSED SYSTEMS

Z. Kožíšek, P. Demo, A. M. Sveshnikov, and P. Tichá

Institute of Physics, Academy of Sciences of the Czech Republic, Cukrovarnická 10,
162 53 Praha 6, Czech Republic
kozisek@fzu.cz

Nucleation is the first step in process of formation of a new phase from supersaturated or undercooled mother phase. Macroscopic new phase appears due to growth of supercritical nuclei. It is necessary to overcome some energy barrier (called nucleation barrier) to form critical nuclei. Undercritical nuclei have tendency to diminish, supercritical one grows to macroscopic size under appropriate conditions. Size of critical nuclei (typically tens of molecules) depends on conditions under which nucleation occurs (supersaturation, surface energy, temperature, etc.).

In standard nucleation theory [1-2] the unchanged conditions are supposed during phase transition. In that case the critical size of nuclei remains unchanged at phase transition and analytical solution of the stationary nucleation rate (i. e. the number of nuclei formed in unit volume per unit time) is well known. Critical nuclei are formed within the considered system after some time delay (or transient time). Time delay is given by nucleation kinetics, which depends on the system under consideration and condition of the phase transformation process (energy barrier of nucleation, transport of molecules to the phase interface, etc.). Time delay of nucleation can be from microseconds (vapor-liquid transition) up to days (glass forming systems).

Phase transition is much more complicated in closed systems. Due to formation of nuclei, part of molecules “is transferred” from the mother phase to a newly forming phase and as a consequence the conditions within system are changing with time. Supersaturation decreases with time, critical size increases and the stationary regime at high initial supersaturation is not reached (nucleation rate reaches some maximum and then decreases to zero). At low initial supersaturations the number of transformed molecules (from the mother phase to a new one) is relatively small and standard model of nucleation can be used. At high initial supersaturations depletion of the mother phase plays important role and kinetics of phase transformation is much more complicated.

We have considered formation of droplets by homogeneous nucleation from supersaturated ethanol vapor [3-5] at $T = 260$ K for initial supersaturations $S_i = 3, 4$ and 5 . As a new phase is developed, the initial supersaturation decreases. It has consequences to the size distribution of nuclei (see Fig. 1) and growth rates (see Fig. 2). It is seen that the maximum size of nuclei is not reached at the same time ($t = 6\mu s$) at the highest initial supersaturation $S_i = 5$ (as standard theory gives), but at $S_i \approx 4$.

At low initial supersaturation ($S_i = 3$) depletion effect is negligible and growth rate increases with time to its analytical limit at flat interface (dashed line in Fig. 2). At higher initial supersaturation ($S_i = 5$) growth rate goes to zero and the system comes to equilibrium. Decrease of growth rate with time at initial supersaturation $S_i = 4$ is relatively small. Growth rate of nuclei is slow down due to decrease of supersaturation. As a consequence the first macroscopic droplets does not appear at the highest initial supersaturations.

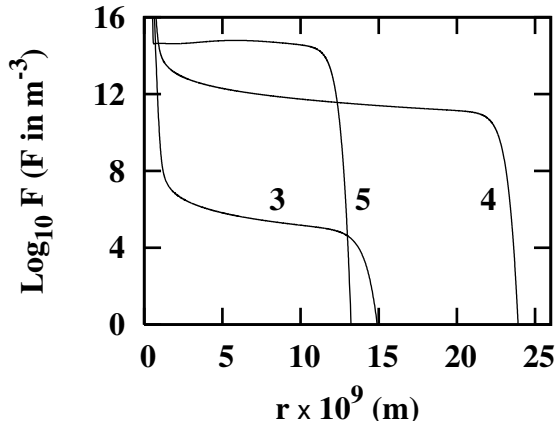


Fig. 1 Decimal logarithm of the number density of nuclei, F , as a function of their radius, r at time $t = 6 \mu\text{s}$ for initial supersaturations $S_i = 3, 4$ and 5 .

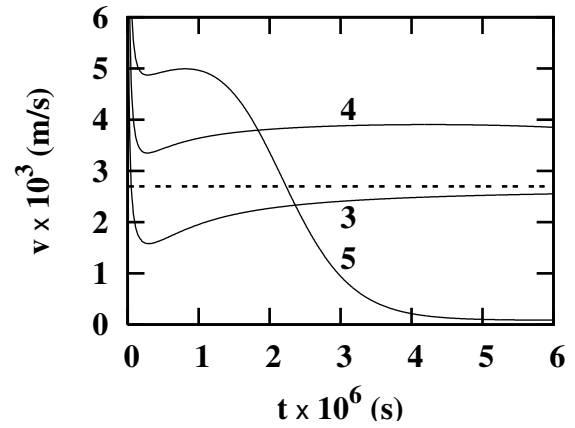


Fig. 2 Growth rate of nuclei, v , as a function of their radius, r as a function of time at initial supersaturation $S_i = 3, 4$ and 5 . Dashed line corresponds to the growth rate in the limit of flat surface at $S_i = 3$.

Resemble behavior of the phase transformation process can be expected in other systems with different time scales and supersaturations (undercoolings).

This work was supported by Grant No. IAA100100806 of the Grant Agency of the Academy of Sciences of the Czech Republic.

- [1] F. F. Abraham, *Homogeneous nucleation theory* (Academic Press New York, 1974).
- [2] D. Kashchiev, *Nucleation: Basic Theory with Applications* (Butterworth-Heinemann, Oxford, 2000).
- [3] Z. Kožíšek and P. Demo, *J. Chem. Phys.* 123 (2005) 144502.
- [4] Z. Kožíšek, P. Demo, and A.M. Sveshnikov, *J. Chem. Phys.* 125 (2006) 114504.
- [5] Z. Kožíšek, P. Demo, *J. Chem. Phys.* 126 (2007) 184510.

THE DETERMINATION OF THE BAR SHAPE CERAMIC MATERIAL YOUNG'S ELASTICITY MODULUS BY MEANS OF THE BEND DEFORMATION

J. Krajčovič and I. Jančuška

Faculty of Materials Science and Technology, Institute of Materials, Dept. of Physics,
Slovak Republic, Paulinska 16, 917 24 Trnava

jozef_krajcovic@stuba.sk

The optical methods are used for the some mechanical parameters of the solid state materials. For example, we can determine the Young's elasticity modulus from the girder bend by means of two-exposure laser holography interferometry method. We obtained interferogram by means of this method. Interferogram contains the system of the light and dark fringes and we determine from its the bend in the point of deformation force activity. Researched object was eutectic composite $\text{Al}_2\text{O}_3 - (\text{Y}_2\text{O}_3)$ ZrO_2 of the parallelepiped shape. This paper contains the used method description, the measured and calculated values of the researched eutectic composite Young's elasticity modulus.

STUDY OF GROWTH OF LEAD HALIDE SINGLE CRYSTALS FROM THE MELT

R. Král and A. Cihlář

Institute of Physics AS CR v. v. i., Cukrovarnická 10, 162 00 Praha 6, Czech Republic
kralr@fzu.cz

Recently there has been growing pressure on the knowledge of influence of temperature field on the shape and position of the crystal/melt interface during the growth of halide single crystals from the melt. This can be obtained by recording the interface when pulling out the ampoule from the furnace during the growth by the vertical Bridgman method. Another way is a creation of induced striations by changing the growth conditions during the crystal growth. This contribution will concentrate on the study of the shape and the position of phase interface by means of induced striations.

Induced striations are closely connected to the admixture concentration at the phase interface. If we have a binary system A – B, where A is a major component and B is an admixture, and if the distribution coefficient k_0 of this admixture is $k_0 < 1$ (Fig. 1a), then the concentration profile in the melt exponentially decreases with distance x from the interface (Fig. 1b). The growing phase always rejects this admixture that lowers the melting point of the liquid [1]. With increasing distance x from the interface to the melt an exponential increment of the equilibrium temperature dT_L/dx is generated, each point of this “isolidus” line T_L strictly defines equilibrium temperature in correspondence to the A – B phase diagram (Fig. 1c). In the melt a linear temperature gradient $G_L = T_A/dx$ is generated, set by temperature profile of the furnace and by crystallization heat removal. This gradient causes that the real temperature can be at the interface lower than the isolidus temperature T_L . This leads to a creation of a supercooling in the melt at the interface. This supercooling is called a constitutional supercooling and the area where it occurs is defined by temperatures T_L and T_A . This area is crosshatched as it is seen in Fig. 1c [2].

A formation of the constitutional supercooling is not required and must be avoided during the growth by an optimization of growth conditions. The supercooled melt can crystallize under the formation of a thin crystalline layer at the interface (striation) that differs from the crystal by the quality and the concentration of the admixture. Striations copy the shape of the interface and so they can be used for study of the dependence of the interface shape and position on the temperature field in the furnace and the pulling rate. However, for this purpose, striations must be artificially generated and visualized [3,4].

In our study striations were induced during the simulated growth of lead chloride (PbCl_2) doped with silver chloride (AgCl) by the vertical Bridgman method. During the growth, the ampoule was pulled out from the furnace to dramatically change growth conditions to achieve the creation of striations. However, this temperature shock caused that the grown crystal cracked and striations could not be observed. Therefore, striations were generated during the growth by lowering the ampoule by 1 mm in the temperature gradient of the furnace. The lowering was performed several times during the experiment to create more striations. Experiments were also performed under different pulling rates and temperature fields in the furnace.

A thin slice was cut from the crystal and polished. The slice was observed under an optical microscope to determine the shape and position of striations. There are two light striations in PbCl_2 single crystal shown in Fig. 2, the first was formed by the change of growth conditions during the ampoule lowering and the other after returning to the stable growth conditions.

This work confirmed that striations can be induced by presented technique and showed that they can give information about the shape and position of the interface crystal/melt.

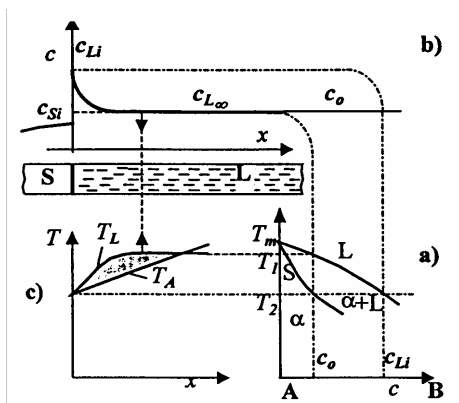


Fig. 1: A – B phase diagram (a), concentration profile of B at the phase interface (b), the temperature course of real temperature T_A and isolidus T_L .



Fig. 2: Induced striation in PbCl_2 single crystal doped with AgCl . Due to insufficient contrast, striations were stressed.

This work was supported from the Grant Agency of the Academy of Sciences of the Czech Republic (Grant No. IAA200100626).

- [1] K. A. Jackson, Kinetic Processes, Wiley-VCH Verlag, Weinheim, 2004, p. 143.
- [2] L. Kuchař, J. Drápala, Segregační jevy při krystalizaci a jejich vliv na strukturní charakteristiky krystalů, Sborník Školy růstu krystalů 2002, September 9-10, 2002, Ostravice, p. 12 – 20.
- [3] K. Nitsch, A. Cihlář, and M. Rodová, Melt supercooling and growth of lead chloride single crystals, Proceedings of the 13th Joint seminar Development of materials science in research and education, September 13-19, 2003, Ráčkova dolina, Slovakia, p.49-50.
- [4] K. Nitsch, M. Rodová, and W. Wilke, Interface shape and crystallisation heat during Bridgman growth of lead bromide single crystals, DGKK - Jahrestagung March 20-22, 2002, Idar-Oberstein, P4.

HEAT CAPACITY, ENTHALPY AND ENTROPY OF Ca(Sr)-Nb-O MIXED OXIDES

J. Leitner¹, K. Růžička², D. Sedmidubský³, P. Svoboda⁴

¹ Department of Solid State Engineering, ² Department of Physical Chemistry,

³ Department of Inorganic Chemistry, Institute of Chemical Technology Prague, Technická 5, 166 28 Praha 6

⁴ Department of Condensed Matter Physics, Faculty of Mathematics and Physics, Charles University, Ke Karlovu 5, 120 00 Praha 2

jindrich.leitner@vscht.cz

Mixed oxides in the system CaO-SrO-Bi₂O₃-Nb₂O₅-Ta₂O₅ possess a lot of extraordinary electric, magnetic and optical properties for which they are used in fabrication of various electronic components. For example Sr₂(Nb,Ta)₂O₇ and (Ca,Sr)Bi₂(Nb,Ta)₂O₉ is used for ferroelectric memories, Bi(Nb,Ta)O₄ and CaNb₂O₆ for microwave dielectric resonators and Ca₂Nb₂O₇ as non-linear optical materials and host for rare-earth ions in solid-state lasers. To assess the thermodynamic stability and reactivity of these oxides under various conditions during their preparation, processing and operation, a complete set of consistent thermodynamic data including heat capacity, entropy and enthalpy or Gibbs energy of formation is necessary.

In a systematic study of thermochemical properties of complex oxides in the Bi₂O₃-CaO-SrO-Nb₂O₅-Ta₂O₅ system, we measured heat capacities and enthalpy increments of Bi₂Ca₂O₅, Bi₂CaO₄, Bi₆Ca₄O₁₃, Bi₁₄Ca₅O₂₆, BiNbO₄, BiTaO₄, BiNb₅O₁₄, SrBi₂Nb₂O₉, SrBi₂Ta₂O₉, SrNb₂O₆, Sr₂Nb₂O₇ and Ca₂Nb₂O₇[1-5]. In this contribution our recent results on CaNb₂O₆, Sr₂Nb₁₀O₂₇ and Sr₅Nb₄O₁₅ are presented together with some generalization of data for calcium and strontium niobates.

The samples were prepared by conventional solid state reactions from high purity precursors CaCO₃ or SrCO₃ and Nb₂O₅. Phase-purity of the samples was checked by XRD at room temperature with an X'Pert PRO θ - θ powder diffractometer. The PPMS equipment (Quantum Design) was used for the heat capacity measurements in the low-temperature region (2–300 K). The measurements were performed by the relaxation method with fully automatic data processing using the two-tau model. A Micro DSC calorimeter (Setaram) in the incremental temperature scanning mode with a number of 5–10 K steps was used for the heat capacity determination in the temperature range of 260–350 K. Enthalpy increment determinations (673–1473 K) were carried out by drop method using high temperature calorimeter, Multi HTC 96 (Setaram).

The fit of the low-temperature heat capacity data consists of two steps. Assuming the validity of the phenomenological formula $C_{p,m} = \beta T^3 + \gamma_{el} T$ at $T \rightarrow 0$ where β is proportional to the Debye temperature θ_D and γ_{el} is the Sommerfeld coefficient, we plot the $C_{p,m}/T$ vs T^2 dependence for $T < 10$ K to estimate the γ_{el} value and the first approximation of θ_D . In the second step of the fit, both sets of the $C_{p,m}$ data (relaxation time + DSC, 2–350 K) were considered. Analysis of the phonon heat capacity was performed as an additive combination of Debye and Einstein models. Both models include corrections for anharmonicity and volume expansion, which are responsible for a small, but not negligible, additive term at higher temperatures and which accounts for the discrepancy between isobaric and isochoric heat capacity. The correction term was

considered in the form $1/(1 - \alpha T)$. The acoustic part of the phonon heat capacity is then described using the Debye model in the form

$$C_{\text{phD}} = \frac{9R}{1 - \alpha_D T} \left(\frac{T}{\Theta_D} \right)^3 \int_0^{x_D} \frac{x^4 \exp(x)}{(\exp(x) - 1)^2} dx, \quad x_D = \frac{\Theta_D}{T} \quad (1)$$

The optical branches, which are empirically grouped into a set of multiple degenerate branches with the same parameters, are described by the Einstein model

$$C_{\text{phEi}} = \frac{R}{1 - \alpha_{Ei} T} \cdot x_{Ei}^2 \frac{\exp x_{Ei}}{(\exp x_{Ei} - 1)^2}, \quad x_{Ei} = \frac{\Theta_{Ei}}{T} \quad (2)$$

The phonon heat capacity then reads

$$C_{\text{ph}} = C_{\text{phD}} + \sum_{i=1}^{3n-3} C_{\text{phEi}} \quad (3)$$

All adjustable parameters (θ_D , α_D , θ_E , α_E) were obtained by a full non-linear fit using the standard simplex routine.

Temperature dependence of heat capacity above room temperature was considered in the simple form

$$C_{\text{pm}} = A + B \cdot T + C \cdot T^{-2} \quad (4)$$

For the assessment of the parameters A , B and C , the heat capacity data from DSC and the enthalpy increment data from drop calorimetry were treated simultaneously. Different weights were assigned to individual points in order to both types of experimental data thus gain comparable significance during the regression analysis.

Our results based on the experimental data were compared with an empirical prediction according to the Neumann-Kopp rule (NKR). While the NKR assumes that the difference between heat capacities of mixed oxide and an appropriate linear combination of heat capacities of the constituent binary ones, $\Delta_{\text{ox}}C_p$, is zero, experimental data give non-zero values of $\Delta_{\text{ox}}C_p$, which are increasing with increasing temperature. This systematic trend is analyzed and the influence for equilibrium calculations at high temperatures is discussed.

This work was supported by the Czech Science Foundation (grant N° 104/07/1209) and Ministry of Education of the Czech Republic (research projects N° MSM6046137302, N° MSM6046137307 and N° MSM0021620834).

- [1] P. Abrman, D. Sedmidubský, A. Strejc, P. Voňka and J. Leitner, *Thermochim. Acta*, 381 (2002) 1.
- [2] M. Hampl, A. Strejc, D. Sedmidubský, K. Růžička, J. Hejtmánek and J. Leitner, *J. Solid State Chem.*, 179 (2006) 77.
- [3] M. Hampl, J. Leitner, K. Růžička, M. Straka and P. Svoboda, *J. Therm. Anal. Cal.*, 87 (2007) 553.
- [4] J. Leitner, M. Hampl, K. Růžička, D. Sedmidubský, P. Svoboda and J. Vejpravová, *Thermochim. Acta*, 450 (2006) 105.
- [5] J. Leitner, M. Hampl, K. Růžička, M. Straka, D. Sedmidubský and P. Svoboda, *J. Therm. Anal. Cal.*, 91 (2008) 985.

FIELD STIMULATED CARBON BLACK AGGLOMERATION IN POLYSTYRENE MATRIX

J. Lipták, L. Turczynová

Faculty of Electrical Engineering, Czech Technical University of Prague, 166 27 Prague,
Czech Republic

Introduction:

The polymer composite materials with inorganic compound combine the properties of polymer matrix and filler. When the filler is electrically conductive, a micro-electronic and nano-applications are reasonable. The composites of conductive polymers with fullerenes are intensively studied for solar cells applications¹. In all applications the formation and final structure of the CB conductive network play the major role. The complicated structure of CB particles and agglomerates provide a wide scale of structural varieties of CB in the polymer. There are many parameters influencing the structure of the CB network as their chemical composition and technology of fabrication. When the concentration of the filler in the composite reaches the percolation value the conductive network is formed. Dependences of conductivity on CB concentration show the sharp rise² (percolation threshold). Also, the network in the bulk increases the viscosity³. The value of the percolation concentration depends on the materials used (polymer², kind of CB⁴) and sample preparation technique (the speed and time of dispersion, , temperature, concentration of added salt, ultrasound acting⁵, intensity of applied electric field⁶). In time-conductivity dependences at constant CB content the percolation can be detected by sharp increase of conductivity in the “percolation time”⁷. This work deals with optical observation of CB agglomerate structures in applying electric field during the sample preparation. In addition, electrical and dielectric measurements were carried out.

Experimental:

Sample preparation: Dry CB was soaked in the toluene solvent for a few days. Secondly, the CB was mixed with the solution of 5 g of polystyrene in toluene and dispersed and pulverized by IKA rotational homogenizer at speed 20000 rpm for the 2 minutes. After that, the ultrasonic homogenizer Sonopuls UW 3200 (Bandelin) was used with the power 40 W for the time 3 x 1 minutes. The series of liquid precursors with CB concentration from 0,5 to 3 w% were prepared. The other precursor series of the same CB contents were prepared from “CB water” which is intermediate forming during the CB production. Both CB and CB water produced by Chemopetrol Group j. s. c. (Czech Republic) and PS produced by Kaučuk j. s. c. (Czech Republic) were used. Toluene was p.a. purity.

Layers preparation and electrical measurements: The composite layers were prepared on the printed circuit cards after toluene evaporation from the coated mixture up to the constant weight. The copper printing on the card was in the form of two mutually dipped racks. The width of the layer between copper electrodes was $d=1$ mm and the total length was $l=1800$ mm. The thickness of the layer was 30-40 μm . The second kind of the samples was prepared by coating into the Petri dishes providing the layers of the thickness approx. from 0,05 to 0,1 mm. Immediately after coating, the

point electrodes were put onto the layer with the voltage from 50 to 300 V. The line electrodes in the layers were also used. The impedance analysis in the frequency region 100 Hz to 1 MHz was carried out with the PM 6306 RLC meter FLUKE at 1 V measurement voltage. From impedance-phase $Z-\varphi$ measurements at the angular frequency $\omega = 2\pi f$ the conductance G and the capacity C were calculated in the parallel $C-G$ combination and the new quantities were defined according equations:

$$C = \frac{-\sin \varphi}{Z\omega}, \quad G = \frac{\cos \varphi}{Z\omega}, \quad e1 = \frac{Cd}{\varepsilon_0 l}, \quad e2 = \frac{Gd}{\varepsilon_0 l \omega}, \quad tg = \frac{e2}{e1},$$

where $e1(m)$ and $e2(m)$ are similar to real and imaginary component of complex permittivity respectively, and tg can be interpreted as loss factor.

Results and discussion:

In static electric field the CB particles form the continual chains (Fig.1) according the shape of the field, time of toluene evaporation, viscosity of polystyrene solution and CB concentration. The alternating field at the same conditions provides more sharp results. For the CB chain formation the CB particles in perpendicular direction are used too, therefore the chain surroundings are transparent. For line electrode arrangements (quasi homogeneous field) the linear chains were observed. The CB chain formations can be stimulated by increasing of the electric field and the process can be registered in situ. On the other hand, for the samples with the higher content of CB the breakdown and high heat production (and sample distortion) were observed. The frequency dependencies of $e1$, $e2$ and tg support our interpretation⁸ of the phenomena by the space charge polarization in CB agglomerates and chains.

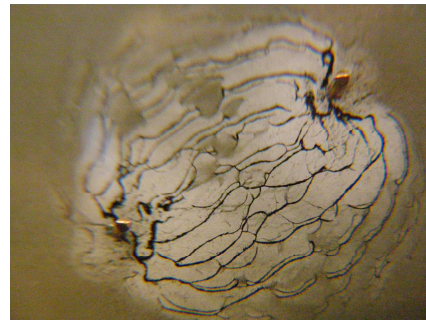


Fig.1: CB chains in the layer of thickness 0,08 mm with 1% CB in the field of 260 V.

Conclusions:

The CB chain formations in the PS-CB composite layers in electric field were observed. The effect of CB concentration, PS solution dilution, temperature of the mixture, electric field intensity and electrodes shape were studied.

There were observed no remarkable differences between the chain structures of the samples from CB or CB water.

- [1] Bjorklund, G.S., Baer, T.M.: Photonics Spectra (2007) 70.
- [2] Miyasaka, K. et al: J. Mater. Sci. 17 (1982) 1610.
- [3] Lakdawala, K., Salovey, R.: Polymer Engineering and Science, 27 (1987) 1043.
- [4] Ezquerro, T.A. et al: J. Mater. Sci. Lett. 5 (1986) 1065.
- [5] Lipták, J., Pilarčíková, I., Bouda, V.: The 11th joint seminar DMSRE 9.-13.9. 2001 Kežmarské Žľaby
- [6] Prasse, T. et al: Appl. Phys. Lett., 72 (1998) 290-3.
- [7] Schueler, R. et al: J. Appl. Polym. Sci., 63 (1997) 1741.
- [8] Lipták, J.: The 17th joint seminar DMSRE, 10.-14.9. 2007 Tatranská Štrba.

BOND AND GRIND-BACK SILICON-ON-INSULATOR

M. Lorenc, J. Šik, M. Pospíšil

ON Semiconductor Czech Republic, 1. máje 2230, 756 61 Rožnov pod Radhoštěm

michal.lorenc@onsemi.com

Silicon-On-Insulator (SOI) replaces traditional bulk silicon [1] wafers used for many semiconductor applications with an ‘engineered’ substrate consisting of three layers:

- A thin, top layer of monocrystalline silicon upon which active circuits are formed (called: active or device layer).
- A fairly thin middle layer of insulating silicon dioxide (called: buried oxide or BOX).
- Substrate (thick bottom layer of bulk silicon), which essentially provides a mechanical support for the two layers above (handle wafer).

SOI technology offers a set of benefits to the traditional semiconductor device process. With correct optimization, specific applications can benefit from device speed improvement, significant reduction in power consumption and from device area reduction. On the other hand SOI structure loss the gettering capability for heavy metals and also heat removal from device region is significantly reduced. Thick SOI is also widely used also for MEMC an MOEMS applications.

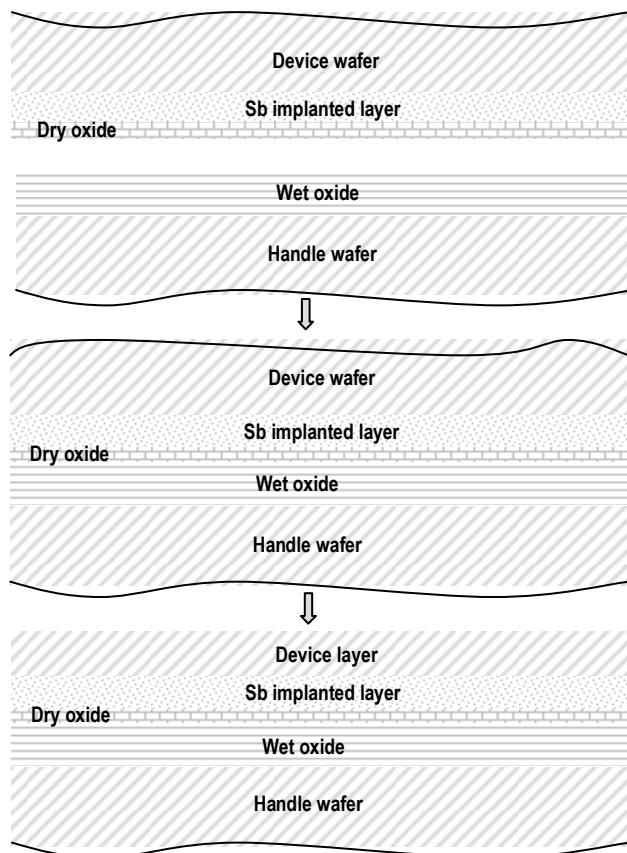


Fig. 1 The scheme of bonding procedure for studied SOI structure.

- A** A) Polished device silicon wafer slightly doped by phosphorus is implanted by antimony (buried layer) and covered by thin layer of silicon oxide. Polished side of slightly boron doped handle wafer is oxidized - silicon oxide layer (BOX) is grown.
- B** B) Both device and handle wafers are RCA cleaned and their surfaces are “activated” by plasma. Wafers are direct - bonded and annealed to strengthen the bonding.
- C** C) Finalization of SOI structure by thinning of device wafer with mechanical grinding and chemical-mechanical polishing.

There are several techniques for SOI manufacturing [2]: bond and grind back or bond and etch-back SOI (BESOI), SMART CUT[®] (the hydrogen exfoliation method of defining an active film), ELTRAN[®] (epitaxial layer transfer, employs selective etching of porous Si as well as water jet splitting), SIMOX (separation by implantation of oxygen below the surface).

In this paper we will focus on SOI with thick device layer (THK ~ 10 μm) manufactured by direct bonding and grinding back according the scheme shown in Fig. 1. We manufactured both device and handle wafer with excellent geometrical parameters. Total thickness variation (TTV) of 150 mm wafers is ~ 0.6 μm , wafers site flatness (STIR) ~ 0.2 μm for site 15x15 μm^2 . Wafers bonding required excellent nanotopography of bonded surface. AFM measurements confirms RMS and Ra values 0.1 nm on the area 2x2 μm^2 for (100) surface. We reached these excellent parameters via single wafer grinding by diamond wheel and single wafer polishing. We used thermal oxidation of handle wafer for BOX layer growth with THK ~ 1 μm . Tested the alternative of High Pressure Oxidation (HiPOx) shows typically twice worse BOX THK variation and surface nanoroughness. For analog bipolar application we implanted antimony to device wafer and re-diffused heavily doped Sb buried layer in substrate slightly doped by phosphorus. Although developed quality of device and handle wafers is fully suitable for spontaneous bonding by SÜSS bonder [3] we added plasma activation of bonded surfaces to reduce hydro-carbons on the surface. With nanopreparation module we evaluated O₂ surface plasma activation as optimal compared to N₂ or no plasma activation. Measured interface energy (bonding strength) after bonding at room temperature was 1.2 J/m² (for O₂ activation) compared to 0.2 J/m² (for N₂ activation) and 0.3 J/m² (no activation). Van der Waals bond between atoms of device and handle wafers surfaces was strengthened to covalent bond by 1050°C annealing. Final thinning of device wafer was done with single wafer grinder and polisher.

SOI structure was characterized by FTIR reflectance, IR camera, Spreading-Resistance-Profiling (SRP) and also by contact and contactless THK measurements. Our measurements fully confirm THK of each layer in the manufactured SOI structure. Also the profile of electrical resistivity (dopant concentration) corresponds with our simulations. Developed structure is intended for analog bipolar applications [4].

We acknowledge to Markus Gabriel and his team (SÜSS MicroTec) for their assistance with wafer bonding and to Josef Humlíček (Masaryk University Brno) and his team for support of SOI characterization (AFM, FTIR reflectance and IR imaging).

- [1] J. Wasselin, SOI to Replace Bulk Silicon, www.euroasiasemiconductor.com, October 2007, p. 84.
- [2] Silicon wafer bonding technology for VLSI and MEMS applications, ed. by S. S. Iyer, A. J. Auberton-Hervé, INSPEC, The Institution of Electrical Engineers, London 2002.
- [3] www.suss.com
- [4] R. Bashir, IEEE transactions on electron devices, 48 (11) 2001, p. 2525.

PREPARATION OF TiNb BASED ALLOY BY ELECTRON BEAM MELTING

M. Losertová, J. Veselý, J. Juřica, J. Drápala

VŠB–Technical University of Ostrava, Faculty of Metallurgy and Material Engineering,
15 av.17.listopadu, 708 33 Ostrava, Czech Republic

mlosertova@vsb.cz

Titanium based alloys are attractive for many biocompatible applications. Shape memory alloys TiNi have been widely used as specific implant materials as orthodontic archwire and orthopedic implant due to its unique properties. To solve the problems with toxicity of some additional elements, such as V, Al, Ni, new Ti-based alloys with biocompatible elements, such as Nb, Zr, Ta, Sn, have been developed. Recently, β -titanium alloys, Ti–Nb, Ti–Ta and Ti–Zr based alloy systems have been studied and found to display both lower elastic module and higher tensile strengths that are preferable for biocompatible metals and alloys.

In this work, the rod of TiNb alloy of diameter of 10 mm and of length of 300 mm was prepared by means of vacuum electron beam melting of Ti rod with wrapped rolled Nb ribbon. The sliced specimens underwent the solution heat treatment at 1173 K for 1 hour in flowing Ar gas and then were cooled into the water. The precipitation hardening was realised at different temperatures: 473, 673 and 873 K for 1 hour in flowing Ar and then was followed by water cooling.

The microstructure characteristics were investigated before and after heat treatment by means of light and scanning electron microscopes and the microhardness measurements with load of 25 g (Table 1).

Table 1. The average values of HV microhardness measurements for different heat treatment of TiNb specimens

heat treatment	as cast	473 K	673 K	873 K
microhardness	273±15.6	244±8.1	292±25.2	271±27.6

The Ti and Nb contents were determined using scanning electron microscope JEOL JSM-6490LV equipped with EDS INCA X-ACT probe. The mean values of microanalysis performed on two as cast specimens are summarised in Table 2.

Table 2. The average values of microanalysis performed on two as cast specimens

specimen	Ti		Nb	
	weight %	atomic %	weight %	atomic %
1	60.27	74.626	39.73	25.373
2	58.415	73.146	41.585	26.853

The results obtained from the microhardness measurement are analogous to that for Ti-25 at.% Nb published in [1]. The microhardness values showed obvious relation with heat treatment and aging. The specimens in the state as cast and aged at 873 K showed

similar microhardness (273 HV and 271 HV, respectively, in Table 1) related with α phase precipitation. The highest microhardness value of 292 HV for aging at 673 K is due of α and ω phases precipitation as it was proved in [1]. Conversely, aging at 473 K caused the decrease of the microhardness to 244 HV.

The X-ray analysis proved that TiNb rod was prepared as single crystal. Also, no grain boundaries were observed in the specimens. Single crystal growing of intermetallic alloys is difficult, so the preparation of TiNb alloy in single crystal state could be considered as extraordinary achievement that for the present, we could not explain using physical or metallurgical theories.

The phase analysis of prepared TiNb alloy was realised in austenitic state, martensite phase was not observed. Generally, the properties of TiNb alloys are strongly affected by content and fraction of α , β and ω phases but the metallographic observation in the present work was limited by microscopy resolution, so next analysis by TEM of aged specimens would be carried out because of very low size of ω phase particles. In following research, resistometric measurements, mechanical property and pseudoelasticity tests completed with complex phase analysis using TEM and X-ray would be performed.

The present work has been supported by Ministry of Education of the Czech Republic under the project No. 6198910013.

[1] Y. Mantani, M. Tajima, Phase transformation of quenched a martensite by aging in Ti - Nb alloys, *Mat. Sci. and Engineering A* 438 - 440 (2006) 315-319.

PREPARATION OF A NANOPARTICULAR SUSPENSION IN THE NEW WATER JET MILL (WJM) DEVICE USING CAVITATION DISINTEGRATION

J. Luňáček¹, R. Dvorský¹, A. Slíva²

¹Department of Physics, ²Laboratory of Bulk Materials, VŠB - Technical University of Ostrava, 17. listopadu 15, 708 33 Ostrava - Poruba, Czech Republic
jiri.lunacek@vsb.cz

In this work, we present a physical analysis of the preparation of submicron (nanoparticulate) suspension by cavitation disintegration. The first experimental results obtained by “top down” method in a new device called “Water Jet Mill” – WJM are presented too. This device (Fig.1) was developed at the Department of Physics, VŠB – Technical University of Ostrava. Principle of the WJM is based on the interaction of particles in liquid suspension with the cavitating water-jet. WJM uses three periodically repeated disintegration effects.

1) Direct mechanical destruction of particles is caused by extremely shear stress during mixing of the carrying liquid suspension with cavitating water-jet whose velocity is about 660 ms^{-1} . The high-speed gradient in the tube (“abrasive nozzle”) can reach extremely high values about $1000 \text{ ms}^{-1}/\text{mm}$ which is cca 100 ms^{-1} at the maximal characteristic particle size. This high-speed gradient develops rotation and radial pressure inside of the jet and subsequently high dynamical straining of the particles.



Fig. 1 Water Jet Mill (WJM)

2) Disintegration of particles is caused by cumulated impact wave generated by cavitation bubble implosions (Fig. 2). That process runs with different intensity in the whole disintegration volume of the device. The technical solution is submitted to the patent application. Extreme tensile stress creates especially high intensity of practically pure steam cavitation. Cavitation of this type generates significantly higher density of the hydraulic water-hammer impact energy. During implosion of the cavitation bubbles this effect take the value about tens GPa. The compressive strength

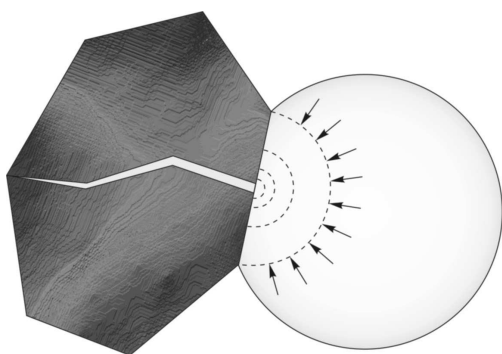


Fig. 2 Mechanism of cavitation breakage

most of the materials is much lower (e.g. $\sigma_{\text{Al}_2\text{O}_3} \approx 3 \text{ GPa}$). There is capillary bond between the bubble wall and particle in submicron range. A disturbance of the spherical symmetry and hydrodynamic instability in this dimensional scale causes asymmetric straining of the particle in the last phase of the cavitation bubble collapse.

3) The last disintegrative mechanism is direct mechanical destruction of particles during their impact to a hard target made of wolfram carbide on the output of cavity tube of the WJM.

The significant technical factor of the whole disintegration process is the multiple circulations of the particles during each of the processes in all the zones. The first milling tests show following results (Fig. 3): The water suspension with Si-fraction was obtained by separation time 180s from input fraction of Si (99,999 w %). During milling process the submicron fraction was increased from 0 vol. % to 6,5 vol. % (Fig. 4).

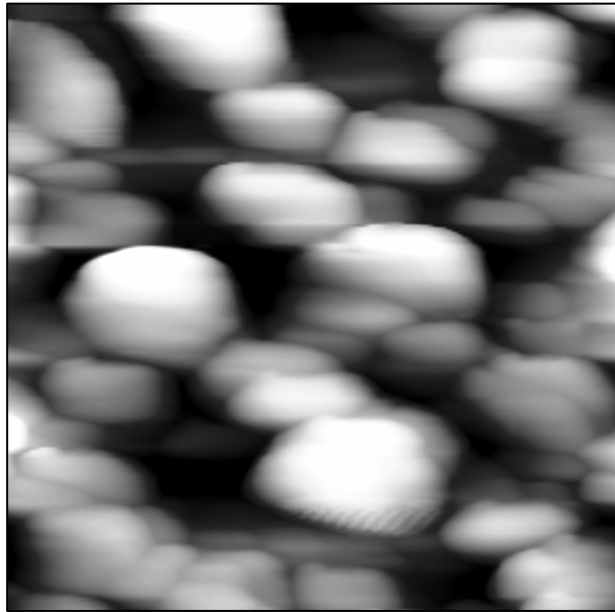


Fig. 3. Silicon submicron particles (photo 1x1 μ m)

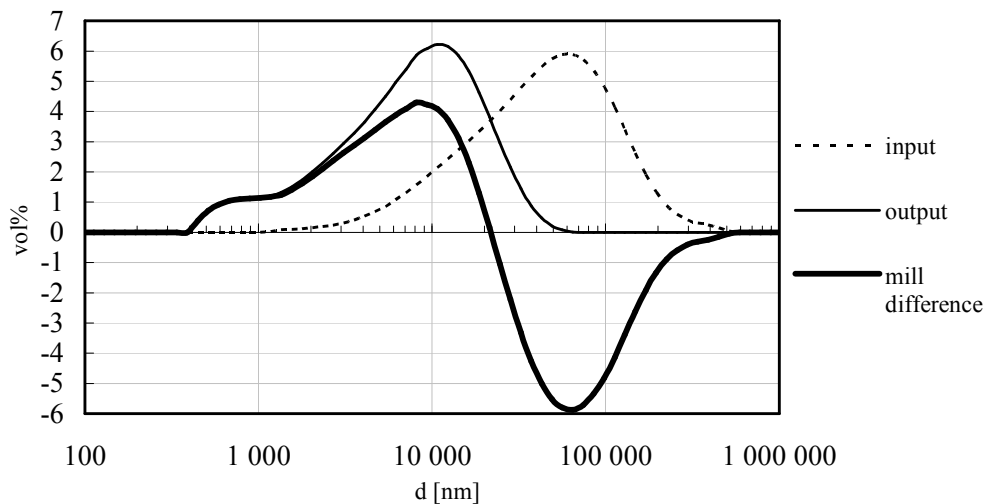


Fig. 4. Submicron fraction increasing

Connection of the WJM with suitable cyclic separator of the rough fraction can set up important technological device for preparation of particles in submicron range with possibility to go to nanometer range.

This research was partially supported by the Grant Agency of the Czech Republic (project No. 106/08/1092), by IGS grant of HGF VŠB-TUO and by the grant MSM 6198910016.

- [1] R. Dvorský, Patent CZ 298 759/2007.
- [2] R. Dvorský, J. Luňáček, A. Slíva, 1st Nanomaterials and Nanotechnology Meeting in Ostrava, September, 2008, two submitted papers.

SPECTRAL REFLECTOMETRY OF SiO₂ THIN FILM ON THE SILICON WAFERS

J. Luňáček¹, Z. Potůček², M. Luňáčková³, P. Hlubina¹, D. Ciprian¹

¹Department of Physics, VŠB - Technical University of Ostrava, 17. listopadu 15, 708 33 Ostrava - Poruba, Czech Republic

²Department of Solid State Engineering, Faculty of Nuclear Sciences and Physical Engineering, Czech Technical University in Prague, Trojanova 13, 120 00 Praha 2,

³Department of Mathematics and Descriptive Geometry, VŠB - Technical University of Ostrava, 17. listopadu 15, 708 33 Ostrava - Poruba, Czech Republic

jiri.lunacek@vsb.cz

Interference fringes are a typical feature of optical reflection spectrum of thin weakly absorbing film on supporting substrate. Film thickness can be simply calculated from a spectral position of interference minima or maxima. However, an observed position of these extremes in the reflection spectrum may be significantly shifted in comparison with their position in the interference pattern if a considerable dispersion of optical constants of thin film or substrate occurs in their vicinity. Moreover, an accurate location of the interference minima or maxima in measured reflection spectra of very thin films with broad interference fringes is relatively questionable. Therefore we developed a method for measurement and computer modelling of reflection spectra of non-absorbing thin films on absorbing substrates in a wide spectral region that enables to determine the thin film thickness more reliably and accurately. This method was successfully tested on SiO₂ thin films on silicon wafers.

When light incidents on a surface of a thin film on a substrate, multiple reflections occur on structure boundaries and the complex reflection coefficient can be written as

$$r(\lambda) = \frac{r_{01}(\lambda) + r_{12}(\lambda) e^{i2\beta(\lambda)}}{1 + r_{01}(\lambda) r_{12}(\lambda) e^{i2\beta(\lambda)}} \quad (1)$$

where $r_{01}(\lambda)$ and $r_{02}(\lambda)$ is the Fresnel reflection coefficient of the boundary air - thin film and thin film - substrate, respectively, and $\beta(\lambda)$ is the change of the reflected wave phase at single thin film passage from one boundary to the other [1]. The reflection coefficient $r(\lambda)$ is a function of the refractive index and the extinction coefficient of optical mediums on both sides of the boundary. Reflectance $R(\lambda)$ is than expressed as $|r(\lambda)|^2$. The phase change $\beta(\lambda)$ at normal incidence of light is given by

$$\beta(\lambda) = \frac{2\pi}{\lambda} n_1(\lambda) d \quad (2)$$

where d is the thickness and $n_1(\lambda)$ is the refractive index of the thin film.

Studied silicon wafers were supplied by company ON Semiconductor Czech Republic. SiO₂ thin films were prepared on silicon wafers by dry oxidation technique at furnace at temperature 1200 °C (Deal-Grove model) [2]. Reflection spectra were recorded on Shimadzu spectrophotometer UV-3600 with specular reflectance attachment that can measure the ratio of reflectance of studied sample and reference mirror of unknown reflectance in the spectral region 185 – 3100 nm. The reflection spectrum of SiO₂ thin film on silicon wafer and the reflection spectrum of respective bare silicon wafer were always measured at the same conditions. Then the ratio of these spectra corresponding to spectral dependence of reflectance of SiO₂ thin film referred to

reflectance of bare silicon wafer was not affected by systematic errors due to optical elements of spectrophotometer and by wafer surface quality. In order to obtain spectral dependence of absolute reflectance of SiO₂ thin film we made an assumption that reflectance of bare silicon wafers was equal to the theoretical reflectance of silicon and multiplied spectral dependence of the reflectance of SiO₂ thin film referred to the reflectance of bare silicon wafer by spectral dependence of reflectance of silicon calculated for normal incidence of light from spectral dependence of the refractive index and the extinction coefficient of silicon tabulated in [3]. Example of reflection spectrum of SiO₂ thin film on silicon wafer corrected in this way is shown on Fig. 1.

A program was written in the software package MATLAB that enables to fit the measured reflection spectrum with a theoretical spectral dependence of reflectance $R(\lambda)$ derived from equation (1) for non-absorbing thin film on absorbing substrate by means of Levenberg-Marquardt least-squares method. The thin film thickness d is the only fitting parameter. Excellent correspondence between the theoretical model and the measured reflection spectrum of SiO₂ thin film on silicon wafer is illustrated on Fig. 1. The spectral dependence of the SiO₂ refractive index appearing in the model was calculated from standard Sellmeier formula and the spectral dependence of refractive index and extinction coefficient of silicon was taken from [3]. The obtained thicknesses of SiO₂ thin films agree very well with that ones determined by means of spectral interferometry [4]. For example, in the case of sample, reflection spectrum of which is on Fig. 1, the difference was only 3 nm.

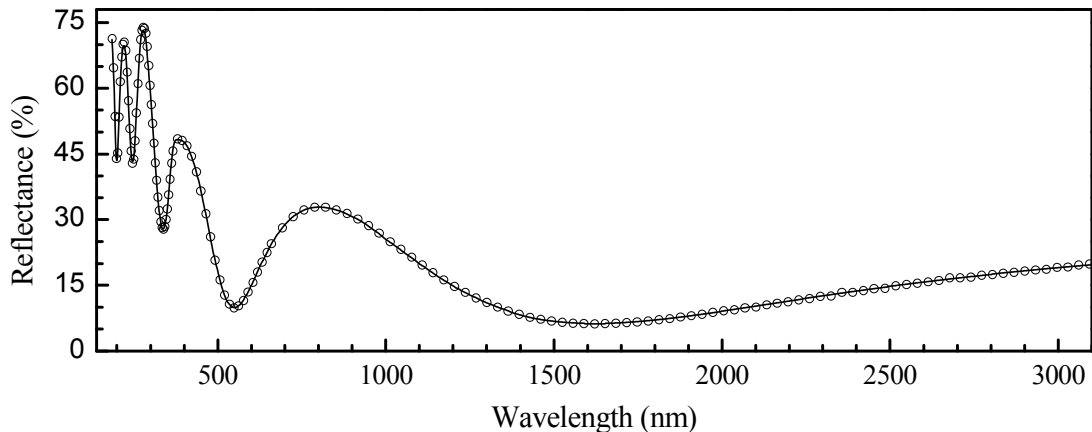


Fig.1. Reflection spectrum (circles) of the SiO₂ thin film on the silicon wafer and its best fit (solid line) by the spectral dependence of reflectance theoretically derived for this structure. Film thickness $d = 280.4$ nm was obtained as a fitting parameter.

This research was supported by the project MSM 6198910016 and MSM 6840770021.

- [1] M. Born, E. Wolf, Principles of Optics, Cambridge University Press, Cambridge, 1999.
- [2] J. D. Plummer, M. D. Deal, P. B. Griffin, Silicon VLSI Technology: Fundamentals, Practice, and Modelling, Prentice Hall, Upper Saddle River, 2000.
- [3] E. D. Palik, Handbook of Optical Constants of Solids, Academic Press, Orlando, 1995.
- [4] P. Hlubina, D. Ciprian, J. Luňáček, M. Lesňák, Appl. Phys. B 84 (2006) 511.

SCINTILLATION RESPONSE OF CRYSTALS – EXCITATION AND MEASUREMENTS USING HPMT

J. A. Mareš¹, P. Průša², M. Nikl¹, A. Beitlerová¹

¹ Institute of Physics, Academy of Sciences of the Czech Republic, Cukrovarnická 10, 162 53 Praha 6

² Faculty of Nuclear Sciences and Physical Engineering, Czech Technical University in Prague, Břehová 7, 115 19, Praha 1

amares@fzu.cz

Scintillating response of crystals is their basic characteristics - it is response due to excitation by X-or γ -rays or by particles as electrons, protons, positrons etc. Generally, the main particle sources are α - or β -rays or electrons. Scintillating response means the following properties: the N_{phels} photoelectron or L.Y. light yields, the energy resolution (mainly characterized by FWHM), linearity or proportionality of the yields or some other special properties [1-3].

Various kinds of excitation of scintillation mentioned above result in different response according e.g. to stopping power of the excitation. Basic difference is between α - or β -rays and γ -ray excitation. The stopping power or penetration depth in crystals for α -rays is around 10 μm , for β -rays up to ~ 1 mm but for γ -rays this depends on crystal composition (on the linear absorption of the individual elements from which crystal is composed) [1-4]. Generally, the heavy scintillating crystals as e.g. LuAG:Ce, LSO:Ce, LuAP:Ce have stopping power of γ -rays around ~ 1 cm. The stopping power is also important if we investigate very thin samples (tenths of μm) because here, we must use another excitation source than γ -ray one – the excitation by α -rays [4].

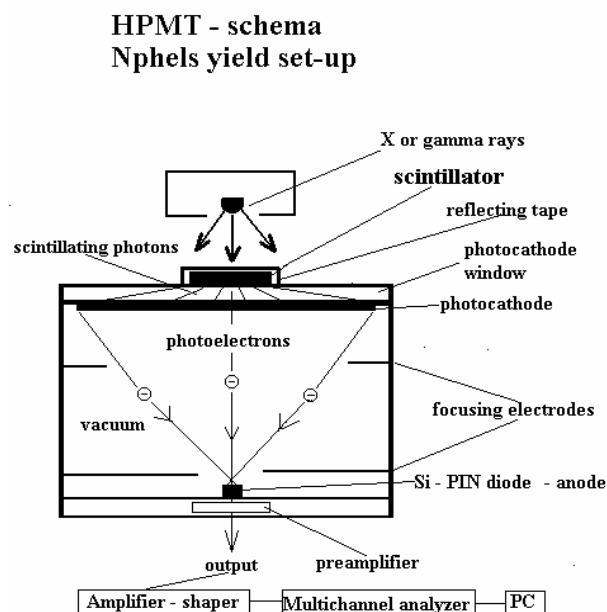


Fig. 1 Experimental set-up using HPMT for scintillation response measurements

Hybrid photomultiplier (HPMT) is a new kind of photomultiplier which consists of only the photocathode and the anode - no dynodes are present [1]. Electrons generated from photocathode by the scintillating photons are accelerated and focused by the electrostatic field of electrodes (see Fig. 1). The anode is Si-PIN diode. Generated electrons which reach the anode create electron-hole pairs [1,2]. Energy needed to create the pair in Si is ~ 3.6 eV and at 1 kV accelerating voltage roughly 280 electron-hole pairs are generated.

The set-up given in Fig. 1 can measure scintillating response of crystals. Calibration spectra of

HPMT are in Figs 2 and 3. If we excite the samples under γ -rays then we must use large volume samples at least of 1 mm of thickness [2]. The most used excitation sources of scintillation crystals are summarized in table below.

^{241}Am	α -rays	5.4857 MeV	140 Bq	$T_{1/2} = 433$ years
$^{90}\text{Sr}/^{90}\text{Y}$	β -rays	0.546 MeV - 2.284 MeV	2 kBq	$T_{1/2} = 29.12$ years
^{137}Cs	γ -rays	661.66 keV	15 kBq	$T_{1/2} = 30$ years

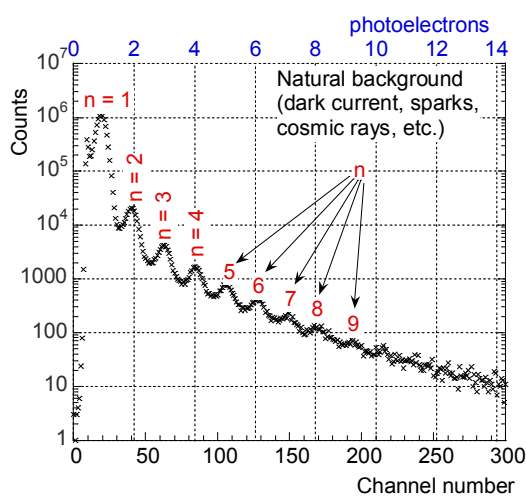


Fig. 2 Pulse-height calibration spectrum of HPMT in logarithmic scale

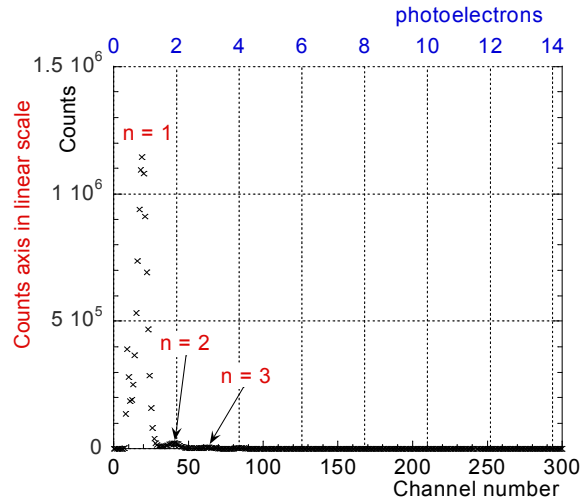


Fig. 3 Pulse-height calibration spectrum of HPMT in linear scale

We have studied various Ce-doped scintillating crystals as garnets, perovskites, silicates prepared mainly by the Czochralski method (but also other methods were used as e.g. μ -pulling-down one). The application of the HPMT to measure scintillation response of crystals was very successful. We can detect very high energy resolution (FWHM) YAP:Ce crystal but we also studied LSO:Ce crystal where large fluctuations in the photo-electron and L.Y. were observed. These measurements were correlated with thermoluminescence measurements [3]. Not only high light yield scintillating crystals were studied but also PWO crystal [5] where L.Y. is below 100 phels/MeV.

- [1] J. A. Mares and C. D'Ambrosio, *Opt. Mat.* 30 (2007) 22.
- [2] J. A. Mares, A. Beitlerova, M. Nikl, N. Solovieva, C. D'Ambrosio, K. Blazek, P. Maly, K. Nejezchleb and F. De Notaristefani, *Rad. Measur.* 38 (2004) 353.
- [3] J. A. Mares, M. Nikl, E. Mihokova, A. Beitlerova, A. Vedda and C. D'Ambrosio, *IEEE Trans. Nucl. Sci.* 55 (2008) 1142.
- [4] M. Kucera, K. Nitsch, M. Kubova, N. Solovieva, M. Nikl and J.A. Mares, *IEEE Trans. Nucl. Sci.* 55 (2008) 1201.
- [5] J. A. Mares, A. Beitlerova, P. Bohacek, M. Nikl, N. Solovieva, C. D'Ambrosio, *phys. stat. sol. (c)* 2 (2005) 73.

STRUCTURE AND PROPERTIES OF BOROPHOSPHATE GLASSES WITH TeO_2 ADDITIONS

P. Mošner, K. Vosejpková, L. Koudelka, M. Vlček

Department of General and Inorganic Chemistry, Faculty of Chemical Technology,
University of Pardubice, 532 10 Pardubice, Czech Republic
petr.mosner@upce.cz

Telluride oxide containing glasses are extensively studied in recent years because of their interesting properties as low melting temperatures, high dielectric constants, good infrared transmissions etc. [1-4]. TeO_2 is only a conditional glass former and melts containing only TeO_2 as the network-forming oxide require special fast-quenching methods to vitrify. Nevertheless, in combination with other network formers like P_2O_5 or B_2O_3 glasses with a high TeO_2 content can be prepared [4,5]. The aim of this work is to study the structure, physico-chemical and thermal properties of $\text{ZnO-B}_2\text{O}_3\text{-P}_2\text{O}_5\text{-TeO}_2$ glasses as a function of TeO_2 content.

Glasses were prepared in compositional series $(100-x)[50\text{ZnO-}10\text{B}_2\text{O}_3\text{-}50\text{P}_2\text{O}_5]\text{-}x\text{TeO}_2$ with $x = 0\text{-}80$ mol% TeO_2 by heating the reaction mixture up to $900\text{-}1250^\circ\text{C}$ with a subsequent slow cooling of the melt in air. The obtained glasses were characterized by the measurements of density, molar volume, chemical durability, glass transition temperature, dilatation softening temperature, crystallization temperature and thermal expansion coefficient. Their structure was studied by Raman and IR spectroscopy.

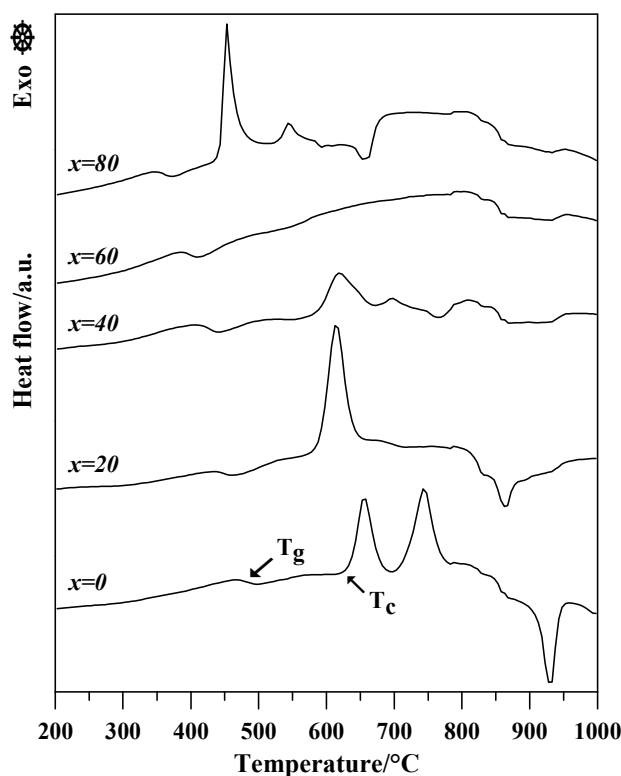


Fig.1. DSC curves of the $(100-x)[50\text{ZnO-}10\text{B}_2\text{O}_3\text{-}50\text{P}_2\text{O}_5]\text{-}x\text{TeO}_2$ glasses.

Study of physico-chemical properties showed that with increasing TiO_2 content glass density linearly increases from $3.1\text{g}\cdot\text{cm}^{-3}$ ($x=0$) to $5.1\text{g}\cdot\text{cm}^{-3}$ ($x=80$ mol% TeO_2) while molar volume and chemical durability decreases. The highest changes of chemical durability were observed especially for the glasses containing 20-40 mol% TeO_2 . Colour of the glasses changed from clear ($x=0$) to brownish.

Thermoanalytical curves obtained by DSC analysis (see Fig.1), showed that glasses crystallize on heating within temperature range of $440\text{-}640^\circ\text{C}$. The crystallization temperature, T_c , decreases with increasing TiO_2 content. The highest thermal stability was observed for glasses with TeO_2 content of 50 and 60 mol%. Crystallization products were identified by X-ray diffraction analysis. This analysis revealed that by heating the glass composition $50\text{ZnO-}10\text{B}_2\text{O}_3\text{-}50\text{P}_2\text{O}_5$ crystalline $\text{Zn}_2\text{P}_2\text{O}_7$ and BPO_4 compounds are formed. With increasing TeO_2 content, these compounds are gradually replaced by crystalline TeO_2 (paratellurite) phase.

Thermomechanical analysis reveal that incorporation of tellurite structural units into the borophosphate network results in its depolymerization and decrease of glass transition temperature and dilatation softening temperature with increasing TeO_2 content while thermal expansion coefficient of glasses increases within the region of $5.8\text{-}11.6$ ppm. $^\circ\text{C}^{-1}$.

Raman spectra of the glasses revealed the incorporation of TeO_x structural units into the disordered network of the glasses and the depolymerization of phosphate chains in the glasses. The Raman spectrum of the starting zinc borophosphate glass with composition $50\text{ZnO-}10\text{B}_2\text{O}_3\text{-}40\text{P}_2\text{O}_5$ is characterized by a strong broad band at 1158 cm^{-1} which is ascribed to the presence of Q^1 phosphate units. In the middle-frequency region there are two small vibrational bands at 666 cm^{-1} and 748 cm^{-1} which can be ascribed to the vibrations of oxygen atoms in B-O-P and P-O-P bridges resp. With increasing TeO_2 content the intensity of these bands decreases and a number of overlapping bands appear in the spectral region of $300\text{-}800\text{ cm}^{-1}$. These bands can be assigned to the stretching vibrations of TeO_4 units and bending vibrations of P-O-Te or Te-O-Te linkages [5,6]. The infrared spectra supply essentially the same information.

The authors are grateful for the financial support from the research project No. 0021627501 of the Ministry of Education of Czech Republic and to the Grant Agency of the Czech Republic (Grant No. 104/07/0315).

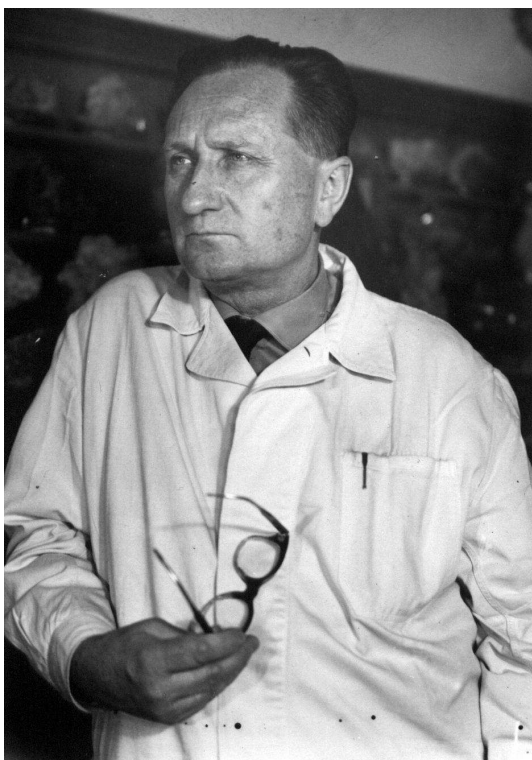
- [1] M. Matsumisago, T. Minami, Y. Kowada, H. Adachi, Phys. Chem. Glasses 35 (1994) 89.
- [2] M.M. Elkholy, L.M. Sharaf El-Deen, Mater. Chem. Phys. 65 (2000) 192.
- [3] D. Zhu, C.S. Ray, W. Zhou, D.E. Day, J. Non-Cryst. Solids 319 (2003) 247.
- [4] A.H. Khafagy, A.A. El-Adawy, A.A.Higazy, S. El-Rabaie, A.S. Eid, J. Non-Cryst. Solids 354 (2008) 1460.
- [5] M.T. Rinke, L. Zhang, H. Eckert, ChemPhysChem 8 (2007) 1988.
- [6] B.V.R. Chowdari, P. Pramoda Kumari, Mater. Res. Bull. 34 (1999) 327.

**PROFESSOR JAN KAŠPAR (1908 -1984)
TO 100th BIRTHDAY ANNIVERSARY**

K. Nitsch

Institute of Physics AS CR, Cukrovarnická 10, 162 00 Praha 6
nitsch@fzu.cz

Professor Jan Václav Kašpar, DrSc., corresponding member of the Czechoslovak Academy of Sciences, was born in Ústí nad Orlicí on April 15, 1908. He graduated from the Faculty of Science of the Charles University in Prague in mineralogy in 1931 and worked there as an assistant professor until 1934. Afterwards he joined the Mineralogical Department of the National Museum in Prague and from 1937 he worked at the Institute of Mineralogy and Petrography at the Institute of Chemical Technological Engineering of the Czech Technical University. He became an extraordinary professor in 1939 but his promising university career was interrupted during the World War Two due to closing down of the Czech universities. He returned to the National Museum and in 1943 he was appointed the manager of the Research Institute for Precious Stones in Turnov and worked there as a manager till 1953. After the war he returned to the Department of Mineralogy of the Institute of Chemical Technological Engineering.



At that time his great attention was paid to the Mineralogical collection of the Department which was almost destroyed during the war. The saddest losses of collection funds were gradually compensated with great effort with donations, purchases, exchanges and collection expeditions to Faeroe Islands, Iceland, USA and Mexico and to other countries. From these expeditions the minerals of total mass above 2 tons were brought. The Collection was increased to more than 23 000 inventory items till 1949. In the fifties and sixties of the 20th century Prof. Kašpar, as an enthusiastic mineralogist, undertook many trips abroad, perhaps in all the continents, and collected minerals in order to enlarge the Department collection.

He worked as a dean of the Institute when in 1952 it branched off the Czech Technical University and the independent Institute of Chemical Technology in Prague (VŠCHT Praha) was established. Prof. Kašpar was appointed as the first rector of the Institute. In the period between 1953 and 1955 he was elected as a dean of the Faculty of Inorganic Technology of the Institute. In 1952 he became a professor and in 1956 as the eighth department professor he took the position of the head of Department and held it till his retirement in 1973. In 1958 he

established a laboratory that was engaged in preparation of minerals resources using floatation methods. This laboratory gradually extended into the Institute of Geochemistry and Mineral Resources of the Czechoslovak Academy of Sciences in 1960 and Prof. Kašpar became the manager of this Institute and held the position until 1978 [1].

Prof. Jan Kašpar died on September 21, 1984 at the age of 76.

Prof Kašpar was an outstanding scientist, teacher and lecturer and organizer of scientific work in the field of crystal growth, mineralogy, crystallography, geochemistry and a competent manager. According to his colleagues he was also an excellent photographer.

Nevertheless, the list of Prof. Kašpar's academic titles and organisation positions is not the main reason, why we commemorate him and the 100th anniversary of his birthday. The main reason is that Jan Kašpar became the leading personality in the field of crystal growth in the former Czechoslovakia both at the very beginning and during development of this field in the fifties and sixties of the 20th century.

Jan Kašpar together with B. Ježek, Professor of the Příbram Academy and Mr. B. Pařízek from Turnov established a Research Institute for Precious Stones in Turnov on June 17, 1943, what was considered as a start of organized growth of synthetic single crystal in the former Czechoslovakia. Jan Kašpar was charged with forming the conception and structure of the Institute and managing the Institute. He had been the manager of this institute until 1953 [2,3]. In the sixties the Institute became the leading research establishment in the former Czechoslovakia. It was several times renamed and has been well known as "Monokrystalý Turnov". Besides the scientific work, development of preparation methods and growth of single crystals of different composition by various methods, it also organized Conferences on crystal growth [4-9].

This work was supported from the Grant Agency of the Academy of Sciences of the Czech Republic (Grant No. IAA200100626).

- [1] V. Seidl, Sborník muzea českého ráje, Acta Musei Turnoviensis 2005, No 1, p. 26.
- [2] R.R. Novotný, Sborník muzea českého ráje, Acta Musei Turnoviensis 2005, No 1, p. 8.
- [3] B. Mánek, Sborník muzea českého ráje, Acta Musei Turnoviensis 2005, No 1, p. 30.
- [4] Proceedings of the 1st National conference on single crystals, Turnov, December 1953.
- [5] Proceedings of the 2nd National conference on single crystals, Turnov, November 1954.
- [6] Proceedings of the 3rd National conference on single crystals, Turnov, December 1957.
- [7] Proceedings of the 4th National conference on single crystals, Turnov, July 1961.
- [8] Proceedings of the 1st Seminary on single crystals, Turnov, 1963.
- [9] Proceedings of the 2nd Seminary on single crystals, Hrubá skála, April 1967.

ELECTROCHEMICAL AND VAPOR GROWN ZnO

D. Nohavica^{1,2}, P. Gladkov^{1,2}, Z. Jarchovský¹

¹Institute of Photonics and Electronics, Academy of Sciences of the Czech Republic, Chaberská 57, 182 51, Praha 8

²Institute of Physics, Academy of Sciences of the Czech Republic, Cukrovarnická 10, 162 53 Praha 6

nohavica@ufe.cz

In this study the procedure proposed by Vayssieres [1] using equimolecular solutions of zinc nitrate hexahydrate and hexamethylenetetramine under an external voltage [2] was used to deposit ZnO on a nanoporous GaP and „bulk“ Si substrates. Nanoporous regions of the GaP are tens of μm thick. Nanoporous dimension of the pores was verified by photoluminescent (PL) spectra of the samples and SEM pictures which demonstrate pores diameter 50 nm. In PL the blue shift of the band to band transition in comparison with the reference not anodized GaP sample from the same monocrystalline plate was observed. Deposit on the „bulk“ Si substrate at identical conditions was less homogeneous with higher nucleation barrier than nanoporous GaP. Obtained ZnO

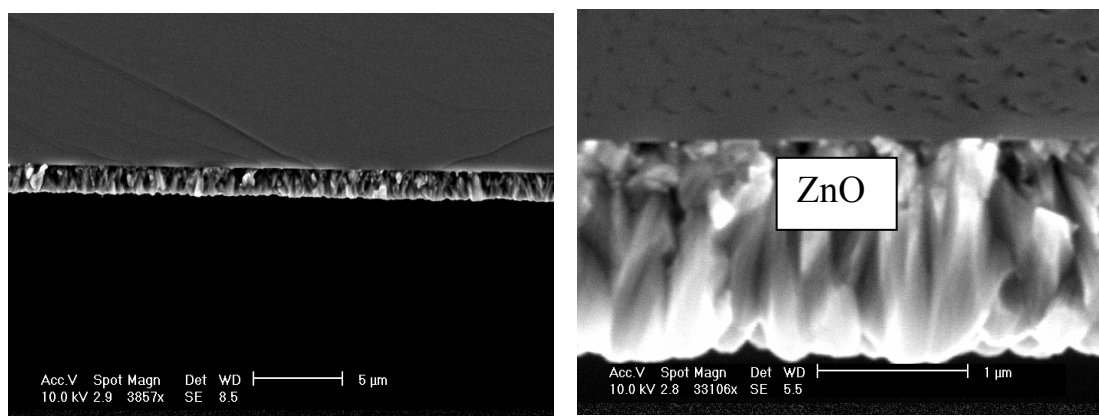


Fig 1. Layer of ZnO on nanoporous GaP substrate

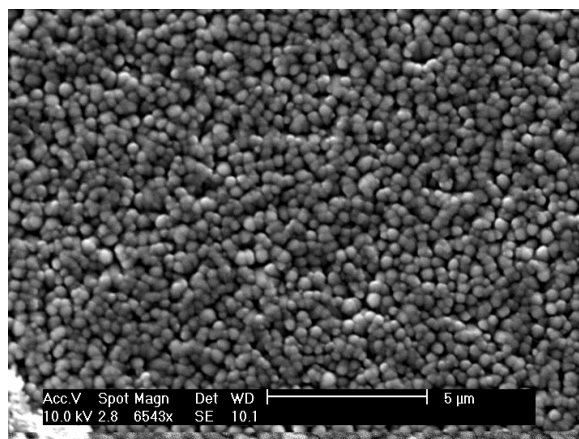


Fig.2. Top view of ZnO micro ribbons on silicon substrate.

layers (Fig. 1.) seems more compact in comparison with nanorods obtained on „bulk“substrates in [1, 2]. Research of the details of the heteroepitaxy on porous substrates is a long term research task in our laboratory.

Photoluminescence spectra (Fig.3.) of the grown ZnO layers excited by He-Cd laser (325 nm) were measured at 4K. PL spectra contain 6 bands which were identified by Gauss deconvolution. According to the literature data BX peak corresponds to bound exciton at neutral acceptor, (Do, Ao) is donor acceptor recombination, BX-LO is LO replica of the BX, SD structural defects, SD-LO is a phonon replica with participation of one phonon, and SD-2LO is a phonon replica with participation of two phonons.

Bond exciton and D-A recombination peaks visibility is indicative for rather low carrier concentration. Structural perfection of the layers is continuously improved.

Main task of the CVD method research is to test UV photo stimulation influence on ZnO clusters formation in the vapor phase. This research has not been finished jet.

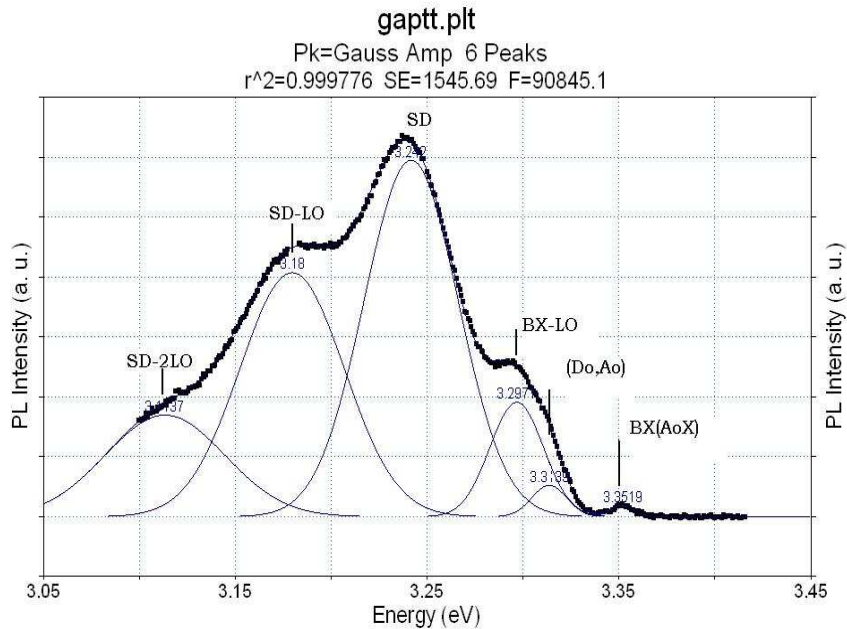


Fig. 3. Low temperature PL spectra of the electrochemically deposited ZnO layer on nanoporous GaP substrate.

[1] L.Vayssieres, Adv. Mater. 15 (2003) 464.
 [2] Ligang Yu, Gengmin Zhang, Shiqi Li, Zhonghe Xi, Dengzhu Guo, J.Crystal Growth 299 (2007) 184.

LUMINESCENCE OF CHALCOHALIDE GLASSES DOPED WITH Pr³⁺ AND Yb³⁺ IONS

J. Oswald¹, K. Kuldová¹, B. Frumarová², and M. Frumar³

¹ Institute of Physics, Academy of Sciences of the Czech Republic, v. v. i., Cukrovarnická 10, 162 00 Praha 6, Czech Rep.

² Joint Laboratory of Solid State Chemistry of Institute of Macromolecular Chemistry of the ASCR, v.v.i., & University of Pardubice, Czech Rep.

³ Res. Center and Dep. of Inorg. Chemistry, Faculty of Chem. Technology, University of Pardubice, 53210 Pardubice, Czech Rep.

oswald@fzu.cz

Rare earth (RE) doped chalcogenide glasses are promising materials for active optical devices in near - and mid-infrared spectral regions [1]. The solubility of RE ions in glassy matrix is often small and many RE doped chalcogenide glasses are unstable. The addition of heavy metal halides to chalcogenide glasses could increase the solubility of RE ions in chalcogenide glassy matrix.

All glasses were synthesized from high purity elements (Ge, Sb and S all of 5N-purity, Pr (99.9%), Yb (99.9%), PbI₂ or PbCl₂ (99.999%) in sealed and evacuated ($p \cong 10^{-4}$ Pa) silica ampoules in a rocking furnace (970°C, 20 hours). After the synthesis, the ampoules with the melt were quenched in undercooled mixture of water with ice and then annealed at temperatures near glass transition. Thermal analysis was performed in the range of 20 to 900°C with the heating rate 10 K/min. Glasses of three systems (100-y((GeS₂)₈₀(Sb₂S₃)_{20-x}(PbCl₂)_x)yPr₂S₃, 100-y((GeS₂)₈₀(Sb₂S₃)_{20-x}(PbI₂)_x)yPr₂S₃, x=0; 2; 5, 8; y= 0.1; 0.5 and 99.9-z((GeS₂)₈₀(Sb₂S₃)₁₈(PbI₂)₂)0.1Pr₂S₃zYb₂S₃, z=0.05; 0.1; 0.15) were prepared in high purity. Homogenous and well transparent glasses were obtained for $x \leq 5$ mol% PbCl₂ (or PbI₂), for $y \leq 0.1$ mol.% Pr₂S₃ and for $z < 0.15$ mol.% Yb₂S₃.

The luminescence spectra were measured in a spectral region from 900 nm to 4250 nm at room temperature. Laser diodes (980 nm, 1064 nm, and 1550 nm) were used for luminescence excitation. The broad luminescence bands near 1350 nm, 1600 nm, 2300 nm and 4200 nm were observed in Pr doped glasses, which were ascribed to ¹G₄ → ³H₅ (maximum ~1340 nm), ³F₃ → ³H₄ (maximum ~1600 nm), not resolved ³F₂ → ³H₄, ³H₆ → ³H₄ and ³F₃ → ³H₅ (2200-2700 nm), and ³H₆ → ³H₅ transition (3900-4200 nm).

The intensity of emission band near 1342 nm (¹G₄ → ³H₅ transition) increases with doping by Yb³⁺ up to 10% of Yb. This is caused by energy transfer between Yb³⁺ and Pr³⁺ ions at excitation by 980 nm. The more efficient population the ¹G₄ state by sensitizing Pr³⁺ with Yb³⁺ is under exploration, since the ²F_{5/2} → ²F_{7/2} emission band of Yb³⁺ overlaps the ³H₄ → ¹G₄ absorption band of Pr³⁺ [2].

The support of Grant Agency of Czech Rep., project 203/06/0627, of the Academy of Sciences of the Czech Rep., projects AV0Z 40500505 and AV0Z 10100521 and of the Ministry of Education of the Czech Rep., projects VZ002167501 and LC523, is highly acknowledged.

[1] Zakery, S.R. Elliott, J. Non-Cryst. Solids 330 (2003) 1.

[2] A.G. Bluiett, E. Pinkney, E.E. Brown, U. Hommerich, P. Amedzake, S.B. Trivedi, J.M. Zavada, Mat. Sci. Eng. B 146 (2008) 110.

MAGNETIC PROPERTIES OF MONONUCLEAR Co(II) AND Ni(II) COMPLEXES.

B. Papánková¹, R. Boča¹, L. Dlhán¹, I. Svoboda², H. Fuess², J. Titiš³

¹ Department of Inorganic Chemistry, Slovak University of Technology, 81237 Bratislava

² Institut für Materials Science, Darmstadt University of Technology, D - 64289 Darmstadt

³ Department of chemistry, University of SS Cyril and Methodius, Trnava
blazena.papankova@stuba.sk

Zero-field splitting (ZFS) is the removal spin microstate degeneracy for systems with $S > 1/2$ in the absence of an applied field. That is, the degeneracy is removed as a consequence of molecular electronic structure and/or spin density distribution. For odd-electron systems, axial ZFS (the „D”ZFS parameter) removes the microstate degeneracy and produces Kramer doublets. Rhombic ZFS (the “E” ZFS parameter) splits the Kramer’s doublets. ZFS causes magnetic anisotropy, and has profound effects on magnetic properties. Understanding the origin of ZFS in molecular magnets is of great importance, because the ZFS determines many of their fundamental properties.

Zero-field splitting of magnetic energy levels in mononuclear complexes is a phenomenon known for decades and it is well described in monographs dealing with electron spin resonance [1]. Nevertheless it is common in magnetochemistry [2,3]. A new impulse for interest in the values of ZFS *D*-parameters has been brought by the speculations about the existence of a single-molecule magnet. It would be appreciated to know of how to fix the sign and how to tune the value of the *D*-parameter in metal complexes [4]. Such a target needs a critical reevaluation of old and determination of new experimental data.

Motivated by the above needs, we prepared a mononuclear cobalt(II) and nickel(II) complexes in which we expect an enhanced magnetic anisotropy.

Our interest is an investigation of interesting coordinating properties of Co(II) and Ni(II) with N - donor base and carboxylate ligand. The heteroleptic complexes with the {MeN₂O₂O₂} [5, 6], {MeN₄O₂} [7, 8] chromophore, where M = Ni and Co have been prepared, structurally characterized and subjected to magnetochemical investigation down to 2 K (susceptibility and magnetization measurement). These parameters can be measured by a variety of techniques. Observation for :

➤ [Ni(imidazole)₄(acetate)₂]

1. Effective magnetic moment drops to a constant value.
2. Magnetization deviates from the Brillouin function progressively.
3. Data are consistent with large **negative** *D* ($D/hc = -29 \text{ cm}^{-1}$).
4. Reason: $k_z = 1$ (very long, ionic bond), $k_x = 0.6$ (normal, covalent bond).

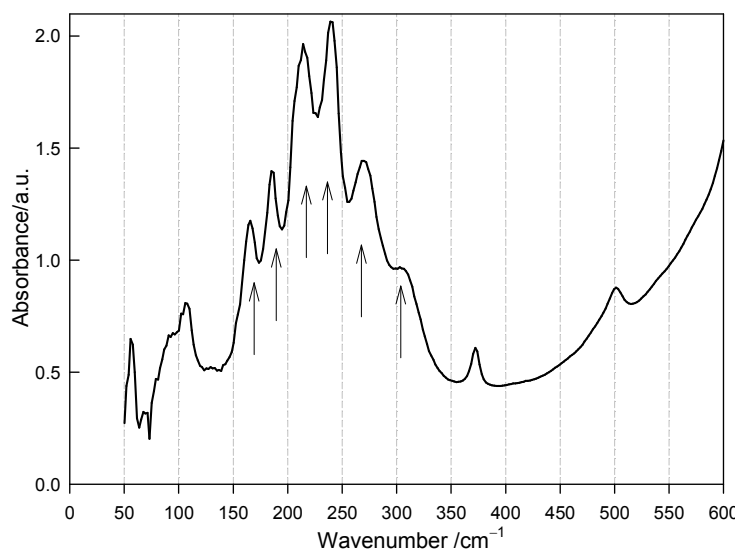
➤ [Ni(pyrazole)₄(acetate)₂] - The coordination polyhedron is a slightly compressed tetragonal bipyramid.

1. Effective magnetic moment drops to the zero.
2. Magnetization at $T = 2.0$ and 4.6 K : not strong deviation.
3. *D* is small and $D > 0$ ($D/hc = + 3.9 \text{ cm}^{-1}$).

➤ [Co(N-methylimidazole)₂(H₂O)₂(ac)₂] - The complex forms a compressed tetragonal bipyramid.

1. The low-temperature effective magnetic moment shows strong deviation from the Curie law.
2. The magnetization deviates strongly from the Brillouin -function behaviour.
3. The complex shows very large zero-field splitting and the magnetic anisotropy. $D = -71.80 \text{ cm}^{-1}$.

The electron spectrum of $[\text{Co}(\text{N-methylimidazole})_2(\text{H}_2\text{O})_2(\text{ac})_2]$ in FAR-IR region exhibits a six-member absorption peak referring to the transition between the members of the split $4T_{1g}$ state ($4A_{2g} + 4E_g$).



The axial parameter of the ZFS, D , adopts either positive or negative values and correlates with axial distortion of the coordination polyhedra.

This work was supported by the Deutscher Akademischer Austauschdienst (DAAD) and by Slovak VEGA Project No 1/0213/08.

- [1] A. Abraham and B. Bleaney Electron Paramagnetic Resonance of Transition Metal Ions, Clarendon, Oxford (1970).
- [2] R.L. Carlin Magnetochemistry, Springer, Berlin (1986).
- [3] O. Kahn Molecular Magnetism, VCH, New York (1993).
- [4] S.M.J. Aubin, Z. Sun, H.J. Eppley, E.M. Rumberger, I.A. Guzei, K. Folting, P.K. Gantzel, A.L. Rheingold, G. Christou and D.N. Hendrickson Inorg. Chem. 40 (2001) 2127.
- [5] R. Ivaníková, R. Boča, Ľ. Dlháň, H. Fuess, A. Mašlejová, V. Mrázová, I. Svoboda and J. Titiš J., Polyhedron 25 (2006) 3261.
- [6] B. Papánková, I. Svoboda and H. Fuess, Acta Cryst.E62 (2006) m1916.
- [7] R. Boča, Ľ. Dlháň, W. Haase, R. Herchel, A. Mašlejová and B. Papánková, Chem. Phys. Lett. 373 (2003) 402.
- [8] B. Papánková, I. Svoboda, H. Fuess and K. Šintálová, Acta Cryst.E61 (2005) m2036.

NANOTECHNOLOGY IN EDUCATION

I. Pilarčíková, J. Sedláček, J. Lipták, A. Mlích

Czech Technical University, Faculty of Electrotechnical Engineering, Technická 2,
166 27 Praha 6, Czech Republic

pilarcik@fel.cvut.cz

Within the scope of the study programme Electrotechnics and Informatics, the subject Nanotechnology is classified among the Electronics and Photonics Engineering block of the course of Electronics. It is of range 2 + 2 and has to be finished by an assessment and examination.

Acquirement of basic knowledge in the sphere of up-to-date nanotechnologies for demands of solving of qualified problems concerning further systems and elements miniaturization, namely in electronics, represents this subject's aim. The subject has its starting point in applications of quantum physics, fractals growth, colloid systems, spontaneous growth of nanostructures and their characterization in nanoelectronics, nanomaterials, organic solar elements, and biomimetical functional structures.

The opening block of lectures deals with quantum physics basics necessary for this subject. The following lectures concern characteristics of nanostructures basic types (fractals, colloids, etc.) being in relation with problems of nanostructures study methods. Particular consideration is applied to Transmission Electron Analysis (TEM), Scanning Electron and Tunnel Microscopy (SEM, STM), and Atomic Forces Microscopy (AFM). Further, the study programme includes one lecture in epitaxial increase methods focused especially on Metalorganic Compounds Epitaxy (MO VPE) and Molecular Beam Epitaxy (MBE). Another lecture in new-generation lithographic methods follows; it includes Extreme Ultraviolet Photolithography (EUV), Electron and Ion Projection Lithography (EPL, IPL), and X-Ray Lithography (XRL). The final lecture block concerns nanomaterial applications. It covers problems of electronic nanoelements, possible development of semiconductor electronics, organic solar elements, and biomimetical nanoactuators.

Practices follow with lectures and complete them in the appropriate way. The practices take place at laboratories and are of demonstration character. Also two excursions are assigned to the study programme. The first one is held at MBE and MO VPE working sites of Physical Department of Czech Academy of Sciences and, the second one, at the nanofibres production site of ELMARCO company in Liberec city.

The first laboratory practice "Study Diffusion-Limited Growth of Fractal Clusters" consists of two tasks. The first one includes an experiment based on electrical deposition (Fig 1). The anode is made of zinc sheet and the cathode is made of carbon bar. The electrolyte consists of zinc sulphate solution on which butyl acetate layer is spread and, so, it creates quasi-2-dimensional interface. After connecting of electrodes to direct-current voltage source, tree fractal grows around the carbon cathode. The second task is based on "viscous fingers" growth (Fig 2). For this experiment, Hele-Shaw cell filled up with highly viscous solution is used. Then, small amount of low viscous solution is injected into the first solution. Finally, diffusion is coming on as well as viscous fingers growth.

The task "Thin Polymeric Layers with Carbon Nanoelements Aggregates Preparation Technology" demonstrates step-by-step preparation of polymeric

composites samples based on polystyrene-carbon particles (PS-CB). Crushed carbon particles are added to the prepared polystyrene solution in toluene. After ultrasonic disintegration and homogenization, the created colloid is cast on microscopical mounts by means of spin-coating method.

The task “Thin Metallic Layers Preparation Technology, Layers Electrical Properties Measurement” follows. As an introduction, students are getting to know with theory of thin layers growth and, then, demonstration of thin aluminium layer on PET carrier by means of vacuum evaporation method follows. On the layer prepared after this manner, optical absorbance measurement and layer thickness (up to 10nm) determination is carried out. Finally, surface resistivity of the created layer is determined according to ASTM D257 – 66 standard.

“Study of Composites and Thin Layers Nanostructure by help of Atomic Forces Microscopy” represents one practice at which the students are practically getting to know with AFM microscopy based on atomic forces mapping on a sample’s surface. At this measurement, the students discover nanostructure of PS-CB composites and thin aluminium layers on PET carriers samples prepared during the previous practices.

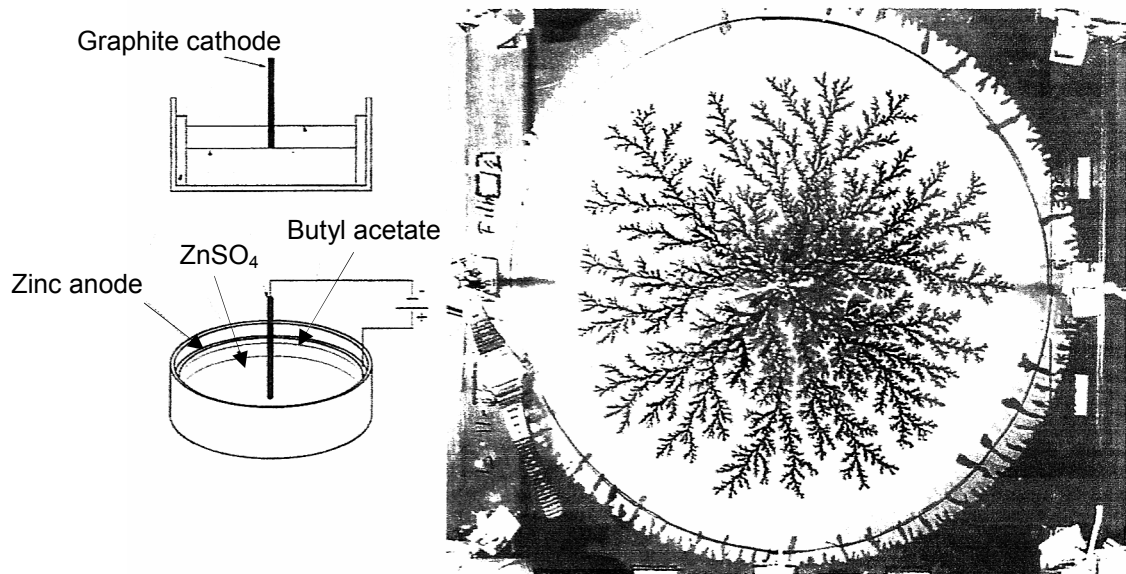


Fig. 1. Electrical deposition of fractal clusters.

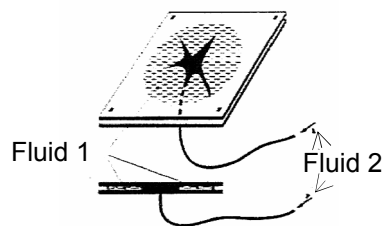


Fig. 2. Growth of “viscous fingers”.

PHOTOLUMINESCENCE OF ERBIUM DOPED KTaO_3 CRYSTALS

Z. Potůček^{1,2}, Z. Bryknar¹, V. Trepakov²

¹Czech Technical University in Prague, Faculty of Nuclear Sciences and Physical Engineering, Trojanova 13, 120 00 Praha 2, Czech Republic

²Institute of Physics, Academy of Sciences of the Czech Republic, Na Slovance 2, 182 21 Praha 8, Czech Republic

potucek@troja.fjfi.cvut.cz

Crystals of incipient ferroelectrics KTaO_3 possess a cubic inversion symmetric perovskite-type structure down to the lowest temperatures although the frequency of temperature-dependent TO_1 soft phonon mode strongly decreases on cooling and the crystal structure appears unstable with respect to phase transitions. Nevertheless phase transitions can be induced even by rather low concentrations of suitable impurities. Very unusual temperature behavior of the zero-phonon line of photoluminescence of Cr^{3+} ions corresponding to ${}^2\text{E} \rightarrow {}^4\text{A}_2$ transition were previously observed on $\text{KTaO}_3:\text{Cr}$ crystals and associated with a strong interaction of the Cr^{3+} impurity center with temperature-dependent TO_1 soft phonon mode and with a local configuration instability of Cr^{3+} ion with the 3d^3 configuration in the ${}^2\text{E}$ excited state with respect to TO_1 mode related polar distortions [1].

Study of optical properties of model erbium ions in KTaO_3 crystals thus appears very attractive because it deepens knowledge of properties of optically active impurity centers in highly polarizable crystals with soft phonon modes and the tendency to structural and ferroelectric phase transitions. It can also bring valuable information about structure and phase transitions of this interesting model crystal. However, to our knowledge, optical properties of erbium doped KTaO_3 crystals have not been studied yet. Therefore, we performed a study of optical absorption and photoluminescence emission spectra on $\text{KTaO}_3:\text{Er}$ crystals within the wide temperature (12 – 300 K) and spectral (300 – 1600 nm) regions in order to reveal luminescence centers related to Er ions and to elucidate their optical properties. The blue tinted $\text{KTaO}_3:\text{Er}$ (500 ppm) crystals were grown in air by the top-seed-solution-growth method from a melt with excess of K_2O .

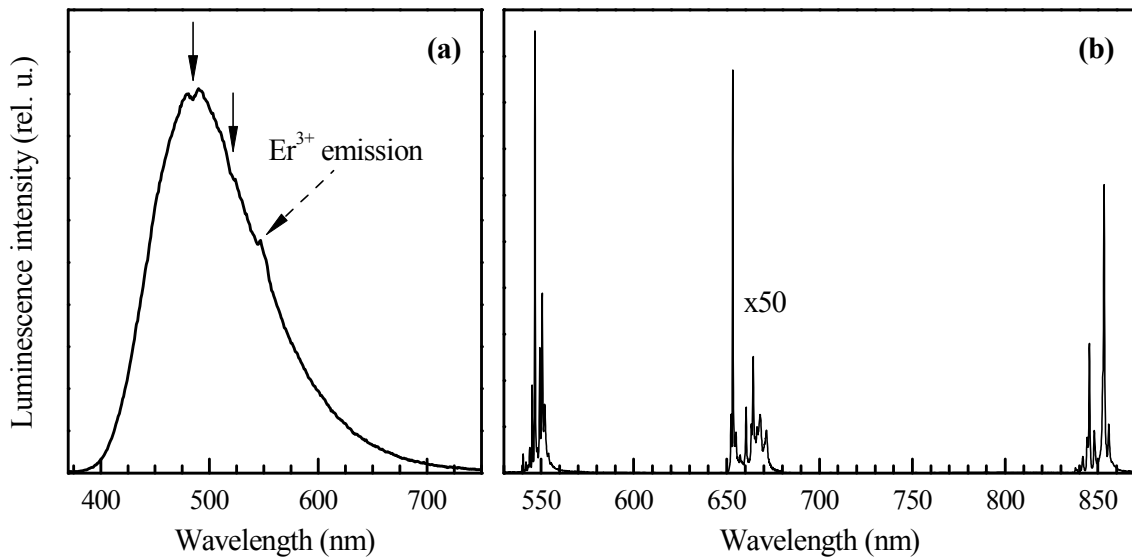
Under excitation with band-gap light ($\lambda < 345$ nm) at low temperatures, the studied $\text{KTaO}_3:\text{Er}$ crystals showed a broad asymmetric emission band peaking near 490 nm at 12 K that belongs to well-known visible photoluminescence of KTaO_3 crystals [2]. Emission spectrum in the Fig. 1a clearly demonstrates two narrow spectral regions in the vicinity of 486 and 522 nm where intensity of this photoluminescence is lower than in the case of usual smooth shape of this asymmetric emission band observed on pure KTaO_3 crystals. This reduction of photoluminescence intensity is caused by reabsorption of luminescence radiation in the $\text{KTaO}_3:\text{Er}$ crystal due to appearance of additional narrow absorption bands as a result of erbium doping. Altogether, five additional absorption bands peaking near 380, 408, 449, 486, and 522 nm were revealed in transmission spectra of the studied $\text{KTaO}_3:\text{Er}$ crystals at room temperature.

Excitation of the crystals via these narrow absorption bands enabled to observe narrow photoluminescence emission bands in the vicinity of 550, 660, and 850 nm. These emission bands consist of pronounced narrow zero-phonon lines accompanied by weak vibrational sidebands as the emission spectrum on the Fig. 1b illustrates. Spectral features of the additional emission and absorption bands appearing as a consequence of

erbium doping are characteristic for photoluminescence and optical absorption of Er^{3+} ions with $4f^{11}$ electron configuration in the visible and near infrared spectral region [3]. Therefore we attribute emission bands in the vicinity of 550, 660, and 850 nm to radiative transitions from the excited states $^4\text{S}_{3/2}$, $^4\text{F}_{9/2}$, and $^4\text{I}_{9/2}$ to the ground state $^4\text{I}_{15/2}$ of Er^{3+} ions in which splitting of free ion states by crystal environment is neglected. The absorption bands peaking near 380, 408, 449, 486, and 522 nm then correspond in this free ion approximation to transitions from ground state $^4\text{I}_{15/2}$ to excited states $^4\text{G}_{11/2}$, $^2\text{H}_{9/2}$, $^4\text{F}_{5/2}$, $^4\text{F}_{7/2}$, and $^2\text{H}_{11/2}$. We assume that Er^{3+} ions are substituted in KTaO_3 crystal in dodecahedral coordinated sites of K^+ ions on the basis of comparison of ionic radius of Er^{3+} , K^+ , and Ta^{5+} ion.

Analysis of temperature behavior of rich structure of zero-phonon lines observed in the photoluminescence emission spectra allowed us to specify a model of energy levels of Er^{3+} ions in the KTaO_3 crystal. However, interpretation of these levels with respect to splitting of states of free Er^{3+} ion by the ligand field will require to perform study of emission spectra on KTaO_3 crystals with a different concentration of erbium in order to exclude possibility that some observed zero-phonon lines originate from aggregations of erbium ions. The origin of vibrational sidebands was suggested on the basis of available Raman and neutron scattering data.

Fig. 1. Photoluminescence emission spectra of $\text{KTaO}_3:\text{Er}$ crystal at 12 K and excitation



with (a) 330 nm and (b) 380 nm light. Arrows mark spectral regions where reabsorption of photoluminescence occurs.

This research was supported by the grant No. 202/08/1009 of the Grant Agency of the Czech Republic and by the project MSM 6840770021.

- [1] V. A. Trepakov, A. V. Babinsky, V. S. Vikhnin, P. P. Syrnikov, *Ferroelectrics* 83 (1988) 127.
- [2] C. Fischer, C. auf der Horst, P. Voigt, S. Kapphan, J. Zhao, *Radiation Effects and Defects in Solids* 136 (1995) 85.
- [3] L. Smentek, B. G. Wybourne, *Optical Spectroscopy of Lanthanides*, CRC Press, London, 2007.

SCINTILLATION RESPONSE OF THE LIQUID PHASE EPITAXY GROWN YAG:CE THIN FILMS

P. Průša¹, J.A. Mareš², M. Nikl², M. Kučera³, K. Nitsch², A. Beitlerová², N. Solovieva², T. Čechák¹

¹ Faculty of Nuclear Sciences and Physical Engineering, Czech Technical University in Prague, Břehová 7, 115 19, Praha 1

² Institute of Physics AS CR, Cukrovarnická 10, 162 00 Praha 6

³ Faculty of Mathematics and Physics, Charles University, Ke Karlovu 3, 121 16 Praha 2
petr.prusa@centrum.cz, prusa@fjfi.cvut.cz

Nowadays, Ce-doped YAG thin crystalline plates are used in high resolution X-ray 2D-imaging with resolution even in μm range [1]. For such high and precise resolution, very thin scintillation films or thin crystalline plates are necessary. Now, the 2D-imaging screens are mainly single crystalline thin plates but also other technologies are used to prepare thin single crystalline films (SCF) or epitaxial layers [2], especially by the liquid phase epitaxy (LPE) method [3].

Generally, various kinds of fluxes are used in the LPE method to prepare SCF. However, using different fluxes could influence optical and scintillation properties of scintillating films, i.e. their photoelectron or light yields, energy resolution (FWHM) or time dependence of these scintillation properties. It has been reported that Pb^{2+} contamination occurring, when PbO based flux is used, leads to smaller light yield of LuAG LPE-grown films in comparison with crystals produced using Czochralski or Bridgman technique [4]. As Pb^{2+} emission is severely quenched at room temperature, decrease of scintillation efficiency due to Pb contamination and related nonradiative losses is expected. On the other hand, scintillation response of LPE-grown films appears to be faster because of the absence of shallow traps related to Lu_{Al} antisite defects [5,6,7]. These defects arise in crystals grown by Czochralski or Bridgman technique at high melting temperature.

As mentioned above, PbO based flux is not the only choice for LPE method and using flux without Pb , like BaO or MoO_3 based ones, luminescence quenching could possibly be avoided. In addition, using these fluxes, based on MoO_3 or BaO could also result in good time dependence of scintillation response.

The aim of this paper is to present and characterize scintillation response and properties, of various Ce-doped YAG LPE garnet crystalline films prepared by the LPE method, especially to compare the performance of samples produced using different fluxes, namely PbO , BaO and MoO_3 based.

Films were prepared from fluxes based on PbO and BaO by standard isothermal dipping technique onto YAG substrates of (111) orientation. MoO_3 samples were prepared using temperature gradient growth on the same substrate. Photoelectron yield (N_{phels}) was measured under α -particle excitation. Three α -emitting radionuclides were used: ^{241}Am (5.4856 MeV), ^{239}Pu (5.1566 MeV), and ^{244}Cm (5.8048 MeV). Dependence of photoelectron yield and energy resolution on the shaping time was measured as well within 0.5 – 10 μs time range. The experimental set-up consists of an HPMT photomultiplier, ORTEC NIM electronic modules and a multichannel buffer in PC

working in pulse-height mode was used [8]. Radioactive source was in direct contact with the measured sample. All measurements were performed at room temperature.

Penetration range (R) of α -particles emitted from ^{241}Am in YAG is $12.28 \mu\text{m}$. Thickness (d) of films of some samples is smaller than the range R of α -particles. However, because of the direct contact, α -particle penetrating under angle θ , $\cos \theta < d/R$, still deposits its entire energy. Ratio of number of α -particles depositing the entire energy to number detected α -particles $N_{\text{entire}}/N_{\text{detected}} = d/R$. For the thinnest sample $N_{\text{entire}}/N_{\text{detected}} = 27 \%$, still enough for determination of N_{phels} yield and FWHM.

Absolute values of $N_{\text{phels}}/\text{MeV}$ show expected results. $N_{\text{phels}}/\text{MeV}$ of samples produced using BaO based flux is the highest followed by $N_{\text{phels}}/\text{MeV}$ of samples produced using MoO₃ based flux, and samples prepared using PbO based flux have lowest $N_{\text{phels}}/\text{MeV}$. While for PbO based flux the Pb contamination is probably reason for lower $N_{\text{phels}}/\text{MeV}$, for MoO₃ based flux the unstabilized production technology may be responsible, as well as for large variations of $N_{\text{phels}}/\text{MeV}$ within this group.

Time dependence of N_{phels} shows slightly different results. Let $N_{\text{phels,fast}}$ be the number of photoelectrons of the fast scintillation component and $N_{\text{phels,entire}}$ number of all photoelectrons. Samples prepared using BaO based flux show the highest value of $N_{\text{phels,fast}}/N_{\text{phels,entire}}$. All samples prepared using MoO₃ based flux have lower $N_{\text{phels,fast}}/N_{\text{phels,entire}}$ than slowest sample produced using BaO based flux. It is possible that some shallow traps were created in these samples due to unstabilized technology of growth. $N_{\text{phels,fast}}/N_{\text{phels,entire}}$ of samples prepared PbO based flux shows high variations.

From the measured scintillation response also the energy resolution was obtained by fitting the Gaussian function to the photo-peak and evaluating full width at half maximum (FWHM). Comparison among the fluxes gives this result: FWHM generally decreases with increase of N_{phels} . FWHM varies from 8.9 % to 48.4 %. FWHM is practically independent on used flux, for best PbO sample FWHM = 10.0 %, for best BaO sample 9.6 %, and for best MoO₃ sample 8.9 %.

The BaO and MoO₃ fluxes are superior to PbO in respect of absolute $N_{\text{phels}}/\text{MeV}$ and BaO flux is superior to MoO₃ flux in respect of time response. Thus, technology of production based on BaO flux could lead to better scintillation thin films than the PbO.

[1] Crytur Ltd., Booklet material (www.crytur.cz), Turnov, Czech Republic.

[2] Yu. Zorenko, Phys. Stat. Sol. 2 (2005) 375.

[3] J.M. Robertson, M.V. van Tool, J.P.H. Heynen, W.H. Smits, T. de Boer, Philips J. Res. (1980) 354.

[4] V. Babin, V. Gorbenko, A. Makhov, J.A. Mares, M. Nikl, S. Zazubovich and Yu. Zorenko, J. Lumin. 127 (2007) 384.

[5] M. Nikl, Phys. Stat. Sol. (a) 202 (2005) 201.

[6] M. Nikl, V. V. Laguta, A. Vedda, Phys. Stat. Sol. (a) 204 (2007) 683.

[7] M. Nikl, E. Mihokova, J. Pejchal, A. Vedda, Yu. Zorenko and K. Nejezchleb, Phys. Stat. Sol. (b) 242 (2005) R119.

[8] J.A. Mares, A. Beitlerova, M. Nikl, N. Solovieva, K. Nitsch, M. Kucera, M. Kubova, V. Gorbenko, Yu. Zorenko, Rad. Measur. 42 (2007) 533.

TMA STUDY ON STRUCTURAL RELAXATION OF Ce DOPED Na-Gd PHOSPHATE GLASSES

M. Rodová^a, M. Chromčíková^b, K. Nitsch^a, and M. Liška^b

^A Institute of Physics AS CR, 162 00 Praha 6, Cukrovarnická 10, Czech Republic

^B ADU Trenčín and RONA, Študentská 2, Trenčín, SK-911 50, Slovak Republic
rodova@fzu.cz

Glasses prepared by quenching of the melt do not reach any equilibrium state but they seek to attain it. The time needed for the glass to reach this state is called structural relaxation and it is connected with time dependent changes in the structure of the glass during the relaxation process.

This contribution deals with the structural relaxation of Na-Gd phosphate glass with nominal composition of NaGd(PO₃)₄. The reason for this study was that this glass doped with Ce³⁺ is a promising material for the detection of neutrons, γ- and X-rays for medical and technical applications due to its low cost and high intensity of radioluminescence.

Glassy NaGd(PO₃)₄ samples were prepared by a rapid quenching technique in air. Structural relaxation of a rectangular glass specimen 4x4x20 mm in size was studied by thermomechanical analysis using a Netzsch TMA 402 under non-isothermal condition. So called intrinsic cycles, cooling and consecutive heating with rates of 10 and 5K/min were done in the temperature range between 550 and 750 K.

The structural relaxation of this glass was described by the Tool-Narayanaswamy-Mazurin model (TNMa) with application of Tool's fictive temperature and the Vogel-Fulcher-Tammann equation (VFT) for the viscosity dependence on temperature. Distribution of relaxation times is expressed by the empirical Kohlrausch-Williams-Watts function (KWW). The common non-linear least squares method was used in which the sum of squares of deviations between measured and calculated values of sample deformation was minimized [1,2].

The following relations are principal for description of structural relaxation in glasses:

$$\tau = \frac{\eta}{K} \quad (1)$$

where τ is the relaxation time and η is the dynamic viscosity a modulus K is the material constant.

Temperature dependence of dynamic viscosity of the melt was expressed by

$$\log \eta(T, T_f) = \left(A + \frac{B}{T_f - T_0} \right) \frac{T_f}{T} + \left(1 - \frac{T_f}{T} \right) \log \eta_0 \quad (2)$$

where T is the thermodynamic temperature, A , B and T_0 are adjustable parameters, T_f is the fictive temperature and η_0 stands for the limited value of the dynamic viscosity.

Distribution of relaxation times was expressed by the empirical KWW:

$$M(\xi) = \exp[-(\xi)^b] \quad (3)$$

where the parameter b ($0 < b \leq 1$) determines the width of the relaxation time distribution and ξ is the dimensionless relaxation time given by

$$\xi = \int_0^t \frac{dt}{\tau[T(t), T_f(t)]} \quad (4)$$

The sample height l is a function of both of thermodynamic and the fictive temperatures, $l = l(T, T_f)$. The viscous flows is included into the model by

$$\frac{1}{l} \left(\frac{\partial l}{\partial t} \right)_{T, T_f} = \frac{\sigma}{3\eta} \quad (5)$$

where σ is the axial stress and t is the time.

The relative sample length change ε can be explained by

$$\varepsilon = \frac{\Delta l}{l_0} \approx \int_{T_1}^{T_2} \alpha_g dT + \int_{T_{f,1}}^{T_{f,2}} \Delta\alpha dT_f - \left(1 + \int_{T_1}^{T_2} \alpha_g dT + \int_{T_{f,1}}^{T_{f,2}} \Delta\alpha dT_f \right) \int_{t_1}^{t_2} \frac{\sigma}{3\eta(T, T_f)} dt \quad (6)$$

where α_g and α_m are the coefficients of temperature expansion of isostructural glass and metastable equilibrium melt, respectively, and $\Delta\alpha = \alpha_m - \alpha_g$.

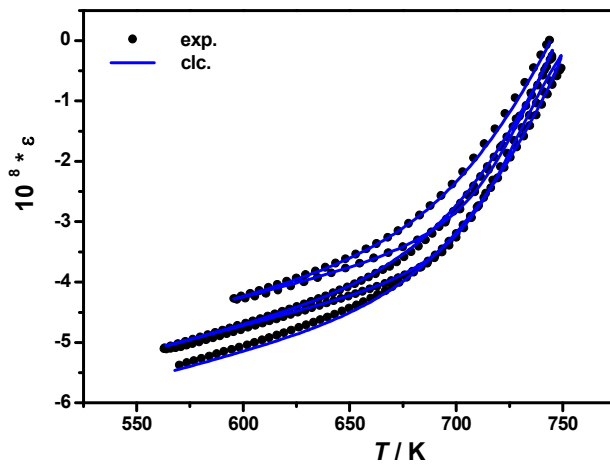


Fig. Temperature dependence of the relative sample length. Points – experiment, line – calculation.

The parameters of relaxation model such as A , B , T_0 and η_0 , were obtained by the non-linear regression analysis of temperature dependence of viscosity, whereas the modulus K , α_g , α_m and b were calculated using non-linear regression analysis of thermo-

mechanical experiments with used time-temperature regimes. The comparison of the temperature dependences of measured and calculated values of relative sample lengths is shown in Fig.

This work was supported from the Agency for Promotion Research and Development APVT-20-P06405, VEGA No. 1/3578/06 and the Grant Agency of the AS CR (No. IAA200100626).

- [1] M. Chromčíková, M. Liška, J. Term. Anal. Calor. 90 (2007) 421.
- [2] M. Chromčíková, K. Nitsch, M. Rodová, M. Liška, 30. Mezinárodní český a slovenský kalorimetrický seminář, Rožnov pod Radhoštěm 26.-30.5.2008, ISBN 978-80-7395-079-8, p. 163-166.

RECRYSTALLIZATION ANNEALING OF WIRES ON THE BASE W-Re UNDER VARIOUS CONDITIONS

K. Skotnicová, J. Drápala

VŠB-Technical Univerzity Ostrava, Department of Nonferrous Metals, Refining and Recycling, 17. listopadu 15, 70833 Ostrava-Poruba

Katerina.Bujnoskova@vsb.cz

The aim of the present work was to evaluate the influence of recrystallization annealing in vacuum electron beam zone melting furnace on the change of structural characteristics of tungsten wires alloyed with rhenium. Influences of the rhenium content, temperature and hot zone pass speed were studied.

Wires W-5 wt.% Re and W-26 wt.% Re, diameter 0.5 mm, delivered by the firm PLANSEE Metall GmbH with chemical certificate, underwent recrystallization annealing under various conditions. The annealing was performed at the Department of Nonferrous Metals, Refining and Recycling, VŠB-TU Ostrava and its conditions for individual specimens are presented in table 1. Several passes of hot zone through the wire specimens at constant speed in the vacuum about 10^{-2} Pa at high temperatures were carried out.

Table 1. Survey of specimens, conditions of recrystallization annealing and average grain size

Sample no.	Composition	Temperature of annealing	Speed of zone pass	Average grain size	Number of passes
	wt.% Re	°C	mm/min	mm	
1	W-26Re	1800-1850	3	30,05	1
2			6	26,91	1
3	W-26Re	2000	1	64,93	1
4			3	53,60	1
5			6	50,61	1
6	W-5Re	2000	1	143,12	3
7			3	117,25	3
8	W-5Re	2100	1	265,23	3
9			3	201,30	3

Crystalline lattice of metals after plastic deformation is characterized by a considerable amount of various types of defects and internal stress. Physical essence of recrystallization consists in creation of new grain nuclei in the deformed metal lattice followed by their growth due to the transition of atoms from the deformed crystalline lattice into the thermodynamically more stable lattice of nuclei. Numerous conditions have to be fulfilled when preparing single crystals of metals from the solid state by the method of recrystallization annealing: Utilization of high purity materials since admixtures obstruct the grain boundary migration and an uniform deformation to a critical degree in the whole specimen volume [1].

Localization of the nuclei formation and ensuring the continuous preferential crystal growth during the heating can be achieved if a convenient temperature gradient is created in the specimen.

In specimens W-26 Re annealed at the temperatures about 1800 and 2000 °C no distinct grain growth happened after one zone pass. The structure of specimens was uniform, greater size of grains was achieved for the lowest zone pass speed – see fig. 1. The temperature increase by cca 200 °C resulted in almost double grain enlargement – see table 1. The specimens W-5 Re were annealed at the temperatures 2000 and 2100 °C by three zone passes and speeds 1 and 3 mm/min. A considerable grain size increase was observed, however, a single crystal structure was not achieved. The structure of specimens annealed at the temperature 2000 °C was uneven for both the used zone pass speeds, it consisted of grains of various size, ranging from 80 to 290 μm for the speed 1 mm/min and from 60 to 180 μm for the speed 3 mm/min. The annealing temperature increase by 100 °C resulted in the grain enlargement, the structure was again uneven and the grain size ranged from 200 to 450 μm for the speed 1 mm/min and from 160 to 300 μm for the speed 3 mm/min – see fig. 2.

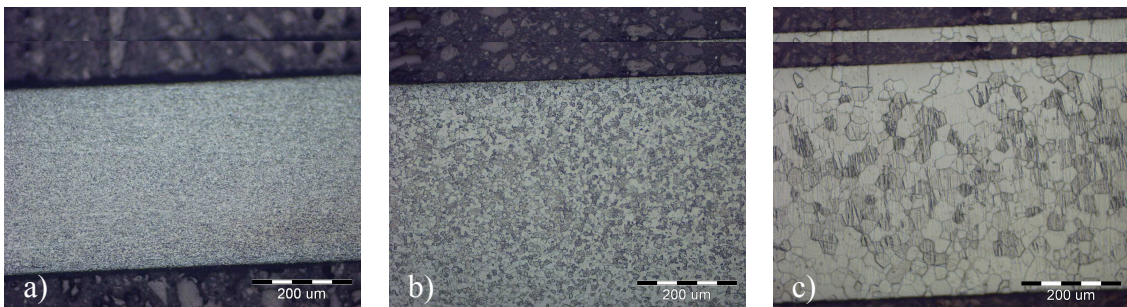


Fig. 1 Structure of specimens W-26 Re a) initial state and annealed at the temperature 1800 °C, one zone pass: b) 3 mm/min, c) 1 mm/min

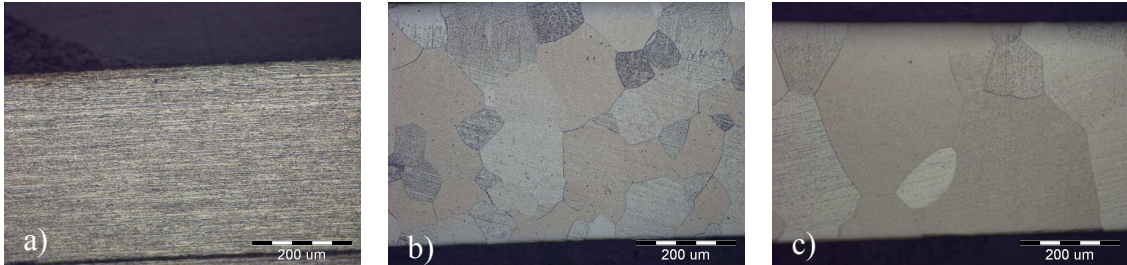


Fig. 2 Structure of specimens W-5 Re a) initial state and annealed at the temperature 1800 °C, one zone pass: b) 3 mm/min, c) 1 mm/min

It is evident that rhenium precipitated on the grain boundaries obstructs an efficient grain boundary migration. A negative property of the material prepared in this way is also its considerable brittleness. High temperatures, low speed and several passes of hot zone, high purity input material and deep vacuum will be necessary for obtaining a single crystal structure of wire on the base W-Re. A prospective application of these materials appears to be the production of thermocouples with long-term lifetime for measuring very high temperatures.

The present work was solved in the frame of the research project of the Czech Science Foundation No. GP106/06/P288 „Preparation and study of characteristic properties of binary and ternary low-alloyed alloys single crystals of tungsten and molybdenum“.

[1] Lyakishev, N.P. and Burkhanov, G.S. Metallic single crystals. Moscow, Eliz, 2002, 312 p., ISBN 5-901179-04-8. in Russian.

GROWTH AND CHARACTERIZATION OF GaN:Mn LAYERS BY MOVPE

Z. Sofer¹, D. Sedmidubský¹, J. Stejskal¹, J. Hejtmánek², M. Maryško², K. Jurek²,
V. Havránek³, A. Macková³, M. Václavů⁴

¹Institute of Chemical Technology, Technická 5, 166 28 Prague, Czech Republic

²Institute of Physics AS CR, v.v.i., Cukrovarnická 10, 162 53 Prague, Czech Republic

³Nuclear Physics Institute of the AS CR, v.v.i., 25068 Řež, Czech Republic

⁴Faculty of Mathematics and Physics, Charles University, Ke Karlovu 3, 12116 Prague 2, Czech Republic

zdenek.sofer@vscht.cz

Gallium nitride doped by manganese belongs to wide band gap diluted magnetic semiconductors. This material is a promising candidate for spintronic applications. The main potential for future application of this material is due to ferromagnetic state persisting well above room temperature. The magnetic behavior was theoretically predicted and experimentally evidenced on thin films prepared by diverse techniques. However, only few reports [1, 2] have appeared on MOVPE growth and characterization for Ga_{1-x}Mn_xN so far.

In this paper we present a growth of Ga_{1-x}Mn_xN layers by MOVPE. GaN templates were grown on (0001) sapphire substrates in a horizontal reactor. These “pseudo substrates” were grown in pure hydrogen atmosphere with V/III ratio 1360. The deposition temperature was 1100 °C and the pressure 200 mbar. The thickness of the whole GaN template was about 2.6 μm. For the deposition of Ga_{1-x}Mn_xN layers, bis(methycyclopentadienyl) manganese was used as Mn - precursor. The precursor was evaporated at a pressure of 1000 mbar and the temperature of the bath was 16 - 25 °C. We used hydrogen carrier gas for this precursor with a flow 100 – 500 sccm. The total flow was 3700 sccm and the concentration of nitrogen in carrier was 40 %. The deposition temperature was varied from 900 to 1100 °C and the pressure was 200 mbar.

V/III ratio was 1360. A typical thickness was 0.25 μm.

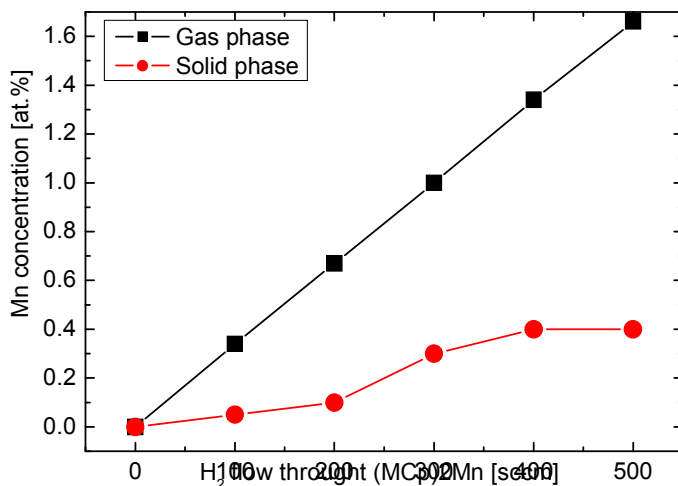


Fig. 1: The dependences of Mn concentration in the layer and in the gas phase on the hydrogen flow through Mn

The X-ray diffraction proved the wurtzite phase without any secondary phase related to Mn. The Mn concentration detected

by electron microprobe and PIXE was well below the solubility limit, ranging from 0.2 to 0.7 at %. The dependence of Mn concentration on hydrogen flow through the bubbler was not linear (figure 1). The surface morphology was influenced by Mn doping of the layer. A small concentration of Mn (below 0.3 at %) acts like a surfactant and led to the improvement of surface morphology compared to undoped layers. The Hall measurements conducted at room temperature revealed n-type charge carriers reaching typical concentrations $1 \times 10^{18} \text{ cm}^{-3}$ and mobilities $230 \text{ cm}^2 \cdot \text{V}^{-1} \cdot \text{s}^{-1}$.

From the isothermal magnetization data recorded on SQUID magnetometer, three main components can be separated – a strong diamagnetic signal from the substrate and GaN template as well as two weak contributions from the $\text{Ga}_{1-x}\text{Mn}_x\text{N}$ film - a paramagnetic component characterized by Brillouin $M(H)$ dependence at the lowest temperatures and a nearly temperature independent ferromagnetic component persisting above 300 K. The dependence of magnetic moment on magnetic field is shown on figure 2. The coercivity of $\sim 70 \text{ Oe}$ taken from hysteresis loops at 120 K also infers a soft FM behavior.

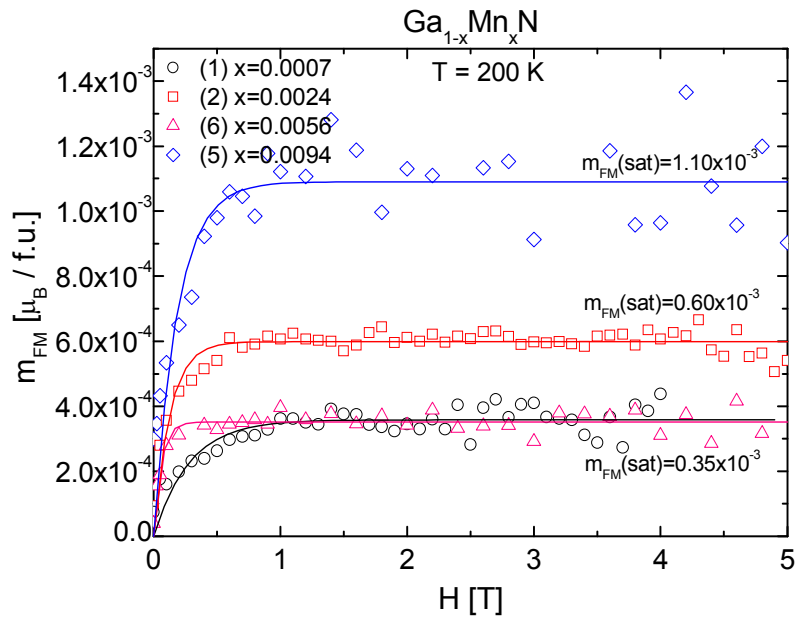


Fig. 2: The dependence of the magnetic moment of the samples at $T = 200 \text{ K}$ on the applied magnetic field.

This work was supported by the Czech Science Foundation, grant GA104/06/0642 and the Ministry of Education of the Czech Republic, project MSM6046137302

[1] M.H. Kane, M. Strassburg, W.E. Fenwick and A. Asghar et.al., J. Cryst. Growth 287 (2006) 591
 [2] X. Yang, Z. Chen, J. Wu and Y. Pan et.al. J. Cryst. Growth 305 (2007) 144

NUCLEATION OF VOIDS IN SOLID MATERIALS: TIME LAG

A. Sveshnikov, P. Demo, P. Tichá, Z. Kožíšek

Institute of Physics, Academy of Sciences of the Czech Republic, Cukrovarnická 10,
162 53, Praha 6

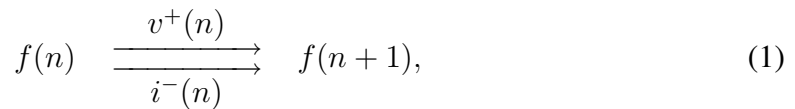
sveshnik@fzu.cz

Nucleation of voids in solid materials under influence of different types of external perturbations (for example, a flux of fast neutrons [1], highly energetic ions or electrons [2], γ -irradiation [3], mechanical tension) is well experimentally studied. However, the theoretical description of the process is quite complicated.

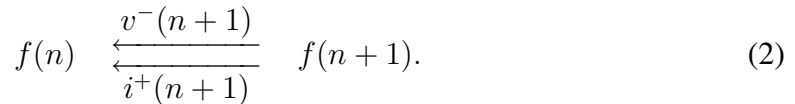
A common approach to the problem is based on a standard nucleation theory, where large “clusters” (pores) are considered to be growing by attachment and detachment of “monomers” (single vacancies). It is clear, though, that the absorption of vacancies is not the only way for the pore to grow. Pores may grow or shrink by absorption of other kinds of defects also, such as, for example, interstitials. Thus, a better method to describe the process of voids formation in a solid matter would involve a consideration of nucleation of at least two different types of monomers — vacancies and interstitials.

Since we have monomers of different kinds in the system, it seems logical to utilize the standard multicomponent nucleation theory. Several such attempts have been made recently [4]. This approach, however, does not take into account the following specifics of voids formation, which makes the application of standard multicomponent nucleation theory in this situation at least questionable. Really, growing voids are characterized by only one variable — their size n . It does not make sense to talk about a number of vacancies and a number of interstitials in the void separately. For example, the void with n_v vacancies and n_i interstitials is physically indistinguishable from the void with $n_v + 1$ vacancies and $n_i + 1$ interstitials.

Consequently, the reaction scheme involves two separate currents of monomers of different kinds which both influence the same state variable of the growing cluster:



and



Here $f(n)$ stands for a distribution function of voids with respect to their sizes, while v^\pm and i^\pm represent transition probabilities of vacancies and interstitials.

The attachment probabilities v^+ and i^+ can be determined from kinetic AI consideration:

$$x^+(n) = \gamma n^{2/3} \frac{N_A kT}{V_M h} C_x, \quad x = v, i, \quad (3)$$

where γ is geometrical factor connected with the shape of void, N_A is Avogadro's constant, V_M represents the molar volume, h is Planck constant and C_x is initial molar fraction of the vacancies (resp. interstitials).

This leads to the following evolution equation of the system:

$$\frac{\partial f(n, t)}{\partial t} = -\frac{\partial J(n, t)}{\partial n}, \quad (4)$$

where the flux $J(n, t)$ is given by the expression

$$J(n, t) = (v^+(n) + i^-(n) - v^-(n) - i^+(n))f(n, t) - \frac{1}{2} \frac{\partial}{\partial n} \left((v^+(n) + i^-(n) + v^-(n) + i^+(n))f(n, t) \right).$$

This equation resembles the standard master equation of one component nucleation theory. If we would have considered the fluxes of vacancies and interstitials independently, we would obtain instead of (4) the equation of 2-component nucleation:

$$\frac{\partial f(n_v, n_i, t)}{\partial t} = -\frac{\partial J_v(n_v, n_i, t)}{\partial n_v} - \frac{\partial J_i(n_v, n_i, t)}{\partial n_i}. \quad (5)$$

After one obtains the solution of (5), he needs to perform the convolution of 2-component distribution function $f(n_v, n_i, t)$ to obtain the physically meaningful distribution function of voids:

$$f(n, t) = \int f(n + n_i, n_i, t) dn_i. \quad (6)$$

On the first glance, the result of convolution (6) will coincide with the direct solution of (4), since equation (4) is, in fact, the result of convolution of (5). The important difference arises, however, from the initial and boundary conditions.

The equation (4) is defined on the positive semi-axis and its boundary condition determines the value of distribution function $f(0, t)$ at the origin. On the other hand, the equation (5) is defined on the quarter of a plane with cyclic boundary conditions. Different topology of domains of definition of both equations exhibits itself in difference of characteristic times of evolution of distribution function. Equation (4) predicts faster growth of voids than equation (5), because in the latter case evolution is slowed down by non-physical diffusion of distribution function in direction of characteristics $n = n_v - n_i$.

Thus, the incorporation of the restriction $n = n_v - n_i$ into the standard nucleation theory yields shorter time lag of formation of voids.

The work is done with the support from project No. IAA100100806 of Grant Agency of the Czech Republic.

- [1] Russel, K. C. (1971) In: Acta Metallurgica 19, pp. 753–758.
- [2] Katz, J. L., Wiedersich, H. (1971) In: J. Chem. Phys. 55, pp. 1414–1425.
- [3] Vodak, F., Trtik, K., Sopko, V., Kapickova, O. and Demo, P. (2005) In: Cement and Concrete Research 35, pp. 1447-1451.
- [4] Demo, P., Vodak, F., Ticha, P. and Sveshnikov, A. M. (2006) In: Physical and Material Engineering 2006, pp. 22-24.

DEVELOPMENT OF 150 MM SILICON WAFER FOR X-RAY SPACE OPTICS

J. Šik¹, P. Kostelník¹, M. Pospíšil¹, R. Hudec²

¹ ON Semiconductor Czech Republic, 1. máje 2230, 756 61 Rožnov pod Radhoštěm

² Astronomical Institute, Academy of Sciences of the Czech Republic, 251 65 Ondřejov
jan.sik@onsemi.com

Future large space X-ray telescopes (such as the ESA's XEUS [1]) require precise and light-weight X-ray optics. Novel approaches are employed to find suitable substrates for mirrors, i.e., to achieve required precise X-ray optics geometries with the fine surface micro-roughness. Among technologies using glass foils, amorphous metals, ceramics, and glossy carbon, the solution based on commercially available silicon wafers manufactured for semiconductor industry is considered as one of the most promising. Collaboration of Si wafer manufacturer ON Semiconductor Czech Republic with Czech scientific institutes (Astronomical Institute ASCR, Czech Technical University, Institute of Chemical Technology and others) has been established in order to study the high precision X-ray optics based on the Si wafers. The first tests of shaping Si wafers (of typical size 10 cm x 10 cm) for mirror application have been already published [2-3].

Relatively light (silicon volume density is 2.33 g.cm^{-3}) and circular shaped wafers are commercially produced in diameters of 100 - 300 mm with the thickness of 380 - 780 μm . During the manufacturing process, wafer is lapped or ground to obtain parallel surfaces with thickness homogeneity better than 1 μm and finally polished to mirror-like surface with very low micro-roughness of about 0.1 nm. To achieve these parameters, the production of Si wafers needs to be modified and optimized during the production stages.

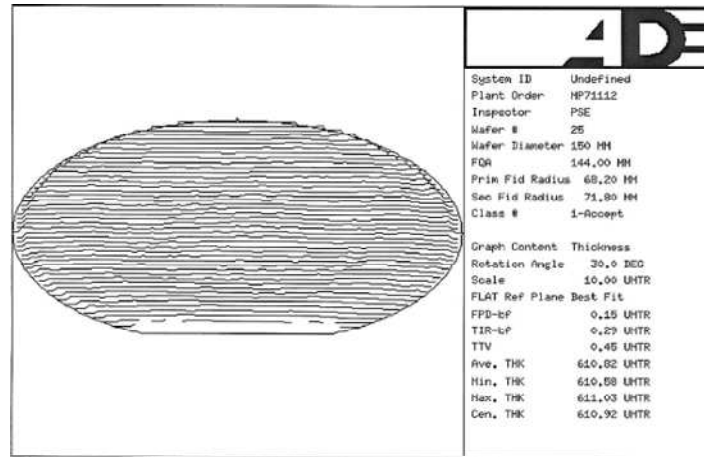


FIG. 1: Example of the flatness measurement of 150 mm silicon wafer developed for sub-micron technologies in ON Semiconductor. Thickness in the wafer center (Cen. THK) is 610.92 μm , minimal measured thickness (Min. THK) is 610.58 μm , and maximal measured thickness (Max. THK) is 611.03 μm . Total thickness variation (TTV = Max. THK – Min. THK) is 0.45 μm . Measured in 1275 points with ADE 7000.

Flatness measurements of 150 mm polished Si wafers recently developed in ON Semiconductor for technologies with sub-micron photolithographic detail can be found in FIG. 1. Thickness variability on the whole wafer area is less than 0.5 μm .

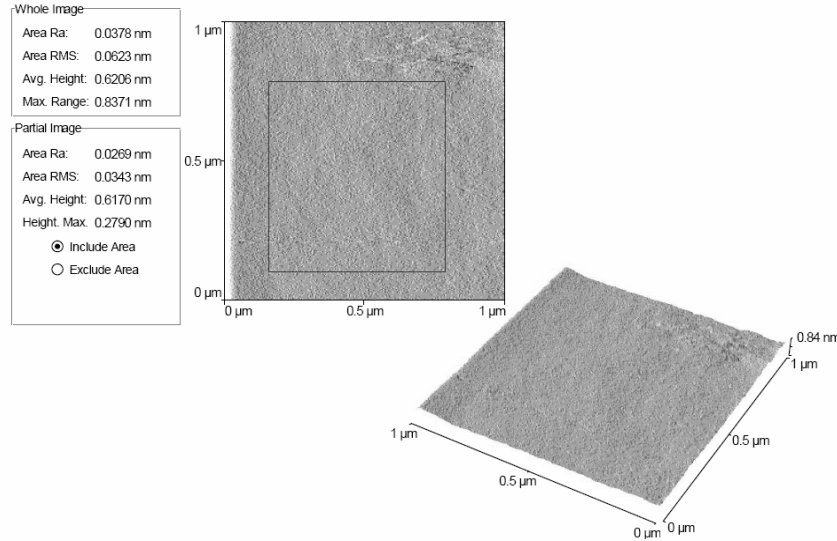


FIG. 2: Surface roughness of polished silicon wafer measured with AFM at Masaryk University Brno. Crystallographic orientation (100), Czochralski Si wafer heavily doped with arsenic. Measured area 1 μm x 1 μm , Ra = 0.04 nm, RMS = 0.06 nm.

Another important parameter for applications in the fine X-ray imaging is the surface micro-roughness. We show the example of surface roughness measurement with AFM in FIG. 2. These results confirm the superior surface micro-roughness of polished Si wafers meeting the requirements of X-ray optics applications. Based on our analysis and early investigations, the crystallographic orientation (100) is the optimal solution due to its superior surface quality. RMS values of polished (100) surface can be as low as ~ 0.1 nm or even slightly lower (measured with AFM).

There are basically only two limitations for achieving superior micro-roughness: (i) defects and particles on the surface and (ii) atomic steps on the surface. In silicon, atomic steps of the high of 0.314 nm are characteristic for surface with crystallographic orientation (111) and only 0.135 nm for (100) surface. The lateral distance between the neighboring steps is determined by surface deviation from (111) or (100) plane (off-orientation). Surface quality after chemical-mechanical polishing depends on silicon mechanical properties given also by impurity concentrations. Native oxide on the surface grown in ambient conditions is usually 1-2 nm thick and does not change surface roughness [4].

[1] <http://www.esa.int/science/xeus>

[2] R. Hudec, et al., Proceedings of SPIE 51st Annual Meeting, San Diego 2006.

[3] R. Hudec, et al., Proceedings of SPIE Astronomical Instrumentation, Marseille 2008.

[4] A. Crossley, et al., Journal of Non-Crystalline Solids 187 (1995) 221-226.

DETERMINATION OF DISTRIBUTION COEFFICIENTS OF ADMIXTURES IN TUNGSTEN AND MOLYBDENUM SINGLE CRYSTALS

J. Štěpánek, K. Skotnicová

Faculty of Metallurgy and Material Engineering, VŠB-Technical University of Ostrava,
17. listopadu 15/2172, CZ 708 33 Ostrava, Czech Republic

jan.stepanek.fmmi@vsb.cz

Single crystals of high-melting metals and their alloys represent new types of perspective materials, which are applied in modern fields of electrical engineering, micro-electronics, opto-electronics, vacuum techniques, nuclear power engineering, etc. The biggest attention during their preparation is paid crystallisation from a melt. The most important material parameter at these methods of preparation is the distribution coefficient k , which indicates distribution of admixtures in solid and liquid phases.

Experiments with use of electron zonal melting required preparation of low-alloyed alloy from the systems W-Mo, W-Ta, W-Nb, Mo-W, Mo-Ta, Mo-Nb. Poly-crystalline tungsten and molybdenum bars of diameter 4 and 6 mm were used as initial materials. Grooves with diameter of 1 mm, depth 0.7 mm and length approx. 20 cm were milled into them. Shreds of Ta and Nb sheets were inserted into these grooves and they were afterwards wrapped with wire made of basic metal. The bars thus prepared were placed into electron zonal furnace, in which the alloying was made.

Alloyed tungsten and molybdenum bars were re-melted in electron zonal furnace progressively by three rates of movement of the molten zone. The beginning of the bar was re-melted at the rate of 3 mm/min, its central part at the rate 5 mm/min and its end part at the rate 1 mm/min over the length 4.5 to 7.5 cm. At the end of each section the molten zone has solidified at high rate so that no diffusion processes could occur in it. Rapid solidification of the zone was achieved by sudden switching stopping of heating, while high rate of solidification was ensured by efficient heat removal by adjoining zones of crystal.

Structure of all the samples of single crystals was composed of sub-grains of the first and second order with disorientation angle of their borders of several minutes. Alloying of tungsten and molybdenum caused crumbling of block structure of single crystals, i.e. reduction of dimensions of sub-grains and increase of disorientation angle of their borders. At the same time density of dislocations increased. In the area of solidified zone a poly-crystalline structure was observed with traces of dendritic formations, as well formation of cell-filamentous structure.

Determination of effective distribution coefficient was realised by three different methods, namely method of solidified zone (MZZ), method by Vigdorovič and Ivlev (VI) and method by Burton-Prim-Slichter (BPS).

Chemical analysis of samples in longitudinal direction was made by electron dispersive wave method in the laboratories of the company Vítkovice – Výzkum a vývoj, s.r.o. The data obtained by the EVDM were used for determination of the value of effective concentration profiles by method of solidified zone. This is comparatively accurate method for determination of the value of effective distribution coefficient at electron zonal melting. Its principle is based on comparison of admixed element in the

zone $\overline{x_{LB}}$, which is solidified at high rate at the experiment, so that no diffusion processes could occur in it with concentration of admixtures at the place right before the solidified zone.

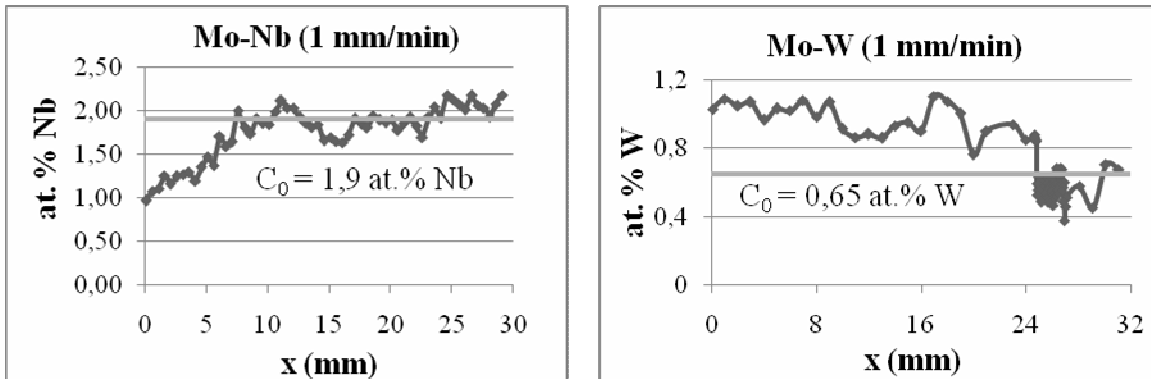


Figure 1. Concentration profiles of two complete samples

Table 1. Comparison of values of effective distribution coefficient for calculations by various methods

It is obvious from comparison of effective distribution coefficients of admixtures in basic metals (tab. 1), that the values for MZZ and BPS are very similar and they fulfil the condition that the value k_{ef} lies between k_0 and 1. The values k_{ef} according VI do not fulfil this condition in the system Mo-Nb. It is probably caused by sensitivity of this method to input data, particularly to the input average concentration of C_0 and to the width of the zone b .

Bujnošková, K., Dissertation thesis, Ostrava, 2004.

Kuchař, L., Drápala, J. R. Kammel Foundation, Košice, 2000, 170 pp.

Kuchař, L., VŠB-TU Ostrava, 1988, 338 pp.

Štěpánek, J., Graduation thesis, Ostrava, 2007, 63 pp.

This work was created within solution of the grant projects GA ČR No. 106/06/P288 „Preparation and investigation of characteristic properties of single crystals of tungsten and molybdenum based binary and ternary alloys”.

ASSESSMENT OF CALCIUM IONS CONCENTRATION IN SETTING CEMENT PASTES WITH VARIOUS WATER/CEMENT RATIOS

P. Tichá^{1,2}, P. Demo^{1,2}, Š. Hošková¹, A. Sveshnikov^{1,2}, Z. Kožíšek²

¹ Department of Physics, Faculty of Civil Engineering, Czech Technical University in Prague, Thákurova 7, 166 29 Prague 6, Czech Republic

² Institute of Physics, Academy of Sciences of the Czech Republic, Cukrovarnická 10, 162 00 Prague 6, Czech Republic
tichap@centrum.cz

Abstract

Formation of clusters from monomers like calcium and hydroxide ions represents basic conception in description of cement paste setting by means of nucleation theory. Decrease of monomers' number density is closely linked to clusters' growth in the system of hydrated cement paste. Monomers' densities are crucial input parameters which enter the equations governing the nucleation processes.

1. Introduction

Setting of cement paste is triggered by chemical processes of hydration when monomers, like Ca^{2+} and OH^- , are formed. These charge carriers, which are free to move within the system, contribute to the acceleration of cement setting. The accelerating impact varies according to their concentration, electric charge, temperature, and geometrical size [1]. Calcium ions are acknowledged to have the strongest accelerating effect in cement paste [2].

Our approach to cement paste setting is based on the model of nucleation when the sub-nanosized domains of a new, solid phase are formed via sufficiently large fluctuations. Such domains, or clusters, grow only if they consist of more particles than n_c , which is the so called critical cluster size. The critical size n_c of cluster can be derived from extremum condition for change of Gibbs free energy [3] and is equal to the third power of temperature dependent surface energy $\sigma(T)$ between cluster and its environment, and to $(\ln \mathcal{S})^{-3}$, where \mathcal{S} is given supersaturation of the system (water + cement). It is evident that critical size decreases with increasing supersaturation, and, therefore, more clusters fulfil the condition of further stable growth. On the other hand, the lower value of the surface energy, the smaller critical size of cluster.

Other vital parameters of setting are temperature and water-to-cement (w/c) ratio. The goal of the executed experiments was to assess the impact of different w/c ratios in respect to the time behaviour of calcium ions concentration. Moreover, temporal dependency of Ca^{2+} concentration represents boundary condition related to equations governing the evolution of newly-forming clusters distribution. The results will be used in the computation of numerical solution of nucleation equations.

2. Experiments and results

Actual concentration of calcium ions has been determined by a modified analytical chelatometric method for cement pastes with w/c ratios ranging from 0.35 to 0.55 in steps of 0.05. Obtained temporal dependencies of calcium concentrations are depicted in Fig. 1.

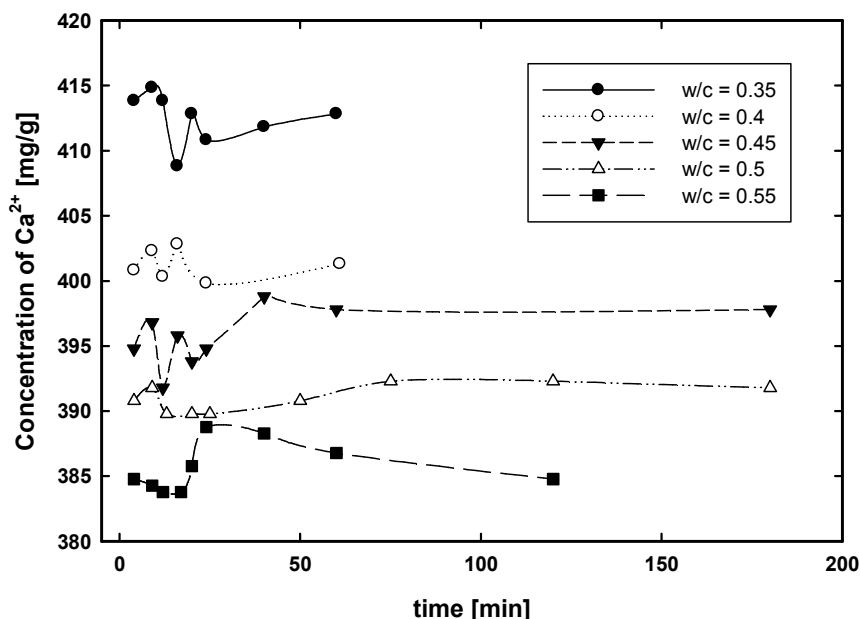


Fig.1. Time evolution of calcium ions concentration in setting cement paste for various w/c ratios. Measurements were taken at constant temperature of 25 °C.

3. Discussion

In general terms, setting of cement paste can be related to a change from a fluid material to a rigid state. Whereas the term setting is used to describe the stiffening of the cement paste, hardening refers to the gain of strength on a set cement paste [4].

Apparently, there exists a simple relation between the parameter of supersaturation and the w/c ratio; by its definition, the supersaturation increases with decrease in w/c ratio. Monomers' concentration and w/c ratio are mutually related when the following model is considered: the bigger supersaturation, the more building units (monomers) are present in the system which increases the probability of cluster creation that inherently accelerates the setting of cement paste. The measured temporal dependencies of calcium concentration are in accordance with such assumptions. The results show lower Ca^{2+} concentrations for larger w/c ratios (ie, smaller supersaturations) which means longer setting of cement paste.

This work was supported by the Ministry of Education of the Czech Republic under project No. CEZ MSM 6840770003. P. Tichá also acknowledges support by CTU under Project No. CTU0800111.

- [1] Taylor H.: Cement Chemistry, second edition, Academic Press 1997, p.335.
- [2] Kantro D. L., J. Testing. Evaln. 3, 1975, p. 312.
- [3] Tichá P., Demo P., Semerák P.: Proceedings of workshop 2007, part A, 2007, vol. 11, p. 44.
- [4] Neville A. M.: Properties of Concrete, third edition, Longman Scientific and Technical, 1986, p. 19.

MAGNETIC CZOCHRALSKI GROWTH OF SILICON

L. Válek, J. Šik, M. Lorenc

ON Semiconductor Czech Republic, 1. máje 2230, 756 61 Rožnov pod Radhoštěm
lukas.valek@onsemi.com

Most of the state-of-the-art electronics is based on silicon technology. Devices and integrated circuits are fabricated on silicon wafers made from silicon single crystals. Silicon crystals are grown predominantly by the Czochralski (CZ) technique [1] based on pulling from the melt. Present CZ processes produce (on the industrial scale) silicon single crystals of 100-300 mm in diameter, and further diameter growth is considered. While growing larger and larger crystals brings many difficulties, at the same time, requirements on crystal parameters steadily toughen. Consequently, novel methods become employed during the industrial growth of silicon, use of magnetic field being one of them. Application of magnetic field for semiconductor crystals can be traced back to 1960'. In 1980, the magnetic field was for the first time used also for the CZ growth of silicon single crystals. Since then the magnetic Czochralski (MCZ) method has received considerable attention and developed mainly in conjunction with the development of large-diameter crystals.

The principal aspect of MCZ lies in the appearance of the Lorentz force, which arises from the interaction of magnetic field with the flow of the highly electrically conductive silicon melt. The specific effect on the melt flow varies among different types of applied magnetic field. Table 1 reviews some of the basic types of magnetic field, describes the effect of the field on the melt flow and gives notes on industrial applications. The most important effects of the magnetic field consist in (a) damping of melt temperature fluctuations and (b) the possibility of tuning incorporation of impurities into the crystal.

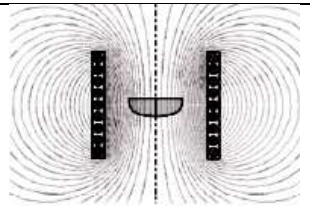
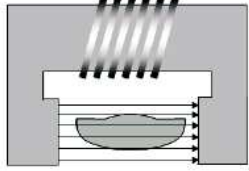
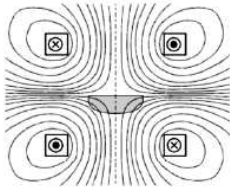
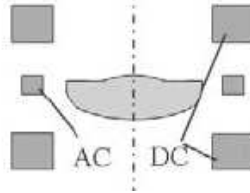
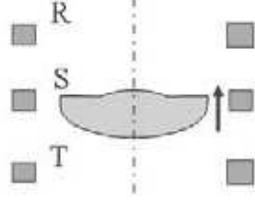
ad (a) Stability of the melt temperature is one of the crucial conditions for the dislocation-free growth of the crystal. Slowing down the melt flow, which is the consequence of static magnetic fields, reduces the turbulent nature of the flow, and thus reduces the fluctuations of melt temperature. Dynamic fields stabilize the flow in a different way, namely by driving the specific flow pattern. Both types of magnetic fields have positive effect on the crystal growth.

ad (b) The silicon melt is intentionally doped with impurities such as B, As, P or Sb in order to control electrical properties of the wafers. Another important impurity inherently bound to CZ silicon is oxygen, which is dissolved into the melt from the silica crucible. The concentration of oxygen in the growing crystal depends on the dissolution rate of silica (driven by the flow conditions near the crucible wall), on the melt flow pattern and on the state of the boundary layer at the melt-crystal interface (which again relates to the melt flow). Incorporation of dopant into the crystal proceeds through the boundary layer as well. Magnetic fields strongly affect the melt flow and so offer wide possibilities for tuning the dopant and mainly oxygen distribution in the grown silicon crystal.

The possibility of oxygen tuning is a strong motivation for use of the MCZ processes. Meeting tough specifications of advanced silicon wafers is often impossible without a precise oxygen control allowed by MCZ. Due to the very low oxygen

concentration achievable, MCZ silicon may even replace the expensive float zone (FZ)

Table 1. Overview of MCZ processes. The pictures show alignment of magnetic field with respect to the silicon melt. O_i - concentration of interstitial oxygen in the crystal.

Field type	Static magnetic fields		
	Axial	Transversal (horizontal)	Cusp
Schema			
Effect	damping of melt flow and temperature fluctuations		
		damped vertical flow	damped flow only near crucible walls
Positives	easiest installation	suitable for low O_i	low O_i possible
Negatives	flow instabilities	disturbed symmetry	not known
Industrial use	not frequently used	common for crystals of diameter > 300 mm	common for crystals of diameter < 300 mm
Field type	Dynamic magnetic fields		
	Rotating	Combined (pulsating)	Travelling
Schema			
Effect	stabilization of melt flow by driving it, damping of temp. fluctuations		
Positives	order of magnitude weaker field (10^{-3} T) compared to static fields		
Industrial use	practically not used, under development and being considered for industrial use		

silicon in certain applications. The many possibilities MCZ brings imply also many new degrees of freedom for the crystal growth process. Therefore, computer simulations are widely employed for study and basic setup of the MCZ processes. Results of MCZ simulations while using the FEMAG code [3] will be presented to demonstrate the effect of magnetic field on the growth process of silicon single crystals.

[1] M. Lorenc, J. Šik, L. Válek, proceedings of The 3rd School on Crystal Growth 2004, editor K. Nitsch, M. Rodová, MAXDORF Praha (2004) 48-57.

[2] W. von Ammon et al., proceedings of The 15th Riga and 6th PAMIR Conference on Fundamental and Applied MHD (2005) 41. <http://ipul.lv/pamir/>.

[3] <http://www.femagsoft.com>.

GROWTH OF INDIUM PHOSPHIDE CRYSTALS FOR RADIATION DETECTION OTHER APPLICATION

L. Pekárek¹, R.Yatskiv²

¹Institute of Physics v.v.i. AS CR, Na Slovance 2, 182 21 Praha 8

²Institute of Photonics and Electronics, v.v.i. AS CR, Chaberska 57, 182 51 Praha 8

yatskiv@ufe.cz

Indium phosphide is commonly used in the high frequency technology and optoelectronics. It is also a promising material for the room temperature X, γ and particle detection. Efficiency of this detection is equal to $\mu\tau E$ product, where μ is carrier mobility, τ is carrier lifetime and E is the applied electric field [1-3]. For application of higher electric fields it is necessary to use semi-insulating InP with resistivity 10^5 to $10^7 \Omega\text{cm}$.

InP single crystals were prepared by the liquid encapsulation Czochralski method, with boron oxide encapsulant. The initial poly-crystalline InP was synthesized and grown by the vertical gradient freeze low pressure method. The growth rate at the Czochralski pulling was 1.5cm/hour under pressure of nitrogen 4.5 to 5.0MPa. Crystals were cut in the [100] and [111] orientation and chemo-mechanical polished on both sides to 400 μm for the epitaxial technology and 200 to 250 μm Schottky barrier method.

InP radiation detector is a thin wafer with two circular metal contacts on the both opposite sides. Cathode and anode electrodes 1mm in diameter were prepared by vacuum evaporation of Au metal {50nm} and eutectic alloy AuGeNi{200nm}, respectively. For radiation detection the P/N junction made of liquid phase epitaxy was also used.

The InP crystals were characterized by measurements of resistivity ρ and Hall coefficient R_H . Concentration (n, p) and mobility ($\mu_{h,e}$) of electrons or holes were evaluated by using relations, $n, p = -1/(q * R_H)$ and $\mu_{e,h} = -R_H/\rho$. Measurements of detector performance were carried by using ORTEC electronic chain. The pulses produced by incident particles were amplified by charge-sensitive preamplifier (CSA) (ORTEC 142A) with bias load resistor 100 M Ω . Following Gaussian shaping used to enhance the signal to noise ratio was performed by the ORTEC 572A spectroscopy amplifier with impedance input about 500 Ω , which accepted positive or negative input pulses with rise and fall times < 650 ns and > 40 ns, respectively. Finally, the signals from the shaping amplifier output were digitized and processed by 8k MCA (PCI Trump Card) and stored on the computer, using Maestro 32 MCA emulator software.

Tab 1. Electrical parameters of InP crystals for the epitaxy and other applications.

Crystal	Dopant	Resistivity [Ωcm]	Hall mobil. [$\text{cm}^2/\text{V.s.}$]	Concentration [cm^{-3}]	Conduc .type
M 125	Tin	$1.8-1.3 \cdot 10^{-3}$	2553-1443	$0.41-2.2 \cdot 10^{18}$	N
G 74	Iron	$3.3-1.3 \cdot 10^7$	2343-2051	$7.9-7.0 \cdot 10^7$	N
G 217	Zinc	$7.5 \cdot 10^{-2}$	90.1	$1.3 \cdot 10^{18}$	P
M 328	Sulfur	$2.55 \cdot 10^{-4}$	590	$4.1 \cdot 10^{19}$	N
R 18	No dopant	0.286	4030	$5.4 \cdot 10^{15}$	N

Electrical parameters of single crystals used for epitaxial and other application are in the Tab.1. If Schottky barrier or photoconductive detectors are prepared, the semi-insulating InP must be used. Fe-doped InP has high resistivity but also high capture cross section for electrons. For this reason we have prepared co-doped crystals with iron

and zinc to lower the Fe concentration necessary for the creation of semi-insulating state and titanium and zinc or titanium and manganese because of the lower electron capture cross section of titanium. Results are shown in the Tab.2.

Tab.2 .Electrical parameters of co-doped semi-insulating InP crystals.

Crystal	Co-dopants	Resistivity [Ωcm]	Hall mobil. [$\text{cm}^2/\text{V.s.}$]	Concentration [cm^{-3}]	Conduc. type
G 264	Iron-zinc	$2.7 \cdot 10^7$	1399	$1.6 \cdot 10^8$	N/P
T 68	Titanium-zinc	$5.9 \cdot 10^7$	1519	$6.9 \cdot 10^7$	N/P
R 10	Titan-mangan.	$2.2 \cdot 10^6$	1815	$1.6 \cdot 10^9$	N/P

Semi-insulating InP can be prepared also by the heat treatment of undoped or gettered crystals. We have used the annealing of pulled crystals at 950°C for 96 hours and slow cooling $4^\circ\text{C}/\text{hour}$. The same procedure was used for tantalum doped and annealed crystals. Electrical parameters of InP:Ta is similar to very pure InP and after annealing convert to semi-insulating state. Crystals doped with copper and quenched from 500°C exhibit even P-type conductivity, meanwhile all other semi-insulating InP prepared at our laboratory or elsewhere are N-type conductivity. In the Tab.3 is the survey of less common InP doped crystals prepared in our laboratory.

Tab.3. Electrical parameters of InP crystals with special dopants

Crystal	Dopant	Resistivity [Ωcm]	Hall mobil. [cm^2/Vs]	Concentr. [cm^{-3}]	Remark
G 222	Mangan.	3.2	120	$1.6 \cdot 10^{16}$	P-type
G 233	Rhenium	0.171	4160	$8.7 \cdot 10^{15}$	N- getter
R 19	Tantalum	0.875	3700	$1.9 \cdot 10^{15}$	N-getter
R 19anneled	Tantalum	$6.3 \cdot 10^6$	2030	$4.9 \cdot 10^8$	N-type
R 20quench.	Copper	$5.5 \cdot 10^5$	120	$9.7 \cdot 10^{10}$	P-type
G162 anneal.	Undoped	$4.1 \cdot 10^8$	4500	$3.6 \cdot 10^6$	N-type
G 267	Gold	0.115	3660	$1.5 \cdot 10^{16}$	N-type
R 26	Nickel	0.375	4130	$4.0 \cdot 10^{15}$	N-type

The first prototype particle detectors based on SI InP co-doped with Ti+Mn operating at room temperature with 60% CCE, and radiation detectors based on SI InP co-doped with Ti+Zn with and without a guard-ring electrode operating at RT have been fabrication in our laboratory. The application of new technology forming an irradiation-exposed electrode consisting of two parts has improved the spectral characteristics of the detectors; better energy resolution and noise level of the detectors with guard-ring electrodes have been obtained. Detector of low energy γ -photons of 122keV (^{57}Co) and 662keV (^{137}Cs) based on new purified InP crystals with Ta admixture, converted to SI state by high temperature annealing, have been reported before.

This work has been supported by the grant GACR 102/06/153 and CAS KAN 400670651 and CAS KAN 40122080.

- [1] Lund, et al., Nucl. Instr. and Meth. A272 (1988) 885.
- [2] Valentini, et al., Nucl. Instr. Meth. A 373 (1995) 47.
- [3] Jayavel, et al., Nucl. Instr. Meth. A 454 (2000) 252.
- [4] V.Gorodyskiy, et al., Nucl. Instr. Meth. 555 (2005) 288.
- [5] RYatskiv, et al., Proc. Int. Conf. IPRM 2008, Versailles, France, May 25-29, 2008.
- [6] L.Pekarek, et al., Proc.Int. Conf. IPRM 2008, Versailles, France, May 25-29, 2008.

Author index

- Behúlová M., 6
Beitlerová A., 41, 56
Boča R., 10, 50
Brožek V., 8, 12
Bryknar Z., 54
- Cihlář A., 27
Ciprian D., 39
Ctibor P., 8
- Čechák T., 56
- Demo P., 24, 64, 70
Dlháň L., 10, 50
Domlátil J., 12
Drápala J., 14, 35, 60
Dvorský R., 37
- Eliáš M., 12
- Frumar M., 49
Frumarová B., 49
Fuess H., 50
Fuhr O., 10
- Gladkov P., 47
Gregora I., 22
Grgač P., 6
Grym J., 16
- Havránek V., 62
Hejtmánek J., 62
Hlubina P., 39
Hošková Š., 70
Hudec R., 66
- Cheong D., 8
Chromčíková M., 58
- Janča J., 12
Jančuška I., 26
- Jarchovský Z., 47
Jurek K., 62
Juřica J., 18, 35
- Kim E., 8
Koman M., 20
Kostelník P., 66
Kotočová A., 20
Koudelka L., 22, 43
Kožíšek Z., 24, 64, 70
Krajčovič J., 26
Král R., 27
Kubíček P., 14
Kučera M., 56
Kuldová K., 49
- Leitner J., 29
Luňáček J., 37, 39
Luňáčková M., 39
Lipták J., 31, 52
Liška M., 58
Lorenc M., 33, 72
Losertová M., 18, 35
- Macková A., 62
Maixner J., 12
Mareš J., 41, 56
Maryško M., 62
Mlích A., 52
Mošner P., 22, 43
- Nikl M., 41, 56
Nitsch K., 45, 56, 58
Nohavica D., 47
- Ondrejovič G., 20
Oswald J., 49
- Papánková B., 50
Pekárek L., 74

Pilarčíková I., 52
Pospíšil M., 33, 66
Potůček Z., 39, 54
Procházková O., 16
Průša P., 41, 56

Rodová M., 58
Růžička K., 29

Sedláček J., 52
Sedmidubský D., 29, 62
Skotnicová K., 60, 68
Slíva A., 37
Sofer Z., 62
Solovieva N., 56
Stejskal J., 62
Sudrová J., 14
Sveshnikov A., 24, 64, 70
Svoboda I., 50
Svoboda P., 29

Šalित्रoš I., 10
Šik J., 33, 66, 72
Štěpánek J., 68
Šubčík J., 22

Tichá P., 24, 64, 70
Titiš J., 50
Trepakov V., 54
Turczynová L., 31

Veselý J., 35
Vlček M., 43
Vosejpková K., 43
Václavů M., 62
Válek L., 72

Yatskiv R., 74

Zavadil J., 16

Žďánský K., 16

LIST OF PARTICIPANTS

Mária Behúlová, Dr.
FMST SUT Trnava
Paulínská 16
917 24 - Trnava - SR
maria.behulova@stuba.sk

Alena Beitlerová, Mrs.
Institute of Physics AS CR
Cukrovarnická 10
162 00 - Praha 6
beitler@fzu.cz

Vlastimil Brožek, Dr
Institute of Plasma Physics AS CR
Za Slovankou 3
182 00 - Praha 6
brozek@ipp.cas.cz

Antonín Cihlář, Mr.
Institute of Physics AS CR
Cukrovarnická 10
162 00 - Praha 6
cihlar@fzu.cz

Pavel Ctibor, Dr
Institute of Plasma Physics AS CR
Za Slovankou 3
182 21 - Praha 8
ctibor@ipp.cas.cz

Miroslav Cukr, Dr.
Institute of Physics AS CR
Cukrovarnická 10
162 00 - Praha 6
cukr@fzu.cz

Pavel Demo, Prof.
Institute of Physics AS CR
Cukrovarnická 10
162 00 - Praha 6
demo@fzu.cz

L'ubor Dlháň, Ph.D.
Faculty of Chemical Technology SUT
Radlinskeho 9
812 37 - Bratislava - SR
lubor.dlhan@stuba.sk

Jiří Domlátil, Mr.
Institute of Chemical Technology Praha
Technická 5
166 28 - Praha 6
jiri.domatil@vscht.cz

Jaromír Drápala, Prof.
VŠB - TU Ostrava, Dept. 636
Tř. 17. Listopadu 15
708 33 - Ostrava - Poruba
Jaromir.Drapala@vsb.cz

Jan Grym, Dr.
Inst. of Photonics and Electronics AS CR
Chaberská 57
182 51 - Praha 8
grym@ufe.cz

Zdeněk Hubička, Ph.D.
Institute of Physics AS CR
Na Slovance 2
182 21 - Praha 8
hubicka@fzu.cz

Eduard Hulicius, Dr.
Institute of Physics AS CR
Cukrovarnická 10
162 00 - Praha 6
hulicius@fzu.cz

Jan Juřica, Mr.
VŠB - TU Ostrava
Tř. 17. Listopadu 15
708 33 - Ostrava - Poruba
jan.jurica.fmmi@vsb.cz

Marian Koman, Prof.
Faculty of Chemical Technology SUT
Radlinského 9
812 37 - Bratislava - SR
marian.koman@stuba.sk

Ladislav Koudelka, Prof.
University of Pardubice
Nám. Legií 565
532 10 - Pardubice
ladislav.koudelka@upce.cz

Zdeněk Kožíšek, Dr.
Institute of Physics AS CR
Cukrovarnická 10
162 00 - Praha 6
kozisek@fzu.cz

Jozef Krajčovič, Mr.
FMST SUT Trnava
J. Bottu 25
91724 - Trnava - SR
josef_krajcovic@stuba.sk

Robert Král, Mr.
Institute of Physics AS CR
Cukrovarnická 10
162 00 - Praha 6
kralr@fzu.cz

Alexander Kromka, Dr.
Institute of Physics AS CR
Cukrovarnická 10
162 00 - Praha 6
kromka@fzu.cz

Jindřich Leitner, Prof.
Institute of Chemical Technology Praha
Technická 5
166 28 - Praha 6
Jindrich.Leitner@vscht.cz

Jan Lipták, Dr.
Faculty of Electrotechn. Engineering CTU
Technická 1
166 28 - Praha 6
liptak@fel.cvut.cz

Michal Lorenc, Mr.
ON SEMICONDUCTOR CR
1. Máje 2230
756 61 - Rožnov pod Radhoštěm
michal.lorenc@onsemi.com

Monika Losertová, Dr.
VŠB - TU Ostrava, Dept. 637
Tř. 17. Listopadu 15
708 33 - Ostrava - Poruba
mlosertova@vsb.cz

Jiří Luňáček, Dr.
VŠB - TU Ostrava
Tř. 17. Listopadu 15
708 33 - Ostrava
jiri.lunacek@vsb.cz

Milena Luňáčková, Mrs.
VŠB - TU Ostrava
Tř. 17. Listopadu 15
708 33 - Ostrava
milena.lunackova@vsb.cz

Jiří A. Mareš, Dr.
Institute of Physics AS CR
Cukrovarnická 10
162 00 - Praha 6
amares@fzu.cz

Petr Mošner, Dr.
University of Pardubice
Nám. Čs. legií 565
532 10 - Pardubice
petr.mosner@upce.cz

Karel Nitsch, Dr.
Institute of Physics AS CR
Cukrovarnická 10
162 00 - Praha 6
nitsch@fzu.cz

Dušan Nohavica, Dr.
Inst. of Photonics and Electronics AS CR
Chaberská 57
182 51 - Praha 8
nohavica@ufe.cz

Jiří Oswald, Dr.
Institute of Physics AS CR
Cukrovarnická 10
162 00 - Praha 6
oswald@fzu.cz

Blaženka Papánková, Dr.
Faculty of Chemical Technology SUT
Radlinského 9
812 37 - Bratislava - SR
blazena.papankova@stuba.sk

Ladislav Pekárek, Dr.
Institute of Physics AS CR
Na Slovance 2
182 21 - Praha 8
pekareklad@volny.cz

Ivana Pilarčíková, Dr.
Faculty of Electrotechn. Engineering CTU
Technická 2
166 27 - Praha 6
pilarcik@fel.cvut.cz

Zdeňka Poláčková, Mrs.
Institute of Physics AS CR
Cukrovarnická 10
162 00 - Praha 6
polackoz@fzu.cz

Zdeněk Potůček, Dr.
Institute of Physics AS CR
Na Slovance 2
182 21 - Praha 8
potucek@fzu.cz

Petr Průša, Mr.
Institute of Physics AS CR
Cukrovarnická 10
162 00 - Praha 6
petr.prusa@centrum.cz

Miroslava Rodová, Mrs.
Institute of Physics AS CR
Cukrovarnická 10
162 00 - Praha 6
rodova@fzu.cz

Jan Šik, Dr.
ON SEMICONDUCTOR CR
1. Máje 2230
756 61 - Rožnov pod Radhoštěm
jan.sik@onsemi.com

Kateřina Skotnicová, Dr.
VŠB - TU Ostrava
17. Listopadu
708 33 - Ostrava - Poruba
katerina.bujnoskova@vsb.cz

Zdeněk Sofer, Mr.
Institute of Chemical Technology Praha
Technická 5
166 28 - Praha 6
zdenek.sofervscht

Bedřich Štěpánek, Dr.
Future Electronics - Praha
Štětkova 5
140 00 Praha 4
bedrich.stepanek@futureelectronic.com

Jan Štěpánek, Mr.
VŠB - TU Ostrava
Tř. 17. Listopadu 15
708 33 - Ostrava - Poruba
jan.stepanek.fmmi@vsb.cz

Alexej Sveshnikov, Dr.
Institute of Physics AS CR
Cukrovarnická 10
162 00 - Praha 6
sveshnik@fzu.cz

Petra Tichá, Mrs.
Institute of Physics AS CR
Cukrovarnická 10
162 00 - Praha 6
ticha@fzu.cz

Ladislava Turczynová, Mrs.
Faculty of Electrotechn. Engineering CTU
Technická 2
166 27 - Praha 6
turcz11@feld.cvut.cz

Lukáš Válek, Mr
ON SEMICONDUCTOR CR
1. Máje 2230
756 56 - Rožnov pod Radhoštěm
lukas.valek@onsemi.com

Roman Yatskiv, Dr.
Inst. of Photonics and Electronics AS CR
Chaberská 57
182 51 - Praha 8
yatskiv@ufe.cz